TECHNISCHE UNIVERSITÄT MÜNCHEN

Lehrstuhl für Tierhygiene

Modulation of apoptosis by SARS-CoV nucleocapsid- and 7a protein

Claudia Wex

Vollständiger Abdruck der von der Fakultät Wissenschaftszentrum Weihenstephan für Ernährung, Landnutzung und Umwelt der Technischen Universität München zur Erlangung des akademischen Grades eines

Doktors der Naturwissenschaften

genehmigten Dissertation.

Vorsitzender:	Univ.-Prof. Dr. R. F. Vogel
Prüfer der Dissertation:	1. Univ.-Prof. Dr., Dr. h.c. J. Bauer
	2. Univ.-Prof. Dr. H. M. Schätzl

Die Dissertation wurde am 03.01.2012 bei der Technischen Universität München eingereicht und durch die Fakultät Wissenschaftszentrum Weihenstephan für Ernährung, Landnutzung und Umwelt am 14.03.2012 angenommen.

SUMMARY

In March 2003, a novel human pathogenic coronavirus had been associated with a worldwide outbreak of atypical pneumonia and was designated as severe acute respiratory syndrome coronavirus (SARS-CoV). Besides the pulmonary tissues which are the primary target of SARS-CoV infection, replicating SARS-CoV has also been detected in the gastrointestinal tract of patients suffering from SARS. Notably, in contrast to the enormous tissue damage of the lung, the gastrointestinal tract showed no histopathological abnormalities. Additionally to an overreaction of immune mediators, the lung tissue damage might also be caused by apoptosis. The histopathological differences observed in SARS-CoV infected patients are also reflected in cell lines infected with SARS-CoV. Vero E6 cells (African green monkey kidney) are highly susceptible to SARS-CoV propagation and show extensive cytopathic effects upon infection. Furthermore, it has been reported that SARS-CoV infection induces apoptosis in Vero E6 cells. In contrast to this observation cell lines of the large intestine such as Caco-2 (human colon adenocarcinoma cell line) cells showed lower replication efficiency and downregulation of proapoptotic proteins during SARS-CoV infection. In order to investigate the interaction of SARS-CoV with the host cell death machinery potentially leading to the extraordinary and distinct human pathology in this thesis the Vero E6 cell line was chosen as a model for lytic infection and the Caco-2 cell line served as a model for persistent infection. To examine the interaction of SARS-CoV with apoptotic pathways in more detail, primarily the structural nucleocapsid protein N and the accessory protein 7a were utilized.

Initially, analysis of the apoptotic properties of N revealed that N was cell-type specifically cleaved by effector caspases 6 and / or 3 upon infection as well as upon transient expression. In contrast to the processing of N in Vero E6 cells (and in A549 cells), no cleavage of N was found in the Caco-2 cell line (or in N2a cells). Further experiments demonstrated that N induces the intrinsic apoptotic pathway, resulting in the processing of N at residues 400 and 403 by caspase-6. Furthermore, the subcellular localization of N was analyzed in these cell lines. N was localized both in the cytoplasm and nucleus in Vero E6 and A549 cell lines, whereas in Caco-2 and N2a cell lines N expression was nearly completely restricted to the cytoplasm. Moreover, this study indicates that the nuclear localization of N is essential for its cleavage by caspase-6. Based on these data we suggest a correlation between the replication cycle of SARS-CoV, the subcellular localization of N, induction of apoptosis and subsequent caspase-mediated cleavage of N.

In order to get insight into the function of the unique 7a protein, a Yeast-Two-Hybrid (Y2H)

screen was performed to identify putative interacting proteins. To find a possible cell type specific interactor of 7a a cDNA-library was prepared from the Caco-2 cell line and used as prey in this screen. Indeed, a protein expressed cell type specifically in Caco-2 cells was identified in this Y2H screen, namely the proapoptotic BH3 only protein Bik. This interaction was further confirmed in other mammalian cell lines by co-immunoprecipitation experiments upon transient overexpression of 7a and Bik, and, more important, even upon infection with SARS-CoV. In a previous study, however, it was shown that the cell type specific expression of Bik is introduced by immortalization of carcinoma cell lines as Bik mRNA was not found in tissues of the gastrointestinal tract. In tissues of the lung, however, mRNA of Bik was detected, enabling a non-artificial interaction of 7a and Bik during SARS-CoV infection. Furthermore, we found that 7a and Bik interact via their transmembrane domains. In addition, like N, 7a also tends to induce cell type specific apoptosis. Expression of 7a in Vero E6 cells resulted in an increased level of activated caspase-3, whereas in Caco-2 cells caspase-3 was not significantly activated by 7a expression. In our hands, however, it was not possible to demonstrate a link between amounts of activated caspase-3 and the interaction of 7a and Bik.

In conclusion, this study has provided new insights in the pro-apoptotic functions of SARS-CoV N and 7a proteins.

ZUSAMMENFASSUNG

Im März 2003 wurde ein neues humanpathogenes Coronavirus entdeckt, das für die pandemische Ausbreitung eines schweren akuten Atemwegssyndroms verantwortlich war und aufgrund des Krankheitsbildes severe acute respiratory syndrome (SARS)-CoV genannt wurde. Neben dem Respirationstrakt, der vorwiegend von SARS-CoV infiziert wird, konnte das Virus außerdem auch im Gastrointestinaltrakt nachgewiesen werden. Bemerkenswerterweise konnten im Gegensatz zu den enormen Gewebeschäden der Lunge im Gastrointestinaltrakt keine histopathologischen Auffälligkeiten gefunden werden. Das zerstörte Lungengewebe in SARS-CoV infizierten Patienten könnte möglicherweise neben der Überreaktion von Immunmediatoren auch das Ergebnis von Apoptosis sein. Diese Unterschiede in der Schädigung der Gewebe von SARS-Patienten konnten ebenfalls in SARS-CoV infizierten Zelllinien beobachtet werden. Vero E6 Zellen (Nierenzelllinie der Grünen Meerkatze) sind sehr empfänglich für die Propagierung von SARS-CoV und weisen nach erfolgter Infektion erhebliche cytopathische Effekte auf. Darüber hinaus wurde beschrieben, dass die Infektion von Vero E6 Zellen mit SARS-CoV Apoptose auslöst. Im Gegensatz dazu konnte in Zelllinien, die aus dem Dickdarm isoliert wurden, beispielsweise in der Caco-2 Zelllinie (humane Colon Adenocarcinomzelllinie), eine geringere Replikationseffizienz von SARS-CoV und eine verminderte Expression von proapoptotischen Genen beobachtet werden. In dieser Arbeit wurden daher Vero E6 Zellen als Modell für die lytische Infektion mit SARS-CoV und die Zelllinie Caco-2 als Prototyp einer persistenten SARS-CoV-Infektion ausgewählt, um die Interaktion des SARS-CoV mit der Zelltodmaschinerie der Wirtszelle zu untersuchen, die möglicherweise zu der außergewöhnlichen und unterschiedlichen Humanpathologie von SARS-CoV führt. Um die Interaktion von SARS-CoV mit apoptotischen Signaltransduktionswegen im Detail zu untersuchen, wurden in dieser Arbeit vorrangig das Strukturprotein N sowie das akzessorische Protein 7a verwendet.

Die Untersuchungen der apoptotischen Eigenschaften von N ergaben, dass während der Expression von N sowie während der Infektion von Zellen mit SARS-CoV, N zelltypspezifisch von den Effektorcaspasen 6 und oder 3 gespalten wird. Im Gegensatz zu der Caspase vermittelten Spaltung von N in Vero E6 Zellen (beziehungsweise bei Expression in A549 Zellen) konnte keine Spaltung von N in Caco-2 Zellen (beziehungsweise bei Expression in N2a Zellen) festgestellt werden. Des Weiteren konnte in dieser Arbeit gezeigt werden, dass N den intrinsischen apoptotischen Signalübertragungsweg aktiviert, was zu der Caspase-6 vermittelten Spaltung von N an den Aminosäurepositionen 400 und 403 führt. Darüber hinaus wurde die subzelluläre Lokalisation von N in den verschiedenen Zelllinien untersucht.

Hierbei konnte festgestellt werden, dass in N exprimierenden Vero E6 und A549 Zellen das Protein sowohl im Cytoplasma als auch im Nukleus lokalisiert ist. Im Gegensatz dazu konnte N in transfizierten Caco-2 und N2a Zellen nahezu ausschließlich im Cytoplasma nachgewiesen werden. Schließlich deuten die Ergebnisse dieser Arbeit darauf hin, dass die Kernlokalisation von N entscheidend für die Caspase-6 vermittelte Spaltung von N ist. Basierend auf diesen Daten schlussfolgern wir einen Zusammenhang zwischen dem Replikationszyklus von SARS-CoV und der Kernlokalisation von N, der Aktivierung von Apoptose und konsequenterweise der Caspase-6 vermittelten Spaltung von N.

Des Weiteren wurde ein Yeast-Two-Hybrid (Y2H) Screen durchgeführt, um mögliche interagierende Proteine von 7a zu identifizieren und schließlich mehr über dieses einzigartige Protein zu erfahren. Um einen möglichen zelltypspezifischen Interaktor von 7a zu finden wurde aus der Caco-2 Zelllinie eine cDNA-Bibliothek hergestellt und in diesem Screen als Prey verwendet. Tatsächlich konnte in dieser Arbeit ein zelltypspezifisches Protein, das proapoptotische, „BH3 only protein“ Bik als interagierendes Protein von 7a identifiziert werden. Die Interaktion von 7a und Bik konnte ferner in Säuger-Zelllinien durch Co-Immunpräzipitations-Experimente sogar während der Infektion mit SARS-CoV bestätigt werden. In einer früheren Studie wurde jedoch gezeigt, dass die zelltypspezifische Expression von Bik durch die Immortalisierung verschiedener Carcinomazelllinien zurückzuführen ist, da keine mRNA von Bik in verschiedenen Geweben des Gastrointestinaltrakt zu finden war. In Geweben der Lunge konnte jedoch mRNA von Bik nachgewiesen werden, was eine nicht artifizielle Interaktion von 7a und Bik ermöglicht. Des Weiteren konnten wir zeigen, dass 7a und Bik über ihre Transmembrandomänen interagieren. Ähnlich wie N scheint auch 7a tendenziell zelltypspezifisch Apoptose auszulösen. Die Expression von 7a in Vero E 6 Zellen führte zu einem erhöhten Maß an aktivierter Caspase-3, wohingegen in 7a transfizierten Caco-2 Zellen Caspase-3 nicht wesentlich aktiviert wurde. Es konnte jedoch nicht gezeigt werden, dass die Interaktion von 7a und Bik die Aktivierung von Caspase-3 maßgeblich beeinflusst.

Zusammenfassend konnten durch diese Arbeit neue Erkenntnisse über die pro-apoptotischen Funktionen der SARS-CoV Proteine N und 7a gewonnen werden.

TABLE OF CONTENTS

1 INTRODUCTION

1.1 SARS-CORONAVIRUS (SARS-COV)

Severe acute respiratory syndrome (SARS) was the first plague of the twenty-first century. In November 2002 SARS emerged in Guangdong Province, China and spread to several countries around the world within months. 8096 people were affected in 32 countries across five continents (WHO, 2011). The disease was described as an infectious atypical pneumonia characterized by progressive respiratory failure. By the end of the pandemic in 2004 the WHO reported 774 deaths with an overall mortality rate of approximately 10 %.

The etiological agent of SARS was rapidly identified to be a new coronavirus (Drosten *et al.*, 2003b;Ksiazek *et al.*, 2003;Peiris *et al.*, 2003b) not endemic in humans. The first cases of SARS had contact with life-game trades (Zhong *et al.*, 2003), suggesting that the virus had originated from animals (Shi and Hu, 2008) and adapted to humans. Animals were collected in wild life game animal market and in raccoon dog (*Nyctereutes procyonoides*), masked palm civet (*Paguma larvata*) and in Chinese ferret badger (*Melogale moschata*) SARS-CoV like viruses were found. Palm civets were suggested to be the natural host of SARS-CoV, since the viral genome sequences between these species and human isolates yielded more than 99 % of nucleotide homology (Guan *et al.*, 2003). However, the virus was not widespread in wild and farmed civets (Wu *et al.*, 2005;Kan *et al.*, 2005). To investigate whether the civet was the natural reservoir or just an intermediate host, civets were experimentally infected with two human strains of SARS-CoV. These animals showed overt clinical symptoms indicating that the civet was not the natural host. Sequences of SARS-CoV like virus isolated from civets showed a high mutation rate, suggesting that the virus had not adapted to civet but that they acquired the virus from another species (Kan *et al.*, 2005;Song *et al.*, 2005).

Bats are reservoir hosts of many viruses including Ebola and Nipah viruses and were present at food and traditional medicine markets in South China. Bats were therefore a putative candidate for a natural host of SARS-CoV and were screened for coronaviral infection. In 2005, Bat coronaviruses closely related to SARS-CoV were discovered in different species of horseshoe bats (*Rhinolophus*) (Li *et al.*, 2005). Subsequent studies ascertained a diversity of coronaviruses in different bat species which seems to be species specific. SARS-CoV like viruses were so far only found in horseshoe bats, indicating that this species is the natural host of SARS-CoV (Tang *et al.*, 2006;Wang *et al.*, 2006).

1.1.1 TAXONOMY OF CORONVIRUSES

In 2003 the etiological agent of severe acute respiratory syndrome was identified as a novel member of the family *Coronaviridae* and denominated SARS-CoV (see 1.1). The name "coronavirus" is deduced from the crown – like morphology observed for these viruses in electron microscope (**Fig. 1**) (Tyrrell, 1965). The *Coronaviridae* family, along with the *Arteviridae* and *Roniviridae* families, constitute the order *Nidovirales*. Previous to the emergence of SARS-CoV, coronaviruses divided into three antigenic groups (I-III) which were consistent with the genetic relatedness of these viruses (Gonzalez *et al.*, 2003). Group I coronaviruses comprise animal pathogens such as transmissible gastroenteritis virus (TGEV) or feline infectious peritonitis virus (FIPV), as well as the human coronavirus HCoV-229E, which causes respiratory infection. Infections with group II coronaviruses also cause respiratory illness or enteric disease of animals and humans. Murine hepatitis virus (MHV), moreover, causes a variety of diseases such as respiratory and enteric disease, encephalitis and hepatitis. Further members of this group are human coronavirus OC 43 and bovine coronavirus BCoV. These pathogens harbor an additional characteristic, namely the hemagglutinin esterase. Pathogens of group III include only avian coronaviruses, such as infectious bronchitis virus which causes respiratory infections of chicken.

SARS-CoV cross-reacts with antibodies against group I coronaviruses, however, phylogenetic analysis revealed that SARS-CoV is distinct from the three classified coronavirus genera and it was proposed to constitute a fourth group. Based on amino acid sequence analysis of the spike protein a closer relationship of SARS-CoV to group II was found (Eickmann *et al.*, 2003). Genome and proteome analysis confirmed that SARS-CoV is probably an early split-off from coronavirus group II lineage (Snijder *et al.*, 2003). Subsequently, SARS-CoV was classified as group 2b coronavirus and the traditionally classified coronaviruses of group II were categorized as group 2a. After the SARS outbreak which has enhanced interest in all directions of coronavirus research, there was an addition of 16 coronaviruses with completely sequenced genome. These include two human coronaviruses, HCoV-NL 63 and HCoV-HKU1, 10 other mammalian coronaviruses, bat-SARS-CoV, bat-CoV HKU4, bat-CoV HKU5, bat-CoV HKU8, bat-CoV HKU9 bat-CoV 512/2005, bat-CoV 1A, equine coronavirus, and beluga whale coronavirus (SW1) (Woo P.C., 2009). Therefore, new phylogenetic analyses were done and two new subgroups of group II (2c and 2d) as well as two subgroups of group III (3b and 3c) have been proposed (Woo *et al.*, 2006;Woo P.C., 2009) (**Fig. 2**).

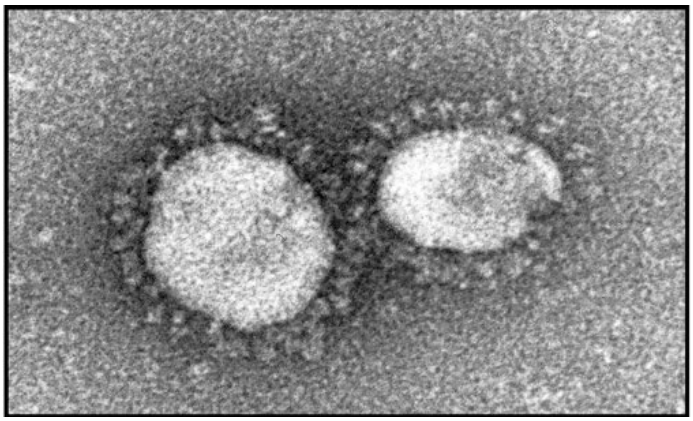

Fig. 1. Electron microscopy of SARS-CoV. Electron microscopy revealed typical coronavirus particle. The crown-like shape is a result of the incorporation of the spike protein in the envelope membrane (Parashar and Anderson, 2004).

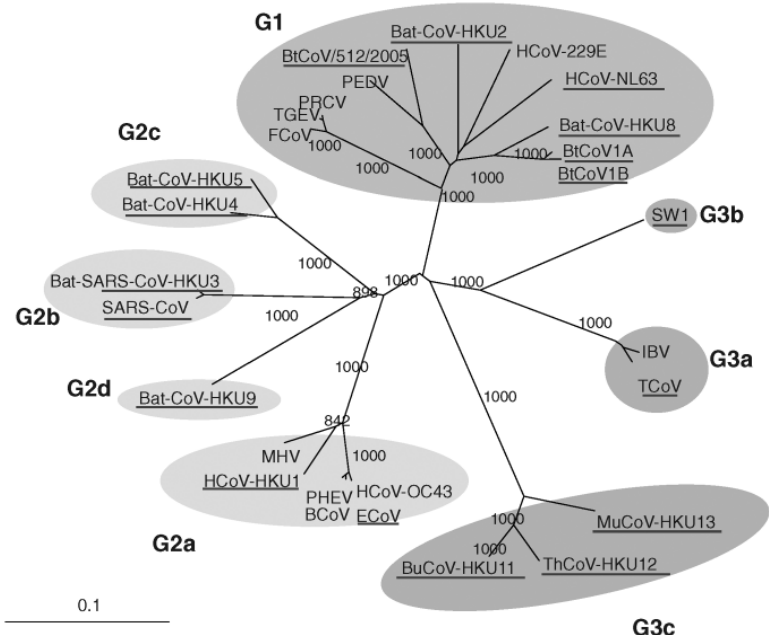

Fig. 2. Taxonomy of coronaviruses. The phylogenetic tree demonstrates the proposed classification of coronaviruses. The viruses were divided into three main groups 1-3 which were in part splitted into 4 (G2a-2d) and 3 subgroups (G3a-G3c). Thus SARS-CoV was classified into subgroup 2b (Woo P.C., 2009)

1.1.2 MORPHOLOGY OF SARS-COV VIRIONS

SARS-CoV is an enveloped virus with spherical virions of approximately 80 -140 nm in

diameter (Ksiazek *et al.*, 2003). A lipid bilayer envelopes the capsid in which three of the main structural proteins the S (spike)-, E (envelope)-, and M- (membrane) proteins are anchored (Lai, 2003) **(Fig. 1 and Fig. 3)**. The S-glycoprotein mediates receptor binding and fusion with the host cell. The E protein together with the M protein is important for viral assembly and budding (Lai, 2003). Further structural components of the SARS-CoV virion are accessory proteins encoded by open reading frames (ORFs) 3a, 7a and 7b (Shen *et al.*, 2005;Huang *et al.*, 2006a;Huang *et al.*, 2006b;Schaecher *et al.*, 2007). Inside of the virion the positive strand RNA genome of SARS-CoV is complexed by the N (nucleocapsid) protein to form a helical nucleocapsid.

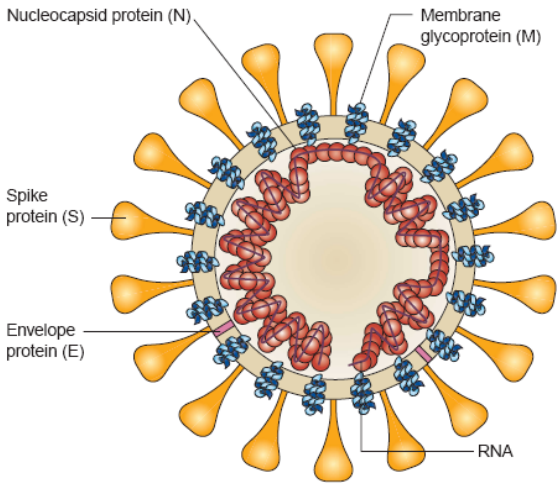

Fig. 3. Schematic illustration of the SARS-CoV viron. The S, E and M proteins are incorporated in a lipid bilayer envelope originated from the host cell. In contrast to group 2a coronaviruses, SARS-CoV does not harbour hemagglutinin esterase glycol-protein. Within the viron the helical nucleocapsid is found consisting of the N protein which complexes the viral RNA genome (Peiris *et al.*, 2004).

1.1.3 GENOME ORGANISATION

The positive strand, polyadenylated RNA genome of SARS-CoV encompasses approximately 30 kilobases (kb), the genome of strain Frankfurt-1 (FFM-1, Genbank AY310120) which was used in this thesis is 29.740 nucleotides in length. The genome organization is typical of coronaviruses with a characteristic order: 5´-ORF 1a, ORF 1b, S, E, M and N-3`. ORF 1a and ORF 1b compose two thirds of the genome and encode 16 nonstructural proteins (Nsp). The last one third of the genome encodes the four structural proteins common to all known coronaviruses and 8 accessory proteins characteristic for SARS-CoV (Rota et al., 2003) **(Fig. 4)**. FFM-1 strain harbours a characteristic deletion of 45 nt in ORF 7b which was generated during passaging in cell culture. This deletion enables

FFM-1 an enhanced growth in cell culture, but has no influence on triggering apotosis (Pfefferle *et al.*, 2009;Schneider, 2011).

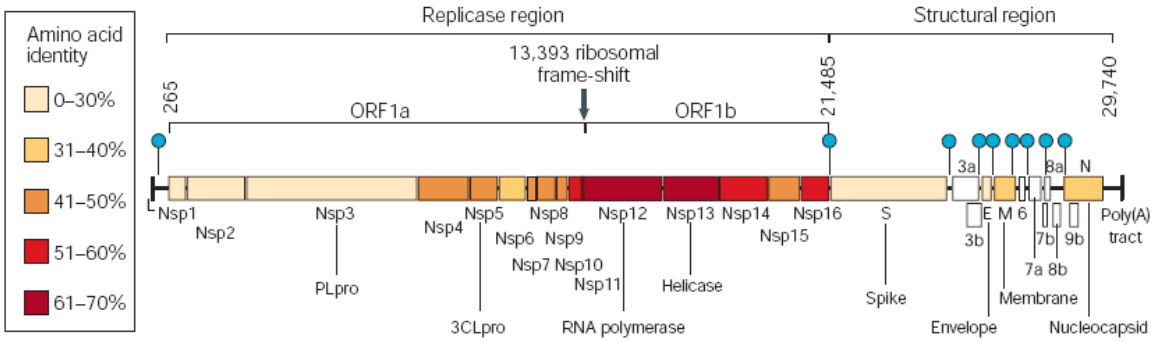

Fig. 4. Genome structure of the SARS-CoV. Two third of the genome consist of the replicase region coding for 16 non structural proteins (Nsps) and the last one third encodes four structural proteins (S, E, M and N) as well as eight SARS-CoV specific accessory proteins. The different colors indicate amino acid sequence homology of the SARS-CoV genome compared to those of other coronaviruses (Stadler *et al.*, 2003).

.

1.1.4 REPLICATION

The life cycle of SARS-CoV starts when the S protein attaches through its S1 domain to ACE-2 (angiotensin-converting enzyme 2), the main receptor of SARS-CoV, and enters the cell via receptor-mediated endocytosis (Wang *et al.*, 2008). In endosomes S is cleaved by acid-activated cathepsin L proteases (Bosch *et al.*, 2005) resulting in the exposure of the S2 fusion domain of the S protein which initiates the fusion of viral envelope and cellular membrane. After fusion the viral genome is released into the cytoplasm where the replication takes place.

The ORF 1a and ORF 1b regions of the genomic RNA are initially translated into two polyproteins (pp1a and pp1ab). The synthesis of pp1ab requires programmed ribosomal frameshift. The polyproteins are autocatalytically cleaved by two viral proteinases (3CLpro and PLpro) resulting in 16 Nsps. Together with cellular components the Nsps form the replication-transcription complex (RTC). This complex is physically anchored by Nsps to intracellular membranes, resulting in the formation of double membrane vesicles (DMV) (Knoops *et al.*, 2008). A former study indicated that these DMVs assemble by utilizing components of autophagosomes (Prentice *et al.*, 2004) but Atg5 which is a key component of autophagosome formation was dispensable for the establishment of DMVs (Zhao *et al.*, 2007). A recent study demonstrates again that components of autophagosomes do not participate in DMV-formation during MHV infection but rather that the DMV derives from

ENDEMosomes originated from the ER (Reggiori *et al.*, 2010). The RTC mediates both genome replication and transcription of a nested set of subgenomic (sg) mRNAs which encode the structural and accessory proteins. The RTC binds to the genome for replication and transcribes the sg RNA. Each of them carries a short 5`-terminal 'leader' sequence derived from 5´-end of the genome which is thought to be fused by discontinuous synthesis which is regulated by transcription regulatory sequences (TRS). The TRS are located downstream of the 5´- leader sequence on the genomic RNA preceding each gene. For template switch during discontinuous transcription base pairing between leader sequence and the newly synthesized minus RNA strand is required. The base pairing is associated with conserved core sequences (CS) within the TRS which direct transcription of sg RNA, for SARS-CoV the CS is ACGAAC (Thiel *et al.*, 2003;Sawicki *et al.*, 2006). The resulting sets of sg mRNA serve as templates for translation of the structural and accessory proteins. The assembly of new virions involves packaging of the genomes into viral particles. This procedure is achieved by the structural proteins N, M and E and takes place in ER and Golgi compartments. N binds to the genome and encapsulates it to form the nucleocapsid while S, M and E distribute to the ER and then transit to the endoplasmic reticulum–Golgi intermediate compartment (ERGIC). Here, they interact with the nucleocapsid to form virions that bud into the ERGIC which are then transported to the cell surface and are released via exocytosis (**Fig. 5**).

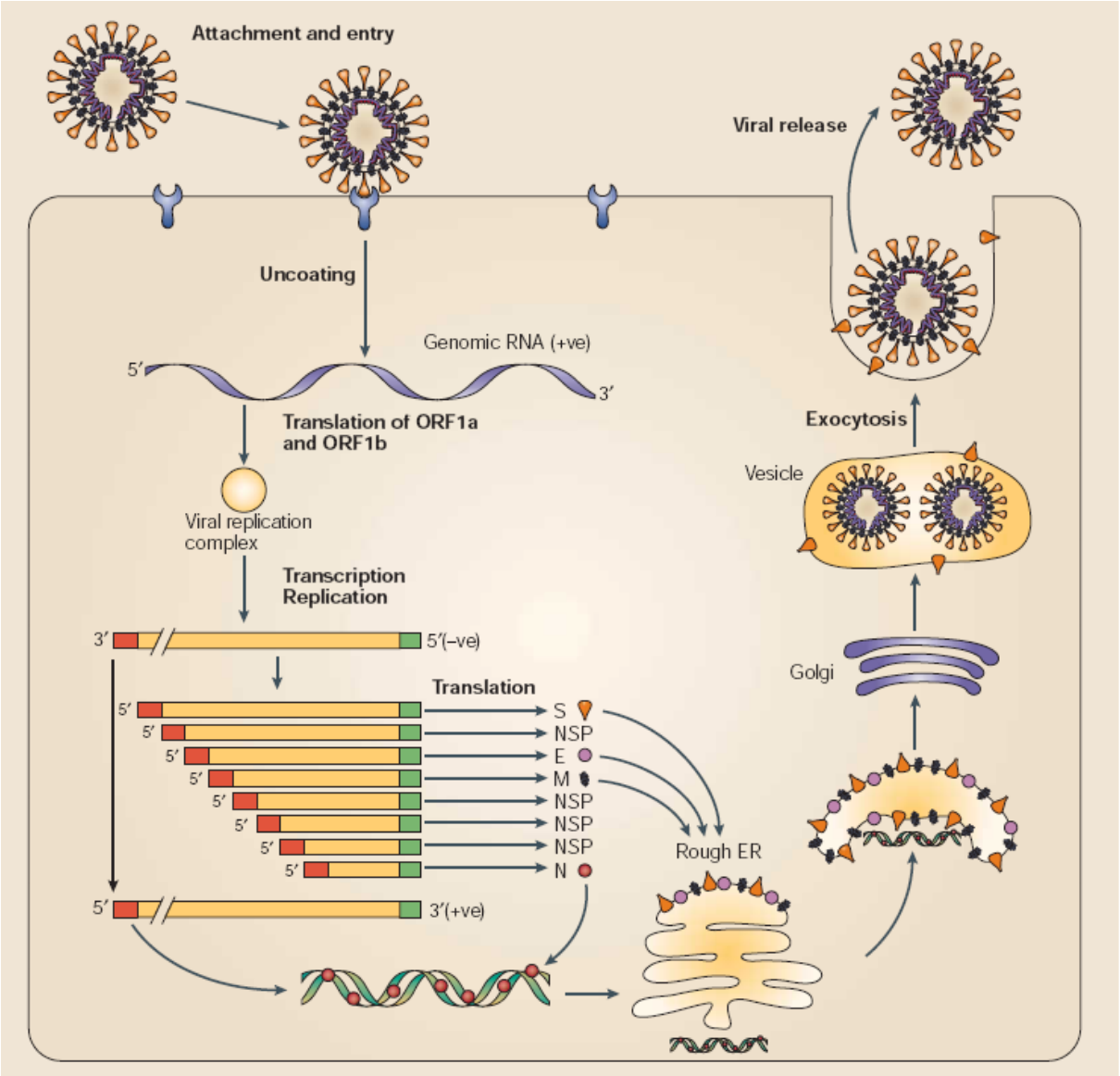

Fig. 5. Model of SARS-CoV life cycle. After receptor interaction, receptor-mediated endocytosis, fusion of envelope and cell membrane, viral RNA and proteins are synthesized in the cytoplasm. Expression of SARS-CoV starts with translation of two polyproteins, pp1a and pp1ab, which undergo autocatalytic processing into the proteins that form together with cellular components the replicase complex. This complex is used to transcribe a 3`-coterminal set of nested subgenomic mRNAs, as well as genomic RNA, that have a common 5`- leader sequence derived from the 5`- end of the genome. Proteins are translated from the 5`- end of each mRNA. Progeny viruses are assembled by budding into intracellular membranes and released through vesicles by the cell secretory mechanisms (Stadler *et al.*, 2003).

1.1.5 EPIDEMIOLOGY

The early SARS cases in Guangdong were more sporadically and occurred among people involved in wild life animal trade (Breiman *et al.*, 2003). A study among animal traders of wild life game animal markets revealed that ~ 9 % of them had IgG antibodies to SARS-CoV

without symptoms (Xu and Gao, 2004). Further studies have also demonstrated that antibodies to SARS-CoV or SARS-like coronaviruses were present in a few healthy humans who had sera banked at least two years prior to SARS-CoV outbreak (Zheng *et al.*, 2004).

In February 2003 the global spread of SARS-CoV started when a physician from Guangdong arrived at the Hotel Metropol in Hong Kong. Previous to his journey he medicated patients with pneumonia at a hospital in Guangzhou. He fell ill and died later of respiratory failure. During his stay in Hong Kong he had transmitted the virus to other hotel guests who got index patients for the viral spread to Singapore, Vietnam and Canada (Booth *et al.*, 2003;Poutanen *et al.*, 2003;Parashar and Anderson, 2004). Simultaneously, the disease began to spread around the world along international air travel routes as infected guests at the hotel flew home. At the end of February a hospital in Hanoi, Vietnam contacted WHO concerning a patient with atypical pneumonia. Dr. Carlo Urbani, a WHO specialist in infectious diseases, concluded that the hospital was faced with an unusual disease and he was the first who recognized the severity of the public health threat. The hospital was put under quarantine and he introduced new infection control procedures to prevent the further spread of the disease in Vietnam (Reilley *et al.*, 2003). On March 12, WHO issued a global alert. Carlo Urbani died at the end of March after acquiring SARS during the work in the hospital. In memorial of Dr. Carlo Urbani the first isolated SARS-CoV was denominated Urbani strain.

In March 2003 SARS had arrived in Germany through a physician who treated patients with atypical pneumonia in Singapore. During a stopover in Frankfurt, Germany on his flight back from New York to Singapore, he, his wife and his mother in law were transferred to an isolation unit at the Frankfurt University Hospital. After a period of 18 days with therapy and entire convalescence the three patients were flown home. From sputum samples of this physician, SARS-CoV was isolated and propagated in cell culture (Drosten *et al.*, 2003a). This SARS-CoV isolate was termed Frankfurt-1 strain (FFM-1) and was used in this thesis.

The mode of spread has been person to person transmission via respiratory droplets. Fecal-oral transmission has also been assumed since SARS-CoV was found in stool. (Peiris *et al.*, 2003a).

The SARS-CoV outbreak was brought under control via patient isolation, infection control in hospitals and travel advisory. In July 2003 no more SARS cases were reported and subsequently, the SARS pandemic was declared to be over by the WHO. After the WHO declaration there were 4 cases of laboratory acquired SARS infection in China, Singapore and Taiwan, with no further spread to human being (Lim *et al.*, 2004;Normile, 2004;Cheng *et al.*, 2007).

1.1.6 PATHOGENESIS AND TISSUE DISTRIBUTION

SARS is predominately a viral pneumonia with diffuse alveolar damage resulting in respiratory failure which could be caused by apoptosis and necrosis. Apoptosis is in contrast to necrosis an active and genetically regulated death of single cells performing physiological function as well as elimination of harmful and abnormal cells. Necrosis, however, occurs coincidentally resulting in the death of tissues or layers of cells. In various studies it was demonstrated that lung epithelial cells such as pneumocytes of SARS-CoV patients undergo apoptosis (Lang *et al.*, 2003;Zhang *et al.*, 2003). SARS-CoV has been detected in several studies in pneumocytes (To and Lo, 2004;Ding *et al.*, 2004;Chow *et al.*, 2004;Gu *et al.*, 2005;Shieh *et al.*, 2005;Nicholls *et al.*, 2006;Ye *et al.*, 2007) as well as in endothelial cells and fibroblasts of the lung (Ye *et al.*, 2007) indicating that pneumocytes are probably the primary target of infection. The clinical course of SARS appears to be a tri-phasic process. In the first phase (week 1) viral replication, increased viral load in the lower respiratory tract (Cheng *et al.*, 2004;Drosten *et al.*, 2004), fever and myalgia can be found. After a few days these symptoms generally decay. The increasing viral load during this phase suggests that the symptoms are related to the effect of viral replication and cytolysis. In the second phase (week 2) the immune response may play an important role, findings are oxygen desaturation, a recurrence of fever and a decline of viral load. About 20% of patients failed to respond to treatment and progress to the third phase, characterized by the development of an acute respiratory distress syndrome (ARDS) (Peiris *et al.*, 2003a). In other cases higher viral loads were significantly associated with patients with a shorter duration from onset of illness to death, indicating virus associated damage of the lung as a contributor to death (Mazzulli *et al.*, 2004). Depending on the age of affected patients the mortality rate varied from 0 to 50%. The total mortality rate is approximately 10 %. People over 65 years old have a higher fatality rate than young people or children.

Although the exact mechanism of SARS pathogenesis is not known the lung damage in patients with SARS appears to be due to both virus induced apoptosis and necrosis as well as indirectly through production of immune mediators. The tri-phasic clinical course of SARS might offer an explanation. In the first phase SARS-CoV damaged tissue directly via apoptosis and necrosis, thereby initiating immunopathology in the second and third phases.

SARS-CoV has also been found in extra-pulmonary tissues, such as brain, liver, kidney, gastrointestinal tract and in the immune system. The tissue distribution of SARS-CoV, however, could not always be correlated with the expression of the main functional SARS-CoV receptor ACE-2 in the respective tissues. Although ACE-2 is highly expressed on the cell surface of endothelial cells of blood vessels of all tissues and the smooth muscle cells of

the intestinal tract there is almost no evidence of SARS-CoV infection at these sites. By contrast in cells and tissues such as colonic enterocytes, liver tissue and immune cells derived from patients SARS-CoV replication has been demonstrated (Hofmann and Pohlmann, 2004). Other receptors or co-receptors such as DC-SIGN which is expressed on dendritic cells and alveolar macrophages as well as L-SIGN which is found on lymph nodes, liver sinusoidal cells, pneumocytes and endothelial cells may explain this discrepancy. *In vitro* experiments, however, showed that cells expressing DC-SIGN as well as L-SIGN without expressing ACE-2 are less or only partially permissive for SARS-CoV infection, implying that DC-SIGN and L-SIGN predominately enhance infection of permissive cells (Jeffers *et al.*, 2004;Marzi *et al.*, 2004;Yang *et al.*, 2004). Furthermore, dendritic cells and immune cells such as macrophages expressing L-SIGN / D-SIGN may transfer SARS-CoV to susceptible cells of the various target organs of SARS-CoV. The different SARS-CoV infected tissues from autopsied or biopsied patients varied in histopathological findings such as necrosis, apoptosis or no tissue damage and are summarized below.

Immune system

In most cases extensive necrosis of the spleen and depletion of lymphocytes have been found (Booth *et al.*, 2003;Li MH, 2004;Lu HY, 2005). Whereas natural killer, CD4, CD8, CD20 and dendritic cell counts have been decreased in the spleen, the average numbers of macrophages have been increased. Indeed, high amounts of SARS-CoV have been detected in lymphocytes as well as in macrophages of patients very early in the onset of illness (< 10 days) in several laboratories (Wang *et al.*, 2004;Gu *et al.*, 2005;Ye *et al.*, 2007). Lymph nodes usually have shown atrophy and reduction of lymphocytes, focal necrosis of hilar lymph nodes has also been found in some cases. SARS-CoV has been detected by electron microscopy (EM) in circulating monocytes and T-lymphocytes and to a lesser extent in natural killer cells and B lymphocytes collected from blood samples in the early stage of illness.

Liver

Liver impairment occured in 60% of SARS-CoV infected patients (Lee *et al.*, 2003;Tsang *et al.*, 2003;Peiris *et al.*, 2003b). In biopsied liver tissue from three patients occurrence of acidophilic bodies, ballooning of hepatocytes and mild to moderate lobular activities was shown (Chau *et al.*, 2004). Moreover, extensive apoptosis in all three cases of this study has been observed.

Urinary system

The kidneys of several autopsied SARS patients have shown various degree of tubular necrosis. SARS-CoV could be detected with both EM and in situ hybridization in epithelial cells of the distal renal tubules (Ding *et al.*, 2004;Gu *et al.*, 2005).

Brain

SARS-CoV has been detected in the cytoplasm of neurons of the brain, predominately in the hypothalamus and the cortex. In this organ degeneration and necrosis of neurons and cellular infiltrates have been observed (Ding *et al.*, 2004;Gu *et al.*, 2005).

Gastrointestinal tract

A considerable number of patients suffering from SARS developed diarhoea (Lang *et al.*, 2003;Leung *et al.*, 2003;To *et al.*, 2004b). The epithelial cells of the mucosa of both the small as well as the large intestine have been infected by SARS-CoV. Beside of the noticeable atrophy of the submucosal lymphoid tissues (Shi *et al.*, 2005) almost no histopathological abnormalities have been found in this organ.

Apart of tissue damage of various SARS-CoV infected organs such as lung, liver, brain, and immune cells potentially due to apoptosis and necrosis, replicating SARS-CoV in the gastrointestinal tract caused no histopathological changes (Lang *et al.*, 2003;Leung *et al.*, 2003;To *et al.*, 2004b).

1.2 MODULATION OF APOPTOSIS BY SARS-COV

The differences in SARS-CoV pathology depending on the infected organ could be confirmed in *in vitro* studies employing SARS-CoV infected cell lines. Vero E6 cells (African green monkey kidney) are highly permissive for SARS-CoV infection and show extensive cytopathic effects upon infection. Furthermore, it was reported that SARS-CoV infection induces apoptosis in Vero E6 cells via the p38 MAPK, caspase and PKR-dependent pathway (Yan *et al.*, 2004;Mizutani *et al.*, 2004c;Ren *et al.*, 2005;Bordi *et al.*, 2006;Krähling *et al.*, 2009). Gene profiling of SARS-CoV infected Vero E6 cells revealed that expression of apoptosis related genes is modified during SARS-CoV infection (Leong *et al.*, 2005). Caco-2 and LoVo are human colon carcinoma cell lines expressing, as well as the Vero E6 cell line, the SARS-CoV specific receptor ACE-2 and, consequently, are permissive for SARS-CoV infection. Although these cell lines from the large intestine are susceptible for SARS-CoV propagation, a lower replication efficiency of SARS-CoV in Caco-2 as well as in LoVo cell lines than in Vero E6 was reported (Chan *et al.*, 2004). This was accompanied by down-regulation of the expression of pro-apoptotic proteins such as caspase-3 and 6 as well as up-regulation of anti-apoptotic factors, for instance Bcl-2 in Caco-2 cells, during SARS-CoV infection (Cinatl *et al.*, 2004). A counterpart to the intrinsic apoptotic pathway is the prosurvival PI3K-Akt signal transduction. PI3K activates several downstream effectors such as the serine-threonine kinase Akt which regulates cell growth, cell cycle and cell survival (Cantrell, 2001). Activated Akt phosphorylates a number of pro-apoptotic proteins including

Bad and caspase-9. Thereby, the pro-apoptotic proteins are inactivated (Kulik *et al.*, 1997). As several other viruses, SARS-CoV also promotes the PI3K-Akt signal transduction to establish persistent infection in Vero cell lines (Mizutani *et al.*, 2005). Moreover, it was shown that the activation of PI3K-Akt is differentiation state-specific in intestinal cells (Gauthier *et al.*, 2001) and inhibits FAS-induced apoptosis in human intestinal epithelial cells (Abreu *et al.*, 2001). In several studies it was demonstrated that SARS-CoV could both induce and inhibit apoptosis in a cell type specific manner (Cinatl *et al.*, 2004;Yan *et al.*, 2004;Mizutani *et al.*, 2004c;Ren *et al.*, 2005;Bordi *et al.*, 2006;Krähling *et al.*, 2009). Activation of PI3K-Akt signal transduction in specific cell lines could offer an explanation, the mechanism of cell type specific modulation of apoptosis, however, needs to be elucidated. Furthermore it was shown that induction of apoptosis by SARS-CoV does not favour viral replication since titers are similar upon overexpression of Bcl-2 (Bordi *et al.*, 2006) or treatment with caspase inhibitors (Ren *et al.*, 2005). SARS-CoV might induce apoptosis after effective replication, potentially to evade immune response as well as to enable spread to other target organs. Otherwise, SARS-CoV may establish persistent infection by inhibition of apoptosis in cell lines derived from the intestine.

These data indicate that the modulation of apoptosis by SARS-CoV seems to be crucial for the cell-type specific phenotype of infection and might subsequently account for the differences of SARS-CoV pathology.

1.2.1 APOPTOSIS

Apoptosis is highly regulated and the molecular mechanism is classically divided into two major apoptotic pathways (Green, 2000), denominated extrinsic and intrinsic pathway **(Fig. 6)**. Extrinsic signals are transmitted by members of the tumor necrosis factor (TNF) superfamiliy. Ligand binding to TNF-family death receptor recruits adaptors and initiator procaspases-8 and/or -10 to form the death-inducing signaling complex (DISC). The DISC formation results in autocatalytic activation of initiator caspases. Once initiator caspases are activated, they directly cleave effector caspases (3, 6, 7) to convert them into their active form. Now effector caspases are able to degrade their targets such as cytoskeletal proteins or nuclear lamins to facilitate cell death. Intrinsic signals are propagated to the mitochondria by the Bcl-2 protein family. There are pro-survival members of this family (Bcl-2, Bcl-xL, Bcl-w, Mcl-1 and A1) which oppose proapoptotic members (Bax, Bak, Bok, Bad, Bid, Bik, Puma and Noxa). Moreover, a cross talk between the intrinsic and extrinsic pathway exists by caspase-8 mediated cleavage of Bid. The intrinsic pathway is highly regulated by the interactions of pro- and anti-apoptotic Bcl-2 proteins. Monitoring of intrinsic signals lead, for

example, to binding of Bad to the prosurvival Bcl-2 proteins and result in release of Bax and Bak from these proteins. Once Bax and Bak are released they oligomerize and insert into the mitochondrial membrane which causes an efflux of cytochrome C. Cytochrome C oligomerizes with Apaf1 and recruits initiator pro-caspase-9 to form the apoptosome, finally resulting in proteolytical activation of caspase-9. Caspase-9 then initiates the caspase cascade by cleaving effector caspases (3, 6, 7) which subsequently degrade their target proteins (Ashkenazi A., 2002;Fulda S, 2006).

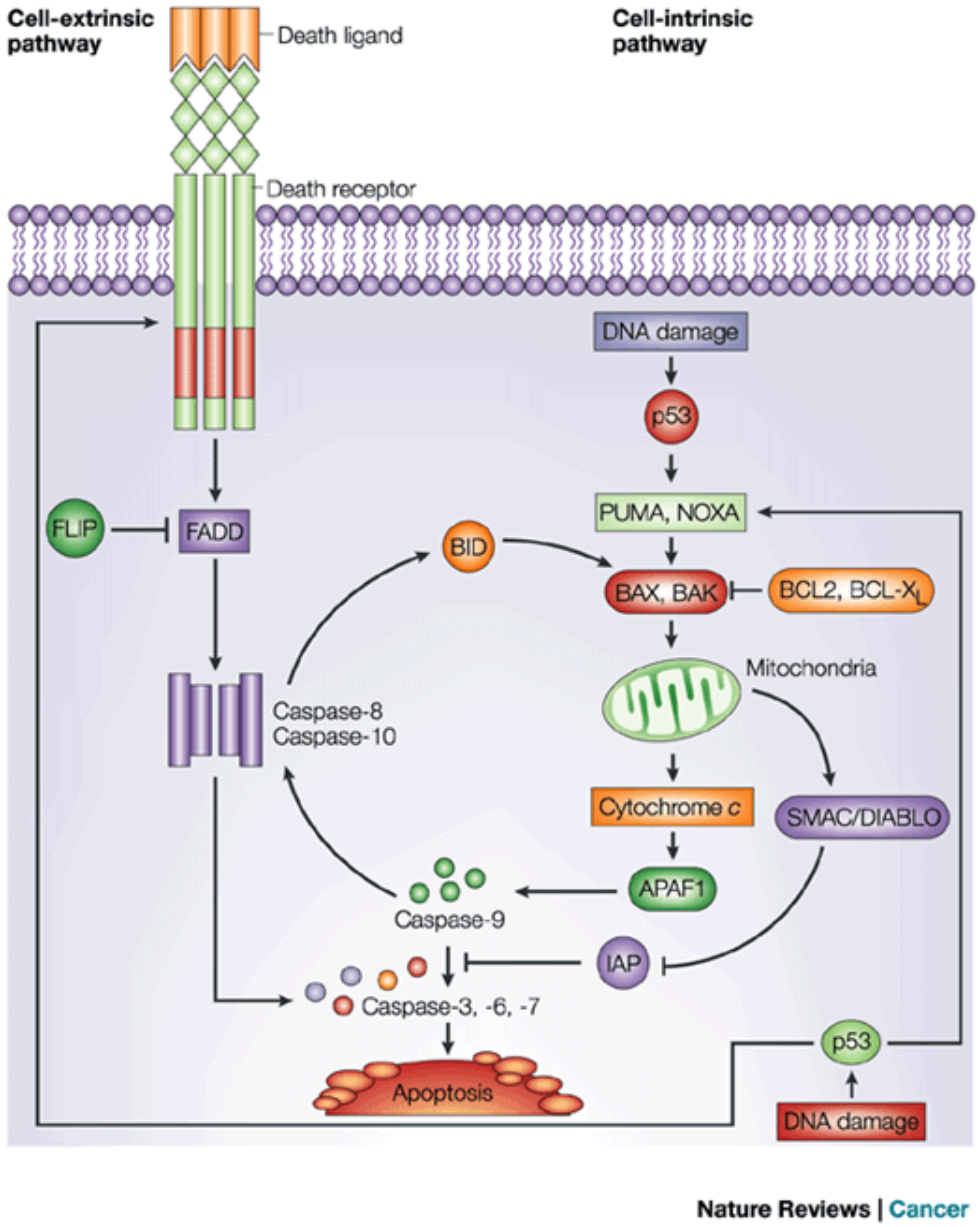

Fig. 6. Extrinsic and intrinsic apoptotic pathway. Apoptosis can be triggered by two different pathways, either through death receptor (extrinsic pathway) or mitochondria signaling (intrinsic pathway). In both cases induction of apoptosis results in the activation of initiator caspases, caspase-8 or -10 for the extrinsic and caspase-9 which is activated through interaction with APAF-1 and cytochrome c for the intrinsic pathway. The

initiator caspases then activate effector caspases which finally lead to apoptosis. In addition there is a crosstalk between these two pathways by caspase-8 mediated cleavage of Bid (source: (Ashkenazi A., 2002).

1.2.1.1 The pro-apoptotic BH3-only protein Bik

Bik is a member of the proapoptotic Bcl-2 family protein consisting of 160 amino acids (aa). The BH3 domain is one of the characteristic of Bik classifying it into the group of BH3 only proteins. The BH3 domain enables Bik to interact with antiapoptotic cellular proteins such as Bcl-2 proteins as well as viral proteins such as adenovirus E1B-19K and EBV-BHRF1 (Boyd *et al.*, 1995;Han *et al.*, 1996). The interaction of BH3 domain with antiapoptotic multidomains is crucial for cell death activity of Bik. In addition to BH3, Bik contains a transmembrane domain (TM) and two phosphorylation sites **(Fig. 7)**. Western blot analysis revealed Bik generally migrates as doublet of 24-25 kDa, with the slower moving band being the phosphorylated one. Mutations that prevent phosphorylation decrease interaction with antiapoptotic proteins and cell death (Verma *et al.*, 2001). Bik predominately localizes to the ER (Germain *et al.*, 2002), mitochondrial localization of Bik, however, has also been found (Han *et al.*, 1996;Hegde *et al.*, 1998). Bik is downregulated by proteasomal degradation and only moderate steady state level of Bik are detected in most cultured cells (Marshansky *et al.*, 2001;Nikrad M, 2005;Zhu *et al.*, 2005). The expression level of Bik is restricted in human tissues (Daniel *et al.*, 1999). Bik expression was predominately found in kidney and pancreas. Whereas in colon and lymphoid tissues no Bik expression was found in certain cell lines derived from these tumor tissues, higher level of Bik mRNA was detectable. Bik induces apoptosis through the release of ER Ca^{2+} resulting in activation of the intrinsic apoptotic pathway (Germain *et al.*, 2002;Mathai JP, 2005;Germain *et al.*, 2005). The Bik mediated ER Ca^{2+} release is dependent on the localization of conformational activated Bak/Bax and deficient in Bak/Bax knock out cells. Furthermore Ca^{2+} release from the ER induced by Bik resulted in the recruitment of the mitochondrial fission protein DRP1 (Dynamin-related protein 1) from the cytosol to the mitochondria and remodeling of the inner mitochondrial membrane cristae (Mathai JP, 2005;Germain *et al.*, 2005). Bik is also able to induce non-apoptotic cell death with autophagic features such as punctuated LC-3 distribution in the absence of activated caspase-9 and -3 in $Bcl^{-/-}$ cells (Rashmi *et al.*, 2008).

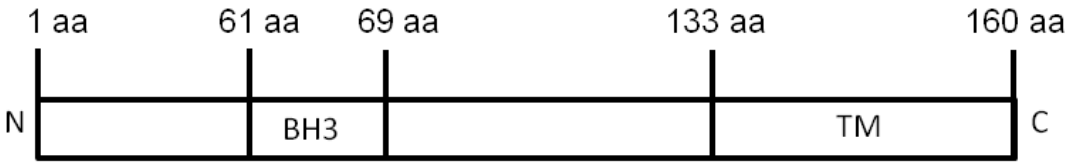

Fig. 7. Schematic illustration of the Bik protein. As a member of the BH3-only protein group Bik harbours a BH3 domain and a further functional segment, the transmembrane domain (TM).

1.2.2 INDUCTION OF APOPTOSIS BY SARS-COV N PROTEIN

The primary function of the SARS-CoV nucleocapsid protein (N) is to bind and encapsulate the viral RNA genome forming a helical nucleocapsid (Masters, 2006). Therefore N is capable of association with the genome and with itself in order to package the genome inside a closed cavity. The interaction of N with the carboxy terminal region of M is essential to form virus like particles (VPL) (Fang *et al.*, 2005).

N is encoded by the ninth ORF of SARS-CoV and is a 46 kDa protein composed of 422 amino acids (Rota *et al.*, 2003). A RNA binding domain consisting of positively charged amino acids has been identified at the amino terminal region of N. The C–terminal region of N is predicted to be capable of self association. The sequence between the RNA-binding site and the self-association domain constitutes the M interaction site. Above the entire protein there are three putative nuclear localization signals distributed (Rowland *et al.*, 2005). The N-terminal region of N contains a pat-7 motif (amino acids 38–44), the middle harbours pat-4 and pat-7 sequences (amino acids 257–265) and, finally, the C-terminal domain exhibits two bipartite motifs, two pat-7 motifs, and one pat-4 motif (amino acids 369–390) **(Fig. 8)**. Unlike the N proteins of many other coronaviruses, SARS-CoV N is more frequently distributed in the cytoplasm, when transiently expressed or in infected cells (You *et al.*, 2005;Rowland *et al.*, 2005;Surjit *et al.*, 2005). Of note, gene regulatory function of N has also been documented in the context of NF-kB, AP-1 and CCAAT/enhancer binding protein (C/EBP)-dependent transcription (He *et al.*, 2003;Yan *et al.*, 2006;Zhang *et al.*, 2007b), interferon (IFN) production (Kopecky-Bromberg *et al.*, 2007) and TGF-β signalling (Zhao *et al.*, 2008).

In a further study it was observed that N is phosphorylated by the cyclin-CDK complex which is known to be active only in the nucleus (Surjit *et al.*, 2005). Furthermore, N associates with the adaptor protein 14-3-3 (tyrosine 3-monooxygenase / tryptophan 5-monooxygenase activation protein) which mediates interaction between components of cellular signaling and cell cycle regulatory pathways. Of note inhibition of 14-3-3 and serum starvation enhances nuclear localization of N (Surjit *et al.*, 2005).

The mechanism how N can enter the nucleus is yet unknown, although the three predicted nuclear localization signals appear to be functional. All of them enable localization to the nucleus or to its components when they were fused to EGFP proteins (You *et al.*, 2005) and experiments with N deletion mutants fused to EGFP confirmed this observation (Timani *et al.*, 2005). Furthermore a potential CRM-1 dependent nuclear export signal was suggested (You *et al.*, 2005). In summary, these observations indicate that N has in principle the physical competence to localize to the nucleus.

Besides its primary function N interferes with various host cell processes such as cell cycle, cytokinesis, translation machinery and Interferon production (Surjit and Lal, 2008). Interestingly, as mentioned above, N also modulates apoptosis. Several studies demonstrated that N leads to apoptotic cell death in the absence of growth factors in COS-1 cells (Surjit *et al.*, 2004;Zhang *et al.*, 2007), HPF (Zhao *et al.*, 2006), or in Vero E6 and A549 (human lung carcinoma) cells. In COS-1 cells, induction of apoptosis was independent of Bax and p53. However, Bcl-2 expression as well as Akt phosphorylation was reduced, whereas the MAPK pathway and caspases were activated. It was speculated that apoptosis was initiated via an integrin dependent pathway (Surjit *et al.*, 2004). In addition, mitochondrial cytochrome C release was observed (Zhang *et al.*, 2007). However, not in all cell lines expressing N apoptosis was induced. In the human hepatoma cell lines Hep-G2 (Zhang *et al.*, 2007) and Huh-7 (Surjit *et al.*, 2004;Zhang *et al.*, 2007) no apoptosis was detectable upon N expression.

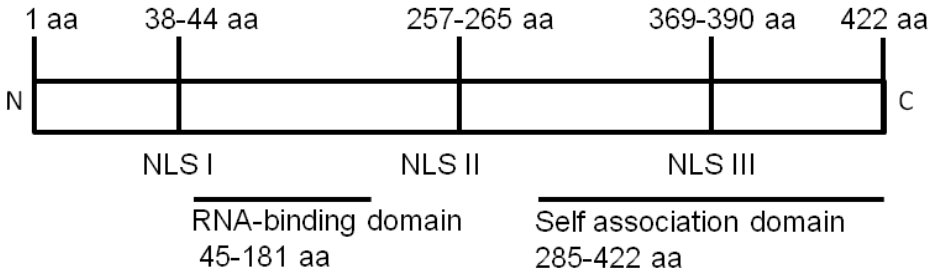

Fig. 8. Schematic representation of SARS-CoV N. The three putative nuclear localization signals are indicated as NLS I-III and are distributed throughout the entire protein. The sequence between the RNA-binding and the self association domain exhibits the interaction site of M.

1.2.3 INDUCTION OF APOPTOSIS BY SARS-COV 7A PROTEIN

7a is encoded by ORF 7 and consists of 122 amino acids (also known as ORF 8, U122 X4) (Marra *et al.*, 2003;Rota *et al.*, 2003;Haijema *et al.*, 2004). It shows no significant sequence

homology with any other known protein. In convalescent sera antibodies against 7a have been detected (Qiu *et al.*, 2005) and the protein has also been found in lung tissue of SARS-CoV infected patients (Chen *et al.*, 2005). In several transfected as well as infected cell lines expression of 7a has been confirmed (Fielding *et al.*, 2004;Tan *et al.*, 2004;Nelson *et al.*, 2005;Kanzawa *et al.*, 2006;Kopecky-Bromberg *et al.*, 2006;Yuan *et al.*, 2006). Crystal structure analysis revealed that the luminal domain of 7a forms a compact structure similar in topology and fold to members of the IgG immunoglobulin superfamily. The 15-17,5 kDa protein is a type I transmembrane protein with a C-terminal transmembrane region **(Fig. 9)**. The amino terminal region includes a signal peptide and the C-terminus contains an ER-retrieval motif. These signal sequences are important for the transport to the ER, enabling 7a to localise to the ER and a recycling between ER and Golgi, respectively and it is posttranslationally processed in a mature form (~15 kDa) (Fielding *et al.*, 2004). Thus, 7a can be found in ER-Golgi intermediate compartment and in the trans Golgi network (Nelson *et al.*, 2005;Tan *et al.*, 2007). 7a is incorporated into viral particles directing it to a structural component of the virion (Huang *et al.*, 2006a). It interacts with 3a, M, E and S proteins but these interactions appear to be non-essential for 7a incorporation into virus-like particles (VLPs) (Huang *et al.*, 2006a). Recombinant SARS-CoV with deleted ORF 7a was viable in infected cell lines and in mice, indicating that 7a is dispensable for virus growth and replication (Yount *et al.*, 2005). Several studies demonstrated that 7a expression in cell culture has diverse biological functions. 7a is capable of blocking cell cycle progression at G0/G1 via the cyclin D3/pRb pathway in HEK293, Cos-7 and Vero E6 cell lines (Yuan *et al.*, 2006). Growth inhibition in 7a-expressing HEK293 cells and blocking of gene expression at the level of translation has been observed. Besides the interaction with the viral proteins, interaction with several host cell proteins has also been found, such as lymphocyte function-associated antigen 1 (LFA-1) (Hanel and Willbold, 2007) human small glutamine-rich tetratricopeptide repeat-containing protein, (hSGT) (Fielding *et al.*, 2006), Ap4 A-hydrolase (Vasilenko *et al.*, 2010) or Bcl_{xl} (Tan *et al.*, 2007). These data indicates that 7a is involved in several pathogenic processes such as inhibition of cellular protein translation, activation of p38 mitogenic pathway and apoptosis

The induction of apoptosis by 7a has been observed in several studies (Tan *et al.*, 2004;Kopecky-Bromberg *et al.*, 2006;Yuan *et al.*, 2006;Tan *et al.*, 2007). Its proapoptotic properties have been verified in many cell lines. The expression of 7a induces the apoptotic pathway in cell lines originating from different tissues like lung (A549 cell line), kidney (Cos-7, Vero E6, HEK293), cervix (HeLa) and liver (Hep-G2) (Tan *et al.*, 2004). The link between apoptosis and 7a has also been investigated in the viral context. Infection of cultured cells with a recombinant virus lacking ORF7a elicited a less efficient DNA fragmentation indicative

for apoptosis compared to infection with wild-type virus (Schaecher *et al.*, 2007).

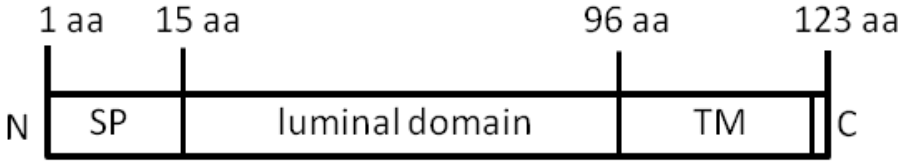

Fig. 9. Schematic diagram of SARS-CoV 7a. Sequence analysis revealed that 7a consists of a N-terminal signalpetide (SP), a luminal domain, a transmembrane segment and a C-terminal ER-retrieval signal.

1.3 OBJECTIVE OF THIS THESIS

All of the structural proteins and nearly all of the accessory proteins induce apoptosis when they were expressed in cell culture (Diemer C *et al.*, 2010). To investigate the role of apoptosis in SARS-CoV pathogenesis in more detail, one structural protein, the nucleocapsid protein and one of the pro-apoptotic accessory proteins, namely the 7a protein, were chosen. For this purpose cell lines were used which may represent models for lytic and persistent infection, respectively. Vero E6 predominately served as model for lytic infection, and for a more persistent infection Caco-2 cells were utilized. They were investigated during SARS-CoV infection and transient overexpression of N and 7a in the context of apoptosis induction. In case of N the goal was to characterize the apoptotic pathway induced by N and the subcellular localization in the different cell models.

Besides the examination of the apoptotic properties of 7a, a further aim was to characterize 7a by identifying interacting proteins. 7a shows no significant sequence homology to any other known protein and to learn more about functional features of 7a a Yeast-Two-Hybrid screen was performed. Therefore, a cDNA-library of Caco-2 cells was generated to find putative protein interactors of 7a in a cell line representing a model for persistent infection. Moreover, putative protein-protein interactions of 7a should be confirmed in relevant mammalian cell culture models for SARS-CoV infection by co-immunoprecipitation (Co-IP) and the interaction site should be identified. Finally, it was desirable to find a link between the pro-apoptotic potential of 7a and the putative interacting protein.

2 MATERIAL AND METHODS

2.1 MATERIAL

2.1.1 CHEMICALS

Adeninhemisulfat	Sigma-Aldrich Chemie GmbH, Steinh., G
Agarose	Invitrogen, Karlsruhe, G
Ammonium peroxodisulfate	Roth, Karlsruhe, G
Bacillol plus	Roth, Karlsruhe, G
Bacto Agar Becton Dickinson	Becton Dickinson, Heidelberg, G
5-Bromo-4-Chloro-3-indolyl α-D-galactopyranoside (α-X-Gal)	Glycosynth, Warrington UK
Bromphenole blue	Sigma Darmstadt, G
Calcium chloride ($CaCl_2$)	Roth, Karlsruhe, G
Caspase-3 Inhibitor II	Calbiochem, San Diego, CA, USA
Caspase-3/7 Inhibitor I	Calbiochem, San Diego, CA, USA
Caspase-8 Inhibitor II	Calbiochem, San Diego, CA, USA
Caspase-9 Inhibitor I	Calbiochem, San Diego, CA, USA
Chloroform	Roth, Karlsruhe, G
Complete Protease inhibitor cocktail	Roche, Mannheim, G
Coomassie Brillant Blue G250	Roth, Karlsruhe, G
Crystal violet	Sigma-Aldrich Chemie GmbH, Steinh., G
β-Mercaptoethanol	Sigma-Aldrich Chemie GmbH, Steinh., G
Dimethylsulfoxide (DMSO)	Sigma-Aldrich Chemie GmbH, Steinh., G
Di-thiothreitol	Sigma-Aldrich Chemie GmbH, Steinh., G
Ethanol p. a. 99 %	Roth, Karlsruhe, G
Ethidium bromide solution (10 mg/ml)	Invitrogen, Karlsruhe, G
Ethylen diamine tetraacetate, sodium salt (EDTA)	Roth, Karlsruhe, G

Formaldehyde	Roth, Karlsruhe, G
Gelantine 40% solution	Sigma-Aldrich Chemie GmbH, Steinh., G
Glucose	Sigma-Aldrich Chemie GmbH, Steinh., G
Glycerol	Roth, Karlsruhe, G
Glycine	Roth, Karlsruhe, G
HCl 37 % (w/w)	Roth, Karlsruhe, G
Hoechst 33342	Sigma-Aldrich Chemie GmbH, Steinh., G
Hybond-P PVDF membrane	GE Healthcare, Freiburg, G
Isopropanol p. a.	Roth, Karlsruhe, G
Isopropyl-β-D-thiogalactopyranosid (IPTG)	Roth, Karlsruhe, G
Kohrsolin	Bode Chemie GmbH, Hamburg, G
Lactacystin	Calbiochem, San Diego, CA, USA
L–Leucine	Sigma-Aldrich Chemie GmbH, Steinh., G
L–Histidine	Sigma-Aldrich Chemie GmbH, Steinh., G
Magnesium chloride	Sigma-Aldrich Chemie GmbH, Steinh., G
Magnesium sulfate	Sigma-Aldrich Chemie GmbH, Steinh., G
Methanol p. a.	Roth, Karlsruhe, G
Methyl-cellulose	Sigma-Aldrich Chemie GmbH, Steinh., G
N,N,N',N'-Tetramethylenediamine (TEMED)	Sigma-Aldrich Chemie GmbH, Steinh., G
Nonidet P40	Sigma-Aldrich Chemie GmbH, Steinh., G
Pefabloc SC	Roche, Mannheim, G
Phenol	Roth GmbH & Co, Karlsruhe, G
Phosphate buffered saline (PBS)	Invitrogen, Karlsruhe, G
Potassium chloride	Sigma-Aldrich Chemie GmbH, Steinh., G
Pro Bond Resin	Invitorgen, Karlsruhe, G
Protein A Sepharose	GE Healthcare, Freiburg, G
Protogel Ultra Pure 30 %,Acrylamide	National Diagnostics, Atlanta, USA
Re-blot Plus Strong Solution	Chemicon Int., Carrigtwohill, IE

Roti-Histofix	Roth GmbH & Co, Karlsruhe, G
SD Minimal Base	Becton Dickinson, Heidelberg, G
Secusept plus	Ecolab, Düsseldorf, G
Skim milk powder	Merck, Darmstadt, G
Sodium chloride	Roth GmbH & Co, Karlsruhe, G
Sodium deoxycholate (DOC)	Roth GmbH & Co, Karlsruhe, G
Sodium dodecylsulfate (SDS)	Roth GmbH & Co, Karlsruhe, G
Sodium hydroxide (NaOH)	Roth GmbH & Co, Karlsruhe, G
Synthetic dropout (SD) supplements	Becton Dickinson, Heidelberg, G
Tris-hydroxy-methyl-aminomethan (Tris)	Roth GmbH & Co, Karlsruhe, G
Triton-X 100	Sigma-Aldrich Chemie GmbH, Steinh. ,G
Trizol	Gibco/Invitrogen, New York, USA
Tryptone	Becton Dickinson, Heidelberg, G
Tween 20	Roth GmbH & Co, Karlsruhe, G
X-ray films Kodak Biomax MS	Sigma-Aldrich Chemie GmbH, Steinh., G
Yeast extract	Becton Dickinson, Heidelberg, G
Z-VAD-FMK, pan-caspase Inhibitor	Sigma-Aldrich Chemie GmbH, Steinh., G
Z-VEID-FMK, caspase-6 Inhibitor	Sigma-Aldrich Chemie GmbH, Steinh., G

2.1.2 KITS

Active recombinant caspase-6	Pharmigen, Heidelberg, G
Bradford Assay	Thermo Fisher Scientific, Rockford, USA
DNA ladder (100 bp and 1 kB)	New England Biolabs, Frankfurt, G
ECL plus Western blotting detection system	GE Healthcare, Freiburg, G
Fugene 6 Transfection Kit	Roche, Mannheim, G
GFX Micro Plasmid Prep Kit	GE Healthcare, Freiburg, G
GFX PCR DNA and Gel Band Purification Kit	GE Healthcare, Freiburg, G
Grow'N'Glow Yeast Plasmid Isolation Kit	MoBiTec GmbH, Göttingen, G

High range protein molecular weight marker	GE Healthcare, Freiburg, G
Lipofectamine 2000	Invitrogen, Karlsruhe, G
Matchmaker Construction & Screening Kit	Becton Dickinson, Clontech Heidelberg, G
Plasmid Maxi Kit	Qiagen, Hilden, G

2.1.3 ENZYMES

Calf intestine alkaline phosphatase (CIP)	Roche, Mannheim, G
DNA-Polymerase Pfu	Metabion, München, G
Restriction enzymes (listed in Tab.)	Metabion, München, G
RNAse free DNAse set	Qiagen, Hilden, G
Trypsin- EDTA	Gibco/Invitrogen, New York, USA
T 4 ligase	Roche, Mannheim, G

2.1.4 ANTIBIOTICS

Ampicillin (Amp)	Sigma-Aldrich Chemie GmbH, Steinh., G
Kanamycin (Kan)	Sigma-Aldrich Chemie GmbH, Steinh., G
Penicillin/Streptomycin	Invitrogen, Karlsruhe, G

2.1.5 ANTIBODIES

Table 1. Antibodies used in this thesis

Primary antibody	Source and Reference	Specifity	Application	Dilution
Anti-active caspase 3	Rabbit polyclonal (Abcam, Cambridge, UK)	Residues 150-250 of human active caspase 3	WB	1:200
Anti-Cleaved Lamin A	Rabbit polyclonal (Cell Signaling Technology, Danvers, MA, USA)	Cleaved Lamin A	WB	1:1000

Anti-Bad	Mouse monoclonal (Santa Cruz Biotechnology, Santa Cruz, CA, USA)	Phosphorylated and Dephosphorylated Bad	WB	1:500
Anti-NBK	Rabbit polyclonal (Santa Cruz Biotechnology, Santa Cruz, CA, USA)	Phosphorylated and Dephosphorylated Bik	WB, IP IF	1:200, 1:10 1:10
Anti-Histone H3	Rabbit polyclonal (Calbiochem, San Diego, CA, USA)	Histone H3	WB	0,2 µg/ml
Anti-Hemagglutinin (HA)	Mouse monoclonal (Santa Cruz Biotechnology, Santa Cruz, CA, USA)	Epitope of hemagglutinin (YPYDYPDYA)	WB IP IF	1:1000 1:10 1:10
Anti-Grb2 (C-32)	Rabbit polyclonal (Santa Cruz Biotechnology, Santa Cruz, CA, USA)	Grb2	WB	1:5000
N-pAb	Rabbit polyclonal (Diemer et., al 2008)	SARS-CoV N	WB IF	1:10000 1:100
Anti-7a mAb	Mouse monoclonal (Tan et al., 2004)	SARS-CoV 7a	WB IP	1:5000 1:500
Anti-β-actin	Mouse monoclonal (Sigma-Aldrich Chemie GmbH, Steinheim, G)	Actin	WB	1:10000
Secondary Antibody	Source and Reference	Specifity	Application	Dilution
HRP-conj. anti-IgG	Sheep (GE Healthcare, Freiburg, G)	Mouse IgG	WB	1:7500
HRP-conj. anti-IgG	Donkey (GE Healthcare, Freiburg, G)	Rabbit IgG	WB	1:7500

Cy2-conj. Anti-IgG	Donkey (Dianova, Freiburg, G)	Mouse IgG	IF	1:100
Cy2-conj. Anti-IgG	Donkey (Dianova, Freiburg, G)	Rabbit IgG	IF	1:100
Cy3-conj. Anti-IgG	Donkey (Dianova, Freiburg, G)	Mouse IgG	IF	1:400
Cy3-conj. Anti-IgG	Donkey (Dianova, Freiburg, G)	Rabbit IgG	IF	1:400

2.1.6 BACTERIA AND YEAST STRAINS

For plasmid generation and propagation *E. coli* XL-1 Blue (*Sup*E44, *hsd*R17, *end*A1, *ec*A1, *gyr*A46, thi-1, *rel*A1, lac-, F' (proABlaclq, lacZΔM15, Tn10 (terR); Stratagene) was used. *E. coli* BL21 (Stratagene) was utilized for the expression of recombinant proteins. Y2H screening and mapping experiments were performed in *S. cerevisiae* AH109 (*MATa, trp1-901, leu2-3, 112, ura3-52, his3-200, gal4Δ, gal80Δ, LYS2:GAL1UASGAL1TATA-HIS3, GAL2UAS-GAL2TATA-ADE2, URA3:MEL1UAS-MEL1TATA -lacZ, MEL1).*

2.1.7 OLIGODEOXYNUCLEOTIDES

All oligodeoxynucleotides were purchased from Metabion (Martinsried, G). Oligodeoxynucleotides were synthesized desalted and purified by HPLC (high performance liquid chromatography). Lyophilized primers were dissolved in A. dest to a final concentration of 10 µM.

2.1.8 PLASMIDS AND CONSTRUCTS

According to their application different plasmids were used to generate various constructs. For recombinant protein expression in mammalian cells pcDNA3.1/Zeo (Invitrogen, Karlsruhe) was utilized. pEGFP-C1 (Clontech, Mountain View, CA, USA) was used to evaluate transfection effenciency. The gene transfer and expression of recombinant protein in yeast were performed by shuttle vectors pGAD-T7 and pGBK-T7 (Clontech, Mountain View, CA, USA). For the expression and purification of recombinant proteins in *E. coli* pQE30 (Qiagen) and pDest (Invitrogen) were used. The maps of all applied plasmids are shown in (**Fig. 10**) and the constructs generated in this study are listed in **(Table 1)**. Sequence analysis (GATC Biotech, Konstanz, G) was always carried out to confirm the correctness of all subcloned DNA-sequences.

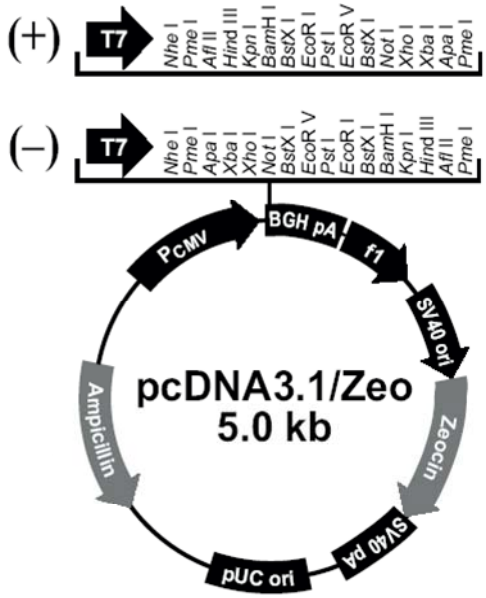

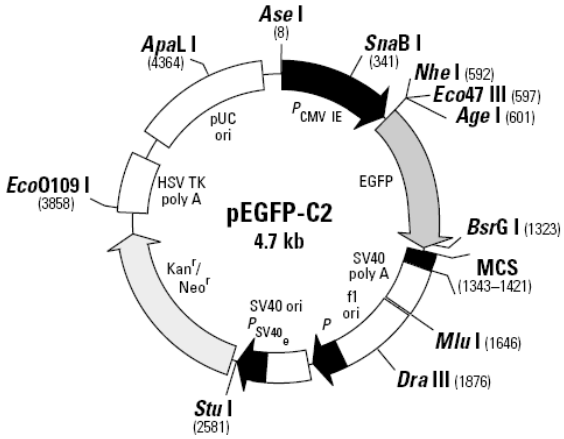

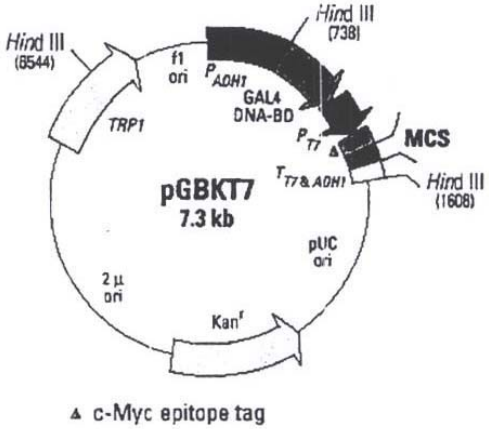

▲ c-Myc epitope tag

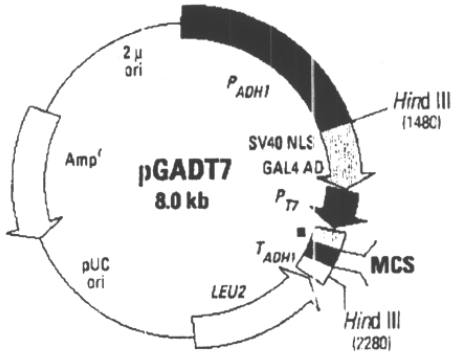

■ HA epitope tag

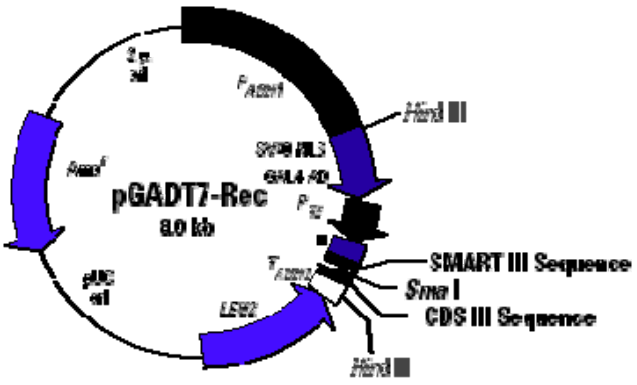

■ HA epitope tag

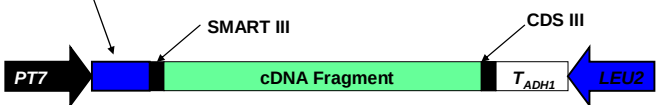

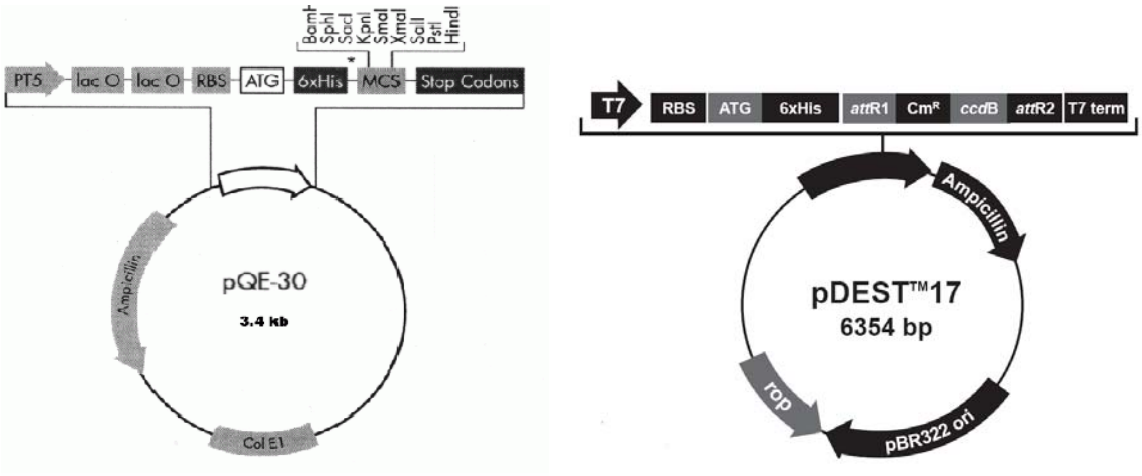

Fig. 10. Plasmid vectors used in this thesis

Table 2. List of constructs

Plasmid + Insert	Description	Restriction enzymes used for cloning
pcDNA N	SARS-CoV nucleocapsid protein (N)	BamHI/XbaI
pcDNA NdeI	SARS-CoV N aa 1-360	BamHI/XbaI
pcDNA NLSII (nuclear localization signal)	Substitution mutant of SARS-CoV N; lysines at pos. 257, 258, 262 were substituted to Glycines	BamHI/XbaI
pcDNA NLSII-Grb2	NLSII is fused to Grb2	BamHI/XhoI
pcDNA 7a	SARS-CoV Orf 7a	EcoRI/XbaI
pcDNA 7a-HA	HA-tag fused to N-terminus of SARS-CoV Orf 7a	EcoRI/XbaI
pcDNA 7aCb5 (cytochrome b5)	Transmembrane substitution (TM) of SARS-CoV Orf 7a with TM of cytochrome b5	EcoRI/XbaI
pcDNA 7aΔTM	TM of SARS-CoV 7a is deleted, construct encodes aa 1-96 of 7a	EcoRI/XbaI

pcDNA Bik	BH3-only protein Bik	BamHI/XbaI
pcDNA BikCb5	Transmembrane substitution (TM) of Bik with TM of cytochrome b5	BamHI/XbaI
pDest N	SARS-CoV N	Homologous recombination
pQE 30 D400/403E	Substitution of aa D to E at position 400 and 403 of SARS-CoV N	BamHI/XhoI
pGBKT7-7a	SARS-CoV Orf 7a	EcoRI/PstI
pGBKT7-Bik	BH3-only protein Bik	EcoRI/PstI
pGADT7-7a-16-46	SARCoV-Orf7a aa 16-46	EcoRI/XhoI
pGADT7-7a-46-76	SARCoV-Orf7a aa 46-76	EcoRI/XhoI
pGADT7-7a-76-106	SARCoV-Orf7a aa 76-106	EcoRI/XhoI
pGADT7-7a-93-123	SARCoV-Orf7a aa 93-123	EcoRI/XhoI
pGADT7-Bik-1-33	Bik aa 1-33	EcoRI/XhoI
pGADT7-Bik-23-55	Bik aa 23-55	EcoRI/XhoI
pGADT7-Bik-40-70	Bik aa 40-70	EcoRI/XhoI
pGADT7-Bik-73-103	Bik aa 73-103	EcoRI/XhoI
pGADT7-Bik-104-133	Bik aa 104-133	EcoRI/XhoI
pGADT7-Bik-134-160	Bik aa 134-160	EcoRI/XhoI
pGADTrec-Caco-2-library	DNA-library of Caco-2 cell line	Homologous recombination

2.1.9 EUCARYOTIC CELL LINES AND VIRUS

Table 3. Used Mammalian cell lines in this thesis

Cell line	Description	Reference
A549	Human lung adencarcinoma epithelial cell line	ATCC-CCL-185
Caco-2	Human epithelial colorectal adenocarcinoma cell line	ATCC-HTB-37
Cos-1	African green monkey kidney epithelial cell line, immortalized by SV-40	ATCC-CRL-1650
N2a	Murine neuroblastoma cell line	ATCC-CCL-131
Vero E6	African green monkey kidney epithelial cell line	ATCC-CRL-1586
SARS-CoV	SARS-CoV isolate Frankfurt-1	Genbank AY291315

2.1.10 CELL CULTURE MEDIA AND ADDITIVES

OptiMEM with Glutamax	Invitrogen, Karlsruhe, G
Dulbeccos MEM (D-MEM) with Glutamax	Invitrogen, Karlsruhe, G
Earles´s MEM with Glutamax	Invitrogen, Karlsruhe, G
Fetal bovine serum (FCS)	Invitrogen, Karlsruhe, G

2.1.11 INSTRUMENTS AND ACCESSORIES

Autoclave V95	Systec, Wettenberg, G
Axiovert 40C microscope	Carl Zeiss Jena GmbH, Göttingen, G
Fuchs-Rosenthal Hemocytometer	Roth GmbH & Co, Karlsruhe, G
CO_2 Incubator	Heraeus GmbH, Hanau, G
Centrifuges:	
Eppendorf 5417C	Eppendorf-Nethaler-Hinz, Köln, G
Sigma 4K15	Sigma-Aldrich, Schnelldorf, G

Beckmann Avanti	Beckmann Coulter GmbH, Krefeld, G
Coverslips and slides	Marienfeld, Bad Mergentheim, G
Cryotubes	Corning Inc., USA
Electrophoresis Power Supply	Pharmacia Biotech, SE
Electrophoresis Power Supply	Consort, Turnhout, BE
Eppendorf tubes (1,5 or 2 ml)	Eppendorf-Nethaler-Hinz, Köln,G
Falcon tubes (15 or 50 ml)	Falcon, Le Pont de Claix, F
Hybond-P PVDF membrane	GE Healthcare, Freiburg
LSM510 confocal laser microscope	Carl Zeiss Jena GmbH, Göttingen, G
Midi protein gel chamber	Peqlab Biotechnologie, Erlangen, G
Minitron Incubation shaker	Infors AG, Bottmingen, CH
Lone Worker tracking and protection system	Multitone Elektronik, Düsseldorf, G
Optimax X-Ray film processor	PROTEC, Oberestenfeld, G
Pipets (0,5-10 µl; 10-100 µl; 100-1000 µl)	Eppendorf-Nethaler-Hinz, Köln, G
Pipetus	Hirschmann Laborg., Eberstadt, G
Power Supplies	GE Healthcare, Freiburg, G
Respirator X plore	Drägerwerk, Lübeck, G
Safety-glasses	Roth GmbH & Co, Karlsruhe, G
Single-use overalls	Roth GmbH & Co, Karlsruhe, G
Single-use gloves	Roth GmbH & Co, Karlsruhe, G
Sonifer	MSE Scientific Instruments, Crawely, Sussex, U.K.
Spectrophotometer	GE Healthcare, Freiburg, G
Sunrise ELISA Reader	Tecan, Maennedorf, CH
Thermomixer 5436	Eppendorf-Netheler-Hinz, Köln, G
Thermocycler GeneAmp PCR System 970	Applied Biosystems, Foster City, CA, USA
Tissue culture dishes and plates	Falcon, Le Pont de Claix, FR

Trans Blot SD Semi-dry Transfer Cell	Biorad Laboratories, München, G
Transfer unit Semi dry (TE77)	GE Healthcare, Freiburg, G
Whatmanpaper	Schleicher & Schüll, Dassel, G
Waste water sterilizer varioklav 80	Thermo Scientific Inc., Waltham, MA, USA
Waterbath	GFL, Burgwede, G

2.2 METHODS

2.2.1 BIOLOGIGAL SAFETY

Based on its relative risk SARS-CoV is categorized in Risk group 3 according to the Biostoffverordnung (BioStoffV). All experiments done with SARS-CoV were performed in a Biosafety level 3 (BSL3) laboratory including all requirements applying to BSL-3 such as low pressure, cabinet class III, change area, double door. Personal equipment such as protective laboratory clothing, protective double gloves, safety glasses and respirator were worn at all times in the BSL3 laboratory. Genetic engineering of organisms was accomplished according to the Gentechnikgesetz (GenTG) under Biosafety level 2.

2.2.2 MOLECULAR BIOLOGICAL METHODS

2.2.2.1 Polymerase chain reaction (PCR) for amplification of DNA fragments

PCR is a highly efficient enzymatic procedure for exponential in vitro amplification of defined DNA fragments through a cyclic repetition. One cycle consists of following steps:

Denaturation: heat denaturation of target DNA (template)

Annealing: hybridization of oligonucleotides (primers) to complement DNA sequences

Elongation: Elongation of primers by a thermo-tolerant DNA-polymerase

The elongation time depends on the PCR product length and on the used DNA-polymerase. To avoid unspecific primer hybridization the annealing temperature is calculated on the basis of the dissociation temperature of the primers used in this reaction (Suggs *et al.*, 1981)

T_D [°C] = 2·(A+T) + 4·(C+G)

(A, T, C, G: number of the respective nucleotides)

PCR reaction mix:		Thermal cycling:	
10 x Pfu buffer	5 µl		
dNTP (5mM)	2 µl	95°C – 5 min	
Primer 5` (10µM)	2 µl	95°C – 5 min	40 cycles
Primer 3` (10µM)	2 µl	x°C – 1 min	
Template (200ng)	1 µl	72°C – y min	
Pfu (5 U)	0,5 µl	72°C – 7 min	
A. dest	Up to 50 µl		

X°C: calculated annealing temperature (see above)

Y min: approximately 1 min per 1,5 kbp (see above)

PCR-Products were separated by agarose gel elektrophoresis and processed further for their application.

2.2.2.2 Site-directed mutagenesis

This method was used to exchange nucleotide(s) within an existing plasmid construct in order to create amino acid exchanges. Therefore, complementary primers to the sequence of the existing construct were designed except the nucleotide(s) of exchange which is substituted to the one of desire. The primer sequences were chosen to flank the position of exchange with 15 specific nucleotides both at the 5`and 3`end, resulting in complementary primers of about 30 nucleotides in length. Mutagenesis was performed during PCR using plasmid DNA which contains the insert for desired substitution as a template. The double stranded plasmid is dehybridised during denaturation and the primers bind to their complementary sequences. For elongation 2 min/1000 bp are calculated and in this time the entire plasmid sequence is complementary synthesized. After 18 cycles the sample is incubated with the restriction enzyme DpnI (10 U) to selectively digest methylated DNA. Synthesized DNA during PCR is, in contrast to plasmid DNA propagated in *E. coli,* not methylated, thus only template DNA is degraded. Then an aliquot (10 µl) of the digested sample is transformed into *E. coli* XL1 and cultivated on LB agar plates containing the adequate antibiotic. From single clones plasmid DNA was purified and the insert was sequenced (GATC Biotech, Konstanz) to confirm successful substitution.

PCR reaction mix:		Thermal cycling	
10 x Pfu buffer	5 µl		
dNTP (5mM)	2 µl	94°C – 5 min	
Primer 5`(10 µM)	2 µl	94°C – 5 min	18 cycles
Primer 3` (10 µM)	2 µl	55°C – 1 min	
Template (200 ng)	1 µl	68°C –14 min	
Pfu 5 U	0,5 µl	72°C – 5 min	
A. dest	Up to 50 µl		

2.2.2.3 Agarose gel electrophoresis

Depending on the size of DNA fragments to be separated 1 – 2 % agarose were dissolved in 1 x TAE buffer by boiling. After cooling to about 55 °C 1,5 µl of ethidium bromide (EtBr) were added and the solution was filled into a gel chamber arranged with a comb. The polymerized agarose gel was then placed into an electrophoresis chamber and overlaid with 1 x TAE buffer. The PCR samples were mixed with an appropriate volume of 5 x loading buffer and applied to the gel. Electrophoretic separation of DNA occurred for 30 min at a constant voltage of 110 V. DNA fragments could be visualized on an UV transilluminator system due to staining with EtBr which intercalates between the DNA strands. Sizes of PCR products were estimated by comparison with 1 kb DNA ladder.

TAE buffer	Tris/Acetat	40 mM
	EDTA	1 mM
5 x loading buffer	Glycerole	50 %
	in TAE buffer	
	Bromphenole blue	0,05 %

2.2.2.4 Elution of DNA fragments from agarose gel

Exact PCR products were excised from the gel and purified using the GFX PCR DNA and Gel Band Purification Kit according to manufacturer´s protocol. Purified DNAs were eluted with 30 µl A. dest.

2.2.2.5 Restriction enzyme digestion

Digestion of DNA with restriction enzymes was used to generate DNA fragments from plasmid DNA or PCR products with defined 5`and 3´ends according to the applied restriction enzyme for subsequent specific ligation reactions or to verify a correct ligation reaction. Treatment of DNA with restriction enzymes was performed according to manufacturer´s protocol (Metabion, München). Commonly 5 µg of plasmid DNA or 30 µl purified PCR product were incubated with 10 U of each enzyme and the adequate buffer for about 3 hours at 37°C. Digested DNA fragments were separated by agarose gel electrophoresis and, for subsequent ligation reaction purified as described.

2.2.2.6 Ligation of DNA fragments

A molar ratio of 1:3 – 1:7 of linearised plasmid DNA and insert were mixed with T4 DNA ligase and the appropriate buffer provided by the manufacturer. The ligation mixture was incubated over night in a water bath at 14 °C. T4 DNA ligase catalyzes the formation of ATP-dependent phosphodiester bonds between 3`-hydroxyl and 5´-phosphate ends. This method was used to generate recombinant plasmids. The recombinant plasmids were stored at – 20 °C or transformed into chemically competent *E. coli*.

2.2.2.7 Preparation of chemically competent *E. coli*

One colony of *E. coli* XL1-blue was inoculated into 5 ml LB medium and incubated with constant shaking (180 rpm) over night at 37 °C. One ml of this culture was added to 100 ml LB medium and was further cultivated as before until it had reached an optical density (OD) measured at a wave length (λ) of 600 nm (OD_{600}) of 0,6 – 0,8. Cells were chilled on ice for 10 min prior to sedimentation at 3500 rpm (Sigma 4K15 centrifuge) at 4 °C. Bacteria were resuspended in 50 ml ice-cold sterile 100 mM $MgCl_2$ and incubated for 30 min on ice before the centrifugation step was repeated. Then bacteria were resuspended in ice-cold sterile 100 mM $CaCl_2$ solution, incubated for 30 min on ice and centrifuged as described above. The cell pellet was resuspended in 2 ml ice-cold sterile 100 mM $CaCl_2$ solution and incubated on ice for 24 hours. Finally 2,5 ml sterile ice-cold $CaCl_2$ solution and 0,5 ml glycerole were added, 100 µl aliquots were prepared and the tubes were immediately stored at -70 °C.

LB (Luria-Bertani-) medium:	Bacto Tryptone	10 g/l
	Bacto Yeast extract	5 g/l
	NaCl	10 g/l in A. dest

2.2.2.8 Transformation of *E. coli* with plasmid DNA

One aliquot (100 µl) of chemically competent *E. coli* was thawed on ice and 1 µl of plasmid DNA, 2-6 µl ligation mix or 10 µl yeast extract were added and incubated on ice for 30 min. At 42 °C a heat shock was performed for 45 s and cells were immediately chilled on ice for 2 min. Addition of 400 µl pre-warmed SOC medium was followed by incubation at 37 °C with constant shaking (180 rpm) for 1 h. For selection of transformants an appropriate volume (100 – 400 µl) of the bacteria solution was plated on LB agar plates containing antibiotics (50 µg/ml ampicillin or 50 µg/ml kanamycin) and incubated over night at 37 °C.

SOC medium:
Bacto Tryptone 2 %
Bacto Yeast extract 0,5 %
NaCl 10 mM
KCl 2,5 mM
$MgCl_2$ 10 mM
$MgSO_4$ 10 mM
Glucose 20 mM in A. dest

LB (Luria-Bertani-) agar:
Bacto Tryptone 10 g/l
Bacto Yeast extract 5 g/l
NaCl 10 g/l
Bacto Agar 15 g/l in A. dest

2.2.2.9 Isolation of plasmid DNA

Analytical scale (Mini Prep)

Isolation of recombinant plasmid DNA from transformed bacteria was performed using GFX Micro Plasmid Prep Kit according to the recommendation of the manufacturer. The purified DNA was eluted in 100 µl A.dest.

Preparative scale (Maxi Prep)

Isolation of high-copy plasmid DNA in a preparative scale was achieved by the Qiagen Plasmid Maxi Kit according to the manufacturer´s protocol. Eluted DNA was precipitated in 0,7 volumes of isopropanol and desalted with 70 % ethanol. The DNA pellet was air-dried and dissolved in A. dest 100 – 500 µl depending on the size of the pellet.

2.2.2.10 Construction of Caco-2 cDNA library

Isolation of RNA with trizol

The trizol method relies on phase separation upon centrifugation of an aqueous sample mixed in two solutions. Trizol consists of guanidiniumthiocyanat, a chaotropic agent which lysed cells and inactivates RNAses. A further component of trizol is phenol which enables the solubilization of DNA. After centrifugation an upper aqueous phase which contains RNA, an interphase and a precipitated organic phase which includes DNA and proteins were separated.

Caco-2 cells were seeded on six 10 cm cell culture dishes. When they reached 60 % of confluence, cells were rinsed with PBS und lysed with 2 ml trizol reagent. For the further steps only RNAse free materials and reagents were used which were in part treated with DEPC- solution to destroy RNAses. One ml of the lysates were transferred to 1,5 ml reaction tubes and centrifuged at 14 000 rpm, 4 °C for 15 min (Eppendorf 5417C) to remove cell debris. 1/10 of the final volume sodium acetate and 200 µl chloroform was aliquoted in 2 ml reaction tube prior supernatant was transferred. Samples were vortexed for 15 sec and incubated at room temperature for 5 min. Afterwards samples were centrifuged at 14 000 rpm, 4 °C for 15 min (Eppendorf 5417C) to enhance a two phase separation. The upper phase in which RNA was included was carefully transferred to 1,5 ml reaction tube, mixed with 0,5 ml isopropanol and incubated for 8 min at room temperature. RNA was sedimented by centrifugation at 14 000 rpm, 4 °C for 10 min (Eppendorf 5417C). The pellet was washed twice with 0,5 ml EtOH (75 %) by centrifugation at 14 000 rpm, 4 °C for 10 min. Afterwards the pellet was air-dried, resuspended in 50 µl Tris/HCl (5 mM, pH 7,5) and shaked at 55 °C for 10 min. Eventually, the samples were chilled on ice and sedimented by short spin. After determination of the RNA concentration, samples were precipitated with 1/10 sodium acetate

and 2,5 volumes EtOH (100%) over night at – 80 °C.

First strand synthesis and long-distance PCR (LD-PCR)

Reverse transcription was performed according to the recommendation of the manufacturer (BD Matchmaker Library construction and screening kit). Two µg total RNA isolated from Caco-2 cells were applied for first strand cDNA synthesis using Oligo dT primer (CD III, BD Smart III Oligonucleotide) and MMLV Reverse Transcriptase. Single-stranded cDNA (ss cDNA) was amplified by Long distance PCR (LD-PCR) to produce a double-stranded cDNA (ds cDNA) library. This PCR-system enables amplification of large cDNA (20 kb) through extended elongation with a high fidelity rate. All used reagents were supplied by the manufacturer (BD Matchmaker Library construction and screening kit).

LD-PCR reaction mix:		Thermal cycling:	
First-Strand cDNA	2 µl		
Deionized H_2O	70 µl	95 °C – 30 sec	
10X BD Advantage buffer	10 µl	95 °C – 10 sec	} 23 cycles
50X dNTP Mix	2 µl	68 °C – 8 min	
5' PCR Primer	2 µl	68 °C – 5 min	
3' PCR Primer	2 µl		
10X GC-Melt Solution	10 µl		
50X BD Advantage Polymerase Mix	2 µl		
Total volume	100 µl		

To exclude DNA fragments < 200 bp from the amplified ds cDNA, LD-PCR sample was purified with BD Chroma spin column centrifugation according to the manufacturer´s protocol (BD Matchmaker Library construction and screening kit).

2.2.2.11 Yeast-Two-Hybrid

The principle of Y2H screenings is based on the reconstitution of the Gal4 transcription factor upon protein-protein interaction, subsequent activation of reporter gene transcription and

finally stringent nutrition selection of interacting proteins in a yeast reporter strain. The Gal4 transcription factor can be physically divided into two domains, the DNA activation domain (AD) and the DNA binding domain (BD). The DNA activation domain of Gal4 is fused to the cDNA-library (prey) and the bait protein is expressed as a fusion protein with the Gal4 binding domain. Through interaction of bait and library fusion proteins in a yeast reporter strain such as AH109 the DNA-BD and AD are brought into proximity and can activate transcription of the reporter genes ADE2, HIS3, LACZ and MEL1. For this thesis the yeast reporter strain AH109 was used which is auxotroph for adenine, tryptophan, leucine and histidine. The transcription of these reporter genes enables the growth of yeast cells harboring bait and prey interactions in the absence of adenine, tryptophan, leucine and histidine. For this thesis BD Matchmaker library construction and screening kit (BD Bioscience, Heidelberg, G) was used. The Yeast-Two-Hybrid screen was performed by yeast mating. Yeast mating only occurs between haploids of opposite mating type which can be Mat *a* or Mat *α*. First, the cDNA library was generated from Caco-2 cells and Orf 7a was subcloned into pGBKT-7 vector. pGADT-rec and the Caco-2 cDNA-library were transformed in AH109 (Mat *a*) (library construction) and pGBKT7-Orf 7a in Y187 (Mat *α*). The transformed yeast strains were cultivated together to fuse and to enable the generation of zygotes. Therefore, 1 ml of pretransformed AH109 pGADT-Caco-2 cDNA library was thawed at room temperature and combined with 5 ml of pretransformed Y187 pGBKT7-Orf7a culture (1 x 10^9 cells / ml). After addition of 45 ml 2 x YPDA/Kan (50 µg / ml) the yeast culture mixture was incubated for at least 24 hours at 30 °C with gentle shaking (40 rpm). After 20 hours of incubation an aliquot was taken to verify the formation of zygotes by light microscopy. At this point of time predominantly dumbbell-shaped cells were present, which indicates the transition phase to zygotes. Therefore, the culture was further incubated for 4 hours. Afterwards the mating culture was centrifuged at 1000 g for 10 min. In the meanwhile the mating flask was rinsed twice with 50 ml 0,5 YPDA/Kan. The rinse was combined and used to resuspend the yeast pellet. Then the cells were pelleted by centrifugation at 1000 g for 10 min and the pellet was resuspended in 10 ml 0,5 YPDA/Kan. After this 200 µl of the yeast solution were plated on media of different stringency (150 mm). The plates were incubated at 30 °C for at least 14 days.

2 x YPDA/Kan	YPD	
	Adenine solution	3 % (v/v)
	Kanamycin	0,1 %

0,5 x YPDA / Kan	YPD	
	Adenine solution	0,75 % (v/v)
	Kanamycin	0,1 %
PEG/LiAc	Tris/HCl pH 7,5	0,01 M
	EDTA	1 mM
	LiAc	1mM
	PEG 3350	40%
QDO	SD Minimal Base	26,7 g/l
	DO Supplement –Ade/-His/-Leu/-Trp	0,60 g/l
	Bacto agar	2 %
SD/-Trp	SD Minimal Base	26,7 g/l
	DO Supplement -Trp	0,73 g/l
	Bacto agar	2 %
SD/-Leu	SD Minimal Base	26,7 g/l
	DO Supplement -Leu	0,69 g/l
	Bacto agar	2 %
α-X-Gal	250 µg/ml in di-methylformamide (DMF)	

2.2.2.12 Preparation of competent yeast cells

Competent yeast cells were prepared using the LiAc-method. Several colonies of AH109 or Y187 or pretransformed cells of these yeast strains were inoculated into 50 ml YPDA medium and incubated 16 – 20 hours with constant shaking (250 rpm) at 30 °C. At an optical density of OD_{600} 0,15 - 0,3 the culture was centrifuged at 700 g for 5 min, the pellet was resuspended in 100 ml YPDA and incubated for another 3 hours at 30 °C with constant

shaking. When the culture reached an OD_{600} of 0,4 -0,6 cells were sedimented by centrifugation as described above. Cells were washed in A. dest and resuspended in 3 ml 1 x TE/LiAc-buffer prior to splitting them into two 1,5 ml reaction tube. The solution was again centrifuged at 14.000 rpm (5415C centrifuge, Rotor F-45-18-11, Eppendorf) for 1 min. After discarding the supernatant, the cell pellets were resuspended each in 600 µl 1 x TE/LiAc-buffer. Competent yeast cells were either used immediately or within two hours after preparation (stored at room temperature) to achieve highest transformation efficiency.

YPDA	Bacto Peptone	20 g/l
	Bacto yeast extract	10 g/l
	Adenine hemisulfate	0,003 %
	Glucose	2 %
TE/LiAc	Tris/HCl pH 7,5	0,01 M
	EDTA	1 mM
	LiAc	1 Mm

2.2.2.13 Transformation of yeast cells with circular or linearized plasmid DNA

Competent yeast cells were transformed either with circular or linearized plasmid DNA. For small scale transformation 200 ng plasmid DNA and 100 µg denaturated Herring testes carrier DNA were pipeted into a 1,5 ml tube, then 100 µl competent yeast cells (AH109 or Y187) were added. Co-transformation occurred simultaneously, however for this 100 ng of pGADT-7-construct and 100 ng pGBKT-7-construct were used. For cDNA library transformation 20 µl Caco-2 cDNA, 6 µl pGADT-rec and 20 µl denaturated Herring testes carrier DNA was added to a sterile, prechilled 1,5 ml tube prior 600 µl competent AH109 were added. The suspension was vortexed carefully and 2,5 ml (library) or 600 µl (small scale) PEG/LiAc solution were applied. After a second vortex step the transformation mixture was incubated at 30 °C for 45 min by mixing every 15 min. After addition of 160 µl (library transformation) or 70 µl (small scale) DMSO the transformation mixture was incubated for 20 min at 42 °C by mixing cells every 10 min. Cells were pelleted by centrifugation at 700 g for 5 min, resuspended in 3 ml YPD plus liquid medium (supplied by manufacuter) and incubated at 30 °C with shaking for 90 min. Cells were sedimented by centrifugation at 700 g for 5 min and resuspended in 30 ml of NaCl solution (0,9%). An aliquot of 150 µl (library) or 100 µl (small scale) of the transformants was plated on 150 mm (library) or 100 mm (small scale) plates containing medium which selects transformed yeast (SD/-Leu or -Trp) and incubated

at 30 °C until colonies were visible (3 – 6 days).

2.2.2.14 Generation of cDNA library in yeast

Homologous recombination between the linearized vector pGADT-rec and the cDNA library occurred in yeast upon transformation. Therefore both were transformed into AH109 as described above. To harvest the library plates were incubated for 4 hours at 4 °C and to each plate 3 ml freezing medium were added. The colonies were transferred to a sterile collection flask. After the colonies of about 200 plates were combined in one flask, cells were mixed gently and aliquots of 1ml were prepared and stored at – 80 °C. After one freezing / thawing process 100 µl of an aliquot were diluted (1:10, 1:100, 1:1000 and 1:10000) and spread on SD/-Leu plates. After incubation for 3 – 6 days colonies were counted to determine the transformation efficiency.

Freezing medium	25 % Glycerol in YPDA

2.2.2.15 Purification of plasmid DNA from yeast cells

One colony of yeast cells was inoculated into 5 ml of the respective dropout medium and incubated over night at 30° C with constant shaking. 1,5 ml of the overnight culture were centrifuged for 30 sec at 14000 rpm (Eppendorf 5417C). Plasmid isolation from the cell pellets was performed with the Grow'n'Glow Yeast Plasmid isolation Kit according to the manufacturer´s protocol. In addition to alkaline lysis, glass beads (supplied by manufactures) were used for mechanical disruption of the yeast cell walls. Since the yield of plasmid was to low for sequencing, plasmids isolated from yeast were transformed into bacteria for sequencing or further applications. Alternatively, inserts of interest were amplified by PCR and purified PCR products were subjected to sequencing.

2.2.2.16 Quantification of nucleic acid

RNA and DNA concentrations were determined by measuring the absorbance at wave length 260 nm using a spectrophotometer. For DNA an absorbance of 1 corresponds to 50 µg/ml DNA, the same absorbance for RNA corresponds to 40 µg/ml, if diluted in A. dest. Samples of DNA and RNA were diluted in A. dest or in RNAse-free A. dest, respectively. The absorbance at wavelength 280 nm monitors aromatic amino acids at their absorption

maximum and this value provides an insight into the protein content of the DNA sample. Therefore, the absorbance at wavelength 280 nm was additionally determined and the ratio between the absorbance at wavelength 260 nm and 280 nm delivers a guide value of the DNA purity. A ratio of 1,8 for DNA and 2,0 for RNA ensures high quality of sample preparation. Concentrations were calculated with the following equations:

DNA: A_{260} x 50 µg/ml x dilution factor = x µg/ml

RNA: A_{260} x 40 µg/ml x dilution factor = x µg/m

2.2.3 PROTEIN BIOCHEMICAL METHODS

2.2.3.1 Expression of recombinant proteins in *E.coli* and purification

SARS-CoV N was subcloned in pDest and the double substitution mutant of SARS-CoV N D400/403 was introduced in pQE30 DNA plasmids. Thereby, 6 histidine residues (His-tag) were fused in frame to the N-termini of the subcloned DNA fragments. Fusion of His-tag enables the purification of recombinant proteins expressed in *E. coli* by chelating with Ni-nitrilotriacetic acid (Pro Bond Resin). By addition of imidazol which displaces the histidine-protein complexes by competitive binding to Ni^{2+} the recombinant proteins can be eluted.

For recombinant protein purification the subcloned constructs were transformed into protease deficient *E. coli* strain BL21. One colony of the plated transformed bacteria was inoculated in 50 ml LB media containing ampicillin and bacteria were grown over night at 37 °C with shaking (200 rpm). Forty ml of this culture were then transferred to 800 ml LB media with ampicillin and incubated at 37 °C with constant shaking. When this culture had reached an OD_{600} of 0,6 – 0,8, expression of recombinant proteins was induced by addition of 1 mM IPTG (pQE) or 0,02% L-arabinose (pDEST) and bacteria were grown further for two hours as described. Bacteria were sediment by centrifugation (4500 rpm, 10 min; Beckmann Avanti, rotor JA 10) and the pellets were stored at -20 °C. After thawing on ice, pellets were resuspended with 10 ml lysis buffer and lysed during rotation for 30 min at 4 °C. Lysates were centrifuged for 20 min at 6000g (Beckmann Avanti, Rotor JA 25,50) and in the meantime resin (Pro Bond Resin, Invitrogen) was equilibrated by washing twice with A. dest, and three times with binding buffer (2 min; 900 rpm; Sigma 4K15; 4° C). Supernatant of lysate was then incubated with the equilibrated resin under rotation for 30 min at 4 °C. Subsequently, resin was transferred to a colum, washed twice with 10 ml binding buffer (2

min; 900 rpm; Sigma 4K15; 4° C) and washing with wash buffer was continued until the OD_{280} of the flow-through was below of 0,6. Recombinant proteins were eluted by addition of 8 ml elution buffer and collected in fractions of 500 µl. Protein concentration of each fraction was determined and fractions containing > 0,5 mg/ml of protein were pooled. The collected samples were dialysed in size exclusion units (Pierce; excluded molecular weight < 10 kDa) over night at 4° C against dialysis buffer to remove urea and to enable renaturation. Re-folded proteins were concentrated by size exclusion chromatography using spin columns (Vivaspin; Pierce; excluded molecular weight < 10 kDa). Purity of proteins was confirmed by SDS-PAGE and Coomassie-Blue staining.

Lysis buffer (pH = 7,8)	Guanidine HCl	6 M
	Na-phosphate	20 mM
	NaCl	500 mM
Binding buffer (pH = 7,8)	Urea	8 M
	Na-phosphate	20 mM
	NaCl	500 mM
Washing buffer (pH = 6,3)	Urea	8 M
	Na-phosphate	20 mM
	NaCl	500 mM
	Imidazole	80 mM
Elution buffer (pH = 6,3)	Urea	8 M
	Na-phosphate	20 mM
	NaCl	500 mM
	Imidazole	500 mM
Dialysis buffer (pH 3,5)	Na-acetate	10 mM

2.2.3.2 *In vitro* caspase-6 cleavage assay

125 ng of purified N and the double substitution mutant D400/403 were each incubated with recombinant active caspase-6 (Mch2, BD Pharmigen; Heidelberg, G) in a final volume of 20 µl assay buffer for 3 hours at 37 °C. As a control for the specificity of reaction both proteins were only treated with assay buffer under the same condition. Finally the reaction was terminated by addition of gel loading buffer and the samples were analyzed by immunoblot.

Assay buffer	Pipes	20 mM
	NaCl	100 mM
	DTT	10 mM
	EDTA	1 mM
	CHAPS	0,1 % (w/v)
	Sucrose (pH 7,2)	10%

2.2.3.3 Preparation of postnuclear lysates

A monolayer of a 6 cm cell culture dish was rinsed twice with PBS before 500 µl of lysis buffer supplemented with 0,5 mM Pefabloc protease inhibitor (Roche) were added. After incubation for 10 min, lysates were transferred to 1,5 ml Eppendorf cups and centrifuged for 1 min at 14.000 rpm in an Eppendorf 5417C centrifuge to remove membranes and nuclei. Proteins in the supernatant were precipitated with the 2.5 - 5 fold volume of methanol and an incubation period of at least 16 hours at -20 °C. At the next day, precipitated proteins were sedimented by centrifugation for 25 min at 3.500 rpm (Sigma 4K15) at 4 °C. Methanol was discarded, and air-dried protein pellets were resuspended in 50-100 µl TNE buffer. After the determination of protein concentration by Bradford assay and addition of an appropriate amount of 3 x SDS loading buffer, samples were stored at -20 °C prior to analysis by SDS-PAGE and Western blot.

Lysis buffer	NaCl	100 mM
	Tris-HCl pH7,5	10 mM
	EDTA	10 mM
	Triton X-100	0,5 % (w/v)

	DOC	0,5 % (w/v) in A. dest
TNE buffer	Tris-HCl pH 7,5	50 mM
	EDTA	5 mM
	NaCl	150 mM in A. dest

2.2.3.4 Preparation of RIPA lysates

For active caspase-3 analysis in western blot RIPA lysis was used. To receive the complete cell population including dead cells, the supernatant of a monolayer of a 6 cm cell culture dish was collected. The cells of the dish were washed and detached by trypsin/EDTA. Then the supernatant was used to inhibit trypsin and to admit the displaced cells from the dish. The cell suspension was centrifuged for 5 min, at 4°C and at 1000 rpm (Sigma 4K15). Afterwards the pellets were resuspended in 100 µl RIPA lysis buffer which was supplemented with 0,5 mM Pefabloc protease inhibitor (Roche) and incubated for 30 min on ice. After this incubation period the lysates were shortly sonified and chilled on ice. To get rid of cell debris the lysates were centrifuged for 10 min at 4°C and at 14000 rpm in an Eppendorf 5417C centrifuge. After determination of the protein concentration of an aliquot, 3 x SDS loading buffer was added, samples were stored at -20 °C prior to analysis by SDS-PAGE and Western blot.

Lysis buffer:	Tris HCl pH 8	50 mM
	NaCl	150 mM
	NP-40	1 %
	Sodium Deoxycholate	0,5 %
	SDS	0,1 %

2.2.3.5 Preparation of nuclear and cytosolic fractionations

For the nuclei fractionation a monolayer of a 6 cm cell culture dish was rinsed twice with PBS prior 1 ml of lysis buffer supplemented with 0,5 mM Pefabloc protease inhibitor (Roche) was added. Lysis occurred on ice for 10 min. Afterwards, cells were carefully detached by using a cell scarper. Lysates were transferred to 15 ml Falcon tube and were centrifuged at 4 °C and 800 g for 10 min to separate nuclei. The supernatant contains the cytotosolic fraction and proteins were precipitated similar as described above. The pellets consisting of nuclei were washed once with lysis buffer without Nonident P-40. Before protein concentration was

determined, pellets were sonified for 3-5 sec and chilled on ice. After addition of 3 x SDS loading buffer, samples were stored at -20 °C prior to analysis by SDS-PAGE and Western blot.

Lysis buffer	Tris–HCl pH 7,4	40 mM
	NaCl	150 mM
	EDTA	1 mM
	Nonidet P-40	0.3% (v/v)
	DTT	1 mM
Wash buffer	Tris–HCl pH 7,4	40 mM
	NaCl	150 mM
	EDTA	1 mM
	DTT	1 mM

2.2.3.6 Determination of protein concentration by Bradford assay

The Bradford assay is a spectroscopic method to measure the concentration of proteins in solution. By binding to proteins the absorption maximum of Coomassie Blue is shifted from a wave length of 465 nm to 595 nm. Cell lysates or proteins dissolved in TNE buffer were diluted 1:20 in water and 5 µl thereof were transferred in duplicate to a 96-well plate. 5 µl of a protein standard dilution series was pipetted onto the plate and 250 µl Bradford reagent was added. Absorption of protein samples was measured at a wave length of λ = 595 nm in an ELISA reader and the protein concentration was calculated according to the values of BSA-protein standard with defined protein concentration.

2.2.3.7 Co-immunoprecipitation (Co-IP)

A monolayer of transfected 6 cm cell culture dish was rinsed twice with cold PBS and lysed for 10 min on ice in 1 ml Co-IP buffer. Cells were detached by using a cell scraper and lysates were transferred to 1,5 ml Eppendorf cups. For infection experiments Caco-2 cells were used and were infected as described below. At day 2 p.i. cell culture medium was

removed, cells were washed once with PBS and were detached by treatment with trypsin / EDTA. To inhibit the trypsin cells were resuspended in 4 ml culture medium, centrifuged at 700 g, 4 °C for 5 min and were rinsed again with PBS. Then cells were transferred to tubes with screw caps and lysed with Co-IP buffer for 10 min on ice. Lysates were centrifuged for 10 min at 14.000 rpm and 4 °C (Eppendorf 5417C) to remove nuclei and membranes. 80 µl Pefabloc proteinase inhibitor (1 %) and antibody (anti-Bik, anti-7a polyclonal or anti-HA) at a 1:100 dilution were added to the supernatants. Samples were incubated for 3 h on a head-over-tail shaker in the cold room. Subsequently, 100 µl protein A-Sepharose and again 80 µl of Pefabloc (1 %) were added, followed by incubation for 90 min on a head-over-tail shaker in the cold room. After centrifugation for 2 min at 14000 rpm and 4° C (Eppendorf 5417C) the protein A-Sepharose pellet with the bound antibody-protein complexes was washed four times with Co-IP buffer by addition of 500 µl buffer followed by centrifugation. The protein A-sepharose pellet was resuspended in 30 µl 3 x SDS sample buffer and boiled for 5 min at 95 °C to release the immune complexes. After a further centrifugation step, supernatants were subjected to SDS-PAGE and immunoblot.

Co-IP buffer	HEPES pH 7,2	10 mM
	NaCl	150 mM
	Nonidet P-40	1% (v/v)

2.2.3.8 Sodium dodecyl sulfate-polyacrylamide gel electrophoresis (SDS-PAGE)

The SDS-PAGE technique allows protein separation upon denaturation with SDS in a two phase gel analysis. SDS is an anionic detergent which linearizes and binds proteins and masks them with negative charges. For reduction of inter- and intramolecular disulfide bonds reducing agent such as 2-mercaptoethanol are used in the loading buffer. The two phase gel system consists of a stacking gel with lower acrylamide concentration (5 – 6 % acrylamide) to focus all proteins in a single sharp band, and a resolving gel with a higher acrylamide content (between 8 – 20 % acrylamide) in which proteins are separated according to their molecular weight during electrophoresis.

Before SDS-PAGE analysis was started an appropriate amount of 3 x SDS sample buffer was added to protein samples resuspended in TNE buffer and boiled at 99 °C for 10 min. Proteins were usually separated on SDS gels containing 12,5 % acrylamide. Different

amounts of sample (5 – 50 µl) of equal protein contents were loaded, together with a molecular weight marker (5 µl). Electrophoresis was accomplished under constant current (30 mA per gel) until the tracking dye reached the bottom of the resolving gel.

4 x Lower gel solution	Tris-HCl, pH 8.8	1.5 M
	SDS	0.4 % (w/v) in A. dest
4 x Upper gel solution	Tris-HCl pH 6,8	0,5 M
	SDS	0,4 % (w/v) in A. dest
APS	10 % (w/v) stock solution in A. dest	
3 x SDS sample buffer	Tris-HCl pH 6,8	83 mM
	SDS	6,7 % (w/v)
	Glycerol	33 % (v/v)
	2-mercaptoethanol	16,6 % (v/v)
	bromphenole blue	in A. dest
10 x SDS electrophoresis buffer	Tris	250 mM
	Glycine	2,5 M
	SDS	1 % (w/v) in A. dest
Resolving gel mixture	A. dest	20,4 ml
(12,5 % acrylamide)	Lower gel solution	15,4 ml
	Protogel	25,9 ml
	APS 10 %	192 µl
	TEMED	90 µl

Stacking gel mixture	A. dest	9,9 ml
(5 % acrylamide)	Upper gel solution	4,2 ml
	Protogel	2,8 ml
	APS 10 %	168 µl
	TEMED	30 µl

2.2.3.9 Coomassie Blue staining of SDS-polyacrylamide (SDS-PA) gels

SDS-PA gels were soaked in Coomassie solution and stained for 30 min with gentle rocking at room temperature. Coomassie solution was removed and the gels were discolored by washing with discoloring buffer until protein bands of interest were clearly visible and no Coomassie blue background staining was present.

Coomassie solution	Coomassie Brillant blue	1,5 g
	Methanol	455 ml
	Acetic acid 99 %	80 ml
	A. dest	ad 1000 ml
Discoloring buffer	Methanol	45 %

2.2.3.10 Westen blot (immunoblot)

Western blot analysis allows the detection of proteins separated by SDS-PAGE by specific antibodies. Transfer of proteins from polyacrylamide gel onto PVDF-membrane was accomplished by an electrophoretic, semi-dry method. The membrane was activated by a short incubation with methanol and equilibrated with A. dest. before it was placed onto 3 layers of blotting paper saturated with blotting buffer. The gel was placed onto the membrane and covered with 3 further blotting paper saturated with blotting buffer. A current of 125 mA per gel (calculated as follows: size of the gel in cm^2 x 0.8 mA) was applied for 1 hour. Then the membrane was incubated with blocking buffer at room temperature for 1 hour. An antibody dilution of the primary antibody in 1 x TBST was prepared, added to the membrane and incubated on a horizontal shaker at 4 °C over night. At the next day the membrane was washed five times for at least 5 min with 1 x TBST, then incubated with a dilution (1 x TBST) of the secondary antibody for 1 hour at room temperature. After 5 further washing steps with

1 x TBST, the membrane was rinsed with A. dest. For detection of antibody-protein-complexes the membrane was covered for 3 min with an adequate mixture of ECL-solution, prepared according to the manufacturer´s protocol in a dark room. Finally the membrane was dried quickly between two blotting papers and exposed depending on expected signal intensity for 20 sec, 1 min, 3 min, 5 min and 3 hours to X-ray films for signal detection.

Blotting buffer	Tris	3 g
	Glycine	14.4 g
	Methanol	20 % (v/v)
	A. dest	ad 1000 ml
10 x TBST	Tris-HCl pH 8,0	100 mM
	NaCl	100 mM
	Tween-20	0,5 % (v/v) in A. dest
Blocking buffer	Skim milk powder 5 % in 1x TBST	
ECL Plus Detection Kit		

2.2.4 CELL BIOLOGICAL METHODS

2.2.4.1 Thawing of mammalian cells

For long-term storage cells were preserved in liquid nitrogen. Thawing of cells was done at 37 °C in a water bath. Afterwards, cells were washed with 10 ml pre-warmed medium by centrifugation at 1000 rpm (Sigma 4K15 centrifuge), 20 °C, for 10 min to remove DMSO contained in the cryoconservation medium. The supernatant was discarded and the cell pellet was gently resuspended in 10 ml fresh culture medium and plated in a 10 cm cell culture dish.

2.2.4.2 Cultivation of mammalian cells

Cells were cultivated at 37° C in a humidified atmosphere containing 5 % CO_2. For virus infection cell culture flasks and for transient transfection cell culture dishes were used. The different cell lines were kept in culture medium as described below.

A549	DMEM + Glutamax + 10 % FCS + Pen/Strep
Vero E6	DMEM + Glutamax + 10 % FCS + Pen/Strep
Cos-1	DMEM + Glutamax + 10 % FCS + Pen/Strep
Caco-2	Earle´s MEM + Glutamax + 10 % FCS + Pen/Strep
N2a	Optimem + Glutamax + 10 % FCS + Pen/Strep

Culture media were changed every other day. When confluence was reached, cells were rinsed once with PBS and detached from cell culture dishes using 1 ml Trypsin-EDTA. Detached cells were suspended in 9 ml medium, the appropriate volume of cell suspension was transferred to a fresh cell culture dish/flask and 10 ml culture medium were added for further cultivation.

2.2.4.3 Cryoconservation of cells

If 80 % of confluence were reached, cells were detached from the culture dish, suspended in culture medium and centrifuged at 1000 rpm (Sigma 4K15 centrifuge), 20 °C, for 5 min. The cell pellet was resuspended in 8 ml freezing medium and 1 ml aliquots in cryovials were immediately placed at -80 °C for at least 24 h before being transferred to liquid nitrogen for long-term storage.

Freezing medium	Culture medium (containing all additives)
	+ 10 % FCS
	+ 10 % DMSO

2.2.4.4 Determination of cell number

Cells were detached from the culture dish and suspended in 10 ml culture medium. An

aliquot of detached cells was diluted 1:2 in PBS and 20 µl thereof were transferred to a Fuchs-Rosenthal hemocytometer. The cell number in four diagonally lying squares consisting of 16 small squares was counted. One square has an area of 1 mm^2 and a depth of 0.2 mm, thus a volume of 0.2 m^3. The cell concentration was calculated according to the following equation:

Cell number/ml = counted cells : no. of counted squares x dil. Factor x 5000

2.2.4.5 Transient transfection of cells

Transient transfection of recombinant plasmids was performed using FuGene transfection kit (Roche) with Vero E6, Cos-1, Caco-2 and N2a. For transient transfection of A549 and CaCo-2 with recombinant plasmid as well as siRNA Lipofectamine 2000 (Invitrogen) was used. Both reagents were applied according to the recommendation of manufacturer. Briefly, cells were plated on 6 cm cell culture dishes, the amount of plated cells depending on the used transfection reagent. After 24 hours cells were transfected and usually were analyzed 24, 48 and 72 hours post transfection.

2.2.4.6 Transient knock down of Bik by siRNA

Short interference RNA (siRNA) enables transient inhibition of gene expression by double-stranded (ds) RNA molecules. This phenomen is initially a host encoded defense machinery activated by dsRNA to protect cells against viral ds genomes. Artificial siRNA are in generally double stranded and designed up to 19 to 22 bases with one strand being complemtary to the mRNA sequence of the protein of interest. siRNA is delivered to the cell by liposome based methods such as transient transfection with lipofectamine 2000 (see below). Once siRNA is arrived in the cytoplasm it is recognized and processed by the enzyme DICER. Cleaved ds RNA together with argonaute proteins form the RNA induced silencing complex (RISC) which enables an epigenetic silencing by RNA cleavage. One strand of the ds siRNA is degraded; RISC binds to the mRNA with its complementary siRNA strand, which then induces mRNA degradation. The siRNA machinery enables a considerable but not complete knock-down of the target protein. Moreover, this effect is only transient (Christian Eggert und Utz Fischer, 2003).

The transient inhibition of Bik expression was performed by two individual siRNAs against human Bik (SI00023317 and SI03044664, Qiagen, Hilden, G). As a negative control one

non-silencing (ns) siRNA (AllStars Neg. Control siRNA, 1027281, Qiagen, Hilden, G) was used. Prior to siRNA transfection, Caco-2 cells were pre-transfected with 7a or empty vector by Fugene reagent. Upon cells reached 80% confluency siRNA transfection was performed. The Lipofectamine 2000 reaction was accomplished in two batches, one includes 100 µl Optimem without antibiotics and 40 nM siRNA, the other consists of 100 µl Optimem without antibiotics and 2,5 µl Lipofectamine 200. After 5 min of separate incubation of these two batches, the reagents were combined and incubated for further 20 min. In the meantime cells were washed twice with Optimem without antibiotics and finally 1,8 ml cultivation medium of Caco-2 (see above) without antibiotics was added to the cells. After 20 min incubation period the transfection reagent batch was transferred to the cells and incubated for 6 h, 37°C in a humidified atmosphere containing 5 % CO_2. Afterwards, cells were washed with PBS and 4 ml cultivation medium was transferred to the transfected cells. At the next day cells were lysed with RIPA lysis buffer or postnuclear lysis buffer.

2.2.4.7 Indirect immunofluorescence assay and confocal microscopy

The indirect immunofluorescence technique was used to visualize antigens *in situ* on a single cell level by binding of fluorochrome-labeled secondary antibody to a primary antibody directed against the protein of interest. Therefore cells were seeded on glass cover slips and were transiently transfected with the respective constructs or left untransfected. On day two or three post transfection cover slips were transferred to 12-well culture plates, rinsed three times with PBS and fixed with 500 µl Roti-Histofix for 30 min at room temperature. Afterwards fixation solution was discarded and cells were quenched with NH_4Cl/glycine solution. Cells were permeabilized with 0,1 % Triton–X 100 solution and blocked with blocking solution. Each step was performed for 10 min and terminated by 3 x rinsing steps with PBS. The primary antibody diluted in blocking solution was added for 45 min at room temperature in a humid chamber. Cells on the glass cover slips were washed three times with PBS prior to incubation with a Cy2- or Cy3- conjugated secondary antibody dilution for 45 min at room temperature in a humid chamber. After three rinsing steps nuclei were stained with Hoechst DNA staining solution for 10 min at room temperature in the dark or left unstained. Again cells on the cover slips were rinsed and were mounted on microscope slides in anti-fading solution Permafluor. Confocal laser scanning microscopy was performed using a LSM510 confocal laser microscope (Zeiss).

Quenching solution	NH_4Cl	50 mM

	Glycine	20 mM in PBS
Permeabilization solution	Triton X-100	0.1 % in PBS
Blocking solution	Gelatine	0.2 % in PBS
Hoechst staining solution	Hoechst	2 µg/ml in PBS

2.2.5 VIRAL METHODS

2.2.5.1 SARS-CoV infection of cells

Vero E6 and Caco-2 cells were cultivated in cell culture flasks until they reached 80 % of confluence. Afterwards cell culture medium was removed, cells were rinsed once with PBS and were inoculated with SARS-CoV in a final volume of 2 ml infection medium (DMEM without additives). After 1 hour incubation at 37 °C, 2 ml culture medium was added. Vero E6 and Caco-2 cells were lysed at 1, 2 and 3 days post infection (p.i.). For preparation of a virus stock Vero E6 cells were chosen to achieve high viral titer. Cells were inoculated as described before and after two days post infection viral supernatant of these cells were harvested and centrifuged at 700 g, 4 °C for 5 min to remove cell debris. One % FCS was added to the viral supernatants and aliquots of 500 µl were distributed to tubes with screw caps and stored at – 80 °C. After one freezing/thawing process an aliquot of viral supernatant was analyzed by plaque assay to determine the virus concentration. Inhibition of caspases was performed by treatment of SARS-CoV infected Vero E6 cells with 100 µM z-VAD-FMK or 100 µM z-VEID-FMK 1 day p.i. After 24 hours inhibition medium was discarded, cells were washed with PBS and lysed.

2.2.5.2 Plaque assay

Vero E6 cells were infected with serial dilutions of viral supernatants that were harvested from Caco-2 and Vero E6 cells on the first or second day p.i. After 1 h, cells were covered with overlay medium. The overlay was removed two days p.i., cells were rinsed with PBS and were fixed in 4% formalin for 1 h. Then cells were stained with a crystal violet solution for

30 min. Afterwards staining solution was discarded and cells were washed with PBS until the plaque assay was evaluable. SARS-CoV propagation induces strong cytopathogenic effects (CPE) on Vero E6 cells such as cell lysis and cell death. After staining the area of dead and destroyed cells appears as holes (plaques) which are visible by the naked eye. To determine the viral titer plaques were counted whereas each plaque arose from a unit of infectious virus and the viral titer is expressed as plaque forming unit of infectious virus per ml (PFU/ml).

Overlaymedium	culture medium	33 ml
	3 % -methylcellulose solution	17 ml

Crystal violet solutions:

Stock solution	Crystal violet	10 g (2% w/v)
	Formaldehyde (37 %)	50 ml (10% v/v)
	Ethanol	100 ml (20% v/v)
	A. dest	ad 500ml
Working solution	stock solution	100 ml
	Formaldehyde (37 %)	100 ml
	A. dest	ad 1000 ml

3 RESULTS

3.1 SARS-CoV

SARS is predominately a viral pneumonia with diffuse alveolar damage. Although the exact mechanism of SARS pathogenesis is not known the lung damage in patients suffering from SARS seems to be due to apoptosis and necrosis, both induced directly by viral replication as well as indirectly by production of immune mediators. To investigate the importance of apoptosis in the pathogenesis of SARS-CoV the apoptotic properties predominately of N as well as 7a were analyzed in different cell culture models. Furthermore, to learn more about the unique protein 7a and which contribution it would have to viral and host interaction a Yeast-Two-Hybrid screen was performed

3.2 APOPTOTIC PROPERTIES OF SARS-COV N

3.2.1 SARS-COV N IS PROTEOLYTICALLY CLEAVED IN A CELL-TYPE DEPENDENT MANNER

The expression pattern of SARSCoV N was examined in different cell lines infected with SARS-CoV or transfected with N. Caco-2 and Vero E6 cells were chosen for infection and their susceptibility as well as the propagation of SARS-CoV was verified. At the second day post infection (p.i.) the titer of SARS-CoV propagated on Caco-2 cells was significantly lower (6,5 x 10^4 pfu/ml) than the titer of inoculated Vero E6 cells (1,8 x 10^6 pfu/ml). Furthermore depending on the cell line differences in the CPE were also observed. While SARS-CoV replication on Vero E6 cells showed strong CPE with cell lysis and death, SARS-CoV propagation on Caco-2 however, caused only low CPE characterized by syncytial cells. Consequently, Caco-2 was used as a model for persistent and Vero E6 for more lytic SARS-CoV infection. Both cell lines were infected with SARS-CoV and lysed at day 1, 2 and 3 post infections. The lysates were analyzed with anti-N antibody by immunoblot. Of note, the immunoblot analysis revealed a different expression pattern of N depending on the cell line. Only one N-specific band corresponding to the expected full-length size of 46 kDa or, in addition, a slightly faster migrating band (indicated by an arrow; **Fig. 11**) was found. In SARS-CoV infected Vero E6 cells full-length N and an additional N-specific signal at each time point

of lysis was found **(Fig. 11A).** In SARS-CoV infected Caco-2 cells, however, at any time point of lysis only the full-length signal of N was detectable **(Fig. 11B)**.

To analyse whether this banding pattern of N in different cell lines is only occurring during viral infection, N was transiently expressed in the same cell lines used for infection. Additionally, the SARS-CoV permissive human epithelial lung carcinoma cell line A549 and the murine neuronal cell line N2a were used to expand the models of persistent and lytic infection. Similar to Caco-2 cells, infection of neural cell lines (Yamashita *et al.*, 2005) with SARS-CoV reveals low or inapparent cytopathological effects (CPEs). These cell lines were transfected with N and lysed at day 1, 2 and 3 post transfection and subjected to immunoblot analysis. Interestingly, again a cell-type specific processing of N was found. In Vero E6 **(Fig. 11C)** and A549 **(Fig. 11E)** cells both forms of N were detectable, whereas in Caco-2 **(Fig. 11D)** as well as in N2a **(Fig. 11F)** cells only the full-length band was observed.

In summary, these experiments demonstrate a cell type-specific processing of SARS-CoV N in transiently expressing and in virus-infected cell lines. It is shown that in SARS-CoV infected Vero E6 cells as well as in transiently transfected A549 and Vero E6 cells two N-specific bands were detectable, indicative for proteolytical cleavage. In contrast, in infected or transfected Caco-2 and N2a cells only full-length N was found.

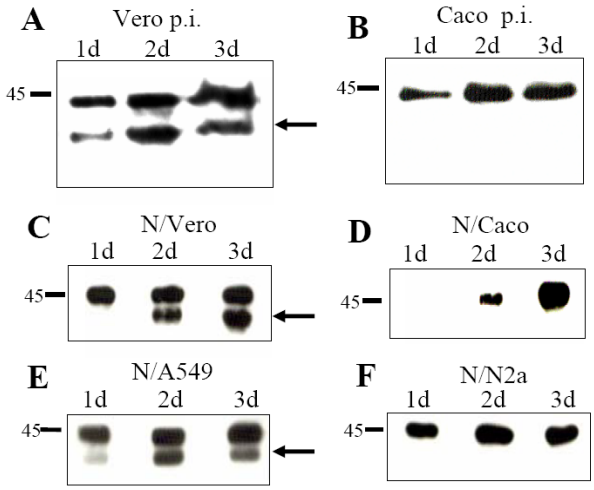

Fig. 11. Expression pattern of SARS-CoV N in different cell lines. Vero E6 (A) and Caco-2 (B) cells were infected with SARS-CoV. In addition Vero E6 (C), Caco-2 (D), A549 (E) and N2a (F) were transfected with N. Cells were lysed at day 1, 2 and 3 post infection and post transfection, respectively, and analysed by immunoblot using N antiserum. Depending on the cell line an additional signal for N indicated by an arrow was observed (Diemer *et al.*, 2008).

3.2.2 SARS-CoV N IS CLEAVED BY CASPASES

In order to test whether this additional signal of N was generated by proteolytical cleavage various protease and caspase inhibitors were used to identify the responsible proteases. N-transfected Vero E6 cells were mock-treated or treated with ammonium chloride (NH_4Cl), lactacystin (LC), or a cell permeable pan-caspase inhibitor (CI). The treatment occurred one day after transfection, at the second day post transfection cells were harvested, lysed and subjected to immunoblot analysis. Whereas treatment with the lysosomal inhibitor ammonium chloride and the proteasome inhibitor lactacystin showed no effect, only full-length N was detectable upon pan-caspase inhibitor treatment **(Fig. 12A**). The treatment prevents activation of caspase-1 and caspase-3 related caspases. This suggests that the lower band of SARS-CoV N is the result of caspase-mediated cleavage. Inhibition of caspase-3 related caspases prevents the activity of effector caspases-3, -6 and -7, which are the executors of apoptosis at the end of the caspase cascade. To ascertain which effector caspase caused the N processing, in a similar procedure as described in **Fig. 12A**, Vero E6 cells were transfected and treated using now cell-permeable caspase-3 or caspase-6 specific inhibitors. As found before, mock-treated, NH_4Cl or lactacystin treated cells still revealed cleavage of N. However, cells treated with caspase-3 **(**CI-3, **Fig. 12B)** or caspase-6 **(**CI-6, **Fig. 12C)** inhibitor showed only the full-length signal of N, indicating that N processing is mediated directly by caspase-6 and -3 or indirectly by activation of caspase-6 by caspase-3.

To verify whether N processing in virus-infected cells is also caused by caspases, SARS-CoV infected Vero E6 cells were mock-treated and treated with pan-caspase inhibitor **(**CI, **Fig. 12D)** or caspase-6 inhibitor at the first day post infection **(**CI-6, **Fig. 12E).** Two days after infection the cells were lysed and analysed by immunoblot. Again, an inhibition of N processing with both inhibitors was found. To confirm the cell-type specific activation of caspase-6 during SARS-CoV infection, cell lysates were analyzed with a specific antibody against cleaved lamin A/C. Lamin A is the main target of caspase-6 and is cleaved by this caspase in one of the final execution steps of apoptosis (Ruchaud *et al.*, 2002). Thus, Vero E6 (Ve) and Caco-2 (Ca) cells were inoculated with SARS-CoV and lysed at the first day post infection. In addition Vero E6 cells were treated were with staurosporine (co) serving as a positive control **(Fig. 12F)**. After analysis of the lysates by immunoblot a signal for cleaved lamin A/C was detectable only in staurosporine-treated and in SARS-CoV infected Vero E6 cells.

Taken together, the cell-type specific cleavage of N can be prevented by both caspase-6 and caspase-3 inhibitors. Proteolysis of the caspase-6 specific substrate lamin A in infected Vero E6 but not in infected Caco-2 cells indicates activity of caspase-6 in certain infected cell

lines.

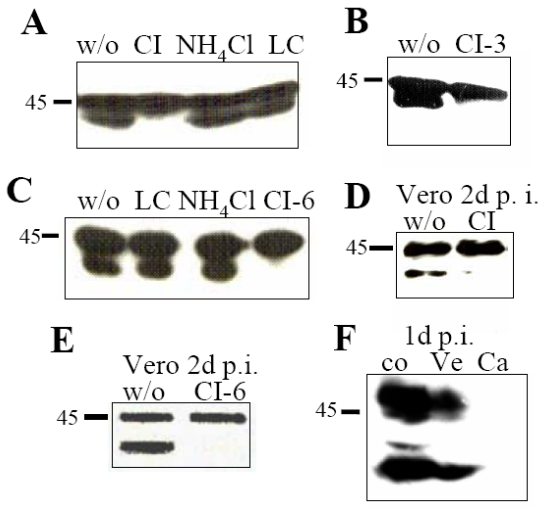

Fig. 12. N is processed by caspases. Vero E6 cells were transfected with N and treated with 10 mM NH_4Cl **(A and C)**, 2 μM LC **(A and C)**, 100 μM z-VAD-FMK (CI) **(A)**, 100 μM z-DEVD-FMK (CI-3) **(B)**, or 100 μMz-VEID-FMK (CI-6) **(C)** or left untreated (w/o) before harvesting. For infection studies Vero E6 cells were infected with SARS-CoV and treated with 100 μM z-VAD-FMK (CI) **(D)**, or 100 μMz-VEID-FMK (CI-6) **(E)**, or left untreated. Cells were lysed 15 h after treatment and subjected to Western blot analysis using N-antiserum. SARS-CoV infected Vero E6 (Ve) and Caco-2 (Ca) or staurosporine treated cells (co) were lysed 1 day post infection **(F)**. Lysates were analyzed by immunoblot utilizing anti-cleaved lamin (Diemer *et al.*, 2008)

3.2.3 CASPASE-6 IS ACTIVATED THROUGH THE INTRINSIC PATHWAY AND MEDIATES C-TERMINAL CLEAVAGE OF SARS-COV N AT RESIDUES 400 AND 403

The next step was to characterize the caspase-6 cleavage site in N. Caspases are aspartate specific cysteine proteases which cleave their substrate after aspartate residues. In general the recognition motif of caspases consists of a tetrapeptide whereat the fourth position contains the aspartate. The size of cleaved N and the presence of aspartates in the C-terminal region of N suggested that the caspase-6 cleavage site is embedded in this region. Thus a deletion mutant of N was created lacking the C-terminal residues 360-422 (Ndel). Vero E6 were transiently transfected with this mutant of N and cells were lysed 1, 2 and 3 days, respectively, post transfection. The immunoblot analysis showed a signal for Ndel of the expected size of ~37 kDa **(Fig. 13A)**. No additional signal for Ndel was detectable at any time point, indicating that the C terminus of N contains the caspase cleavage site. To confirm

this observation and define the putative caspase-6 cleavage site of N, site-directed mutagenesis was performed to exchange two aspartates, which might constitute the putative cleavage site, at position 400 as well as 403 to glutamates. This substitution mutant (D400/403E) and full-length N were expressed in *E.coli* and purified. Both recombinant proteins were incubated *in vitro* in caspase activation buffer with recombinant caspase-6 as well as left without caspase-6 for 3 h at 37° C. Then the proteins were subjected to immunoblot analysis. Treatment of wild-type N with caspase-6 resulted in a signal shift to a lower molecular weight compared to untreated N, indicating that recombinant caspase-6 completely processed wild-type N. In contrast, the substitution mutant (D400/403E) showed a signal with the same size as for uncleaved wild-type N, suggesting that the caspase-6 cleavage site was in fact destroyed by the double mutation **(Fig. 13B)**.

Further, it was analyzed which apoptotic pathway is induced by N. In general, there are two apoptotic pathways, namely the extrinsic and intrinsic signal cascade, both leading to activation of effector caspases. In the extrinsic cascade caspase-8 and in the intrinsic caspase-9 play a crucial role. To investigate which pathway is activated by N, Vero E6 cells were transfected with N, treated with inhibitors of both initiator caspases or left untreated. After 15 h the cells were lysed and analyzed by immunoblot **(Fig. 13C)**. The treatment with caspase-9 inhibitior (CI-9) prevented cleavage of N. In contrast, in caspase-8 inhibitor treated cells (CI-8) cleavage of N still occurred comparable to mock-treated controls (w/o). This data indicates that the intrinsic apoptotic pathway is triggered by N, resulting in activation of initiator caspase-9 and subsequent activation of effector caspases-3 and -6.

To confirm this observation and to investigate the mechanism of activation of the intrinsic pathway by N in more detail the phosphorylation state of the BH3-only protein Bad, which is activated in the intrinsic apoptotic pathway by dephosphorylation, was examined. Cos-1 cells were transiently transfected with N or empty vector (neg) and cells were treated with staurosporine serving as a positive control (pos). Three days post transfection the lysates were analysed by immunoblot. The immunoblot analysis revealed only in the positive control (pos) and in N-transfected cells one signal for Bad, indicating complete dephosphorylation. In the negative control (neg) **(Fig. 13D)** two signals for Bad were detectable. This data indicate that N enables dephosphorylation of Bad and subsequent activation of the intrinsic pathway.

In summary, it was shown that expression of SARS-CoV N triggers the intrinsic apoptotic pathway by dephosphorylation of Bad and activation of caspas-9 and effector caspases-6 and 3. Activated caspase-6 in turn mediates the C-terminal cleavage of N at residues 400 and 403.

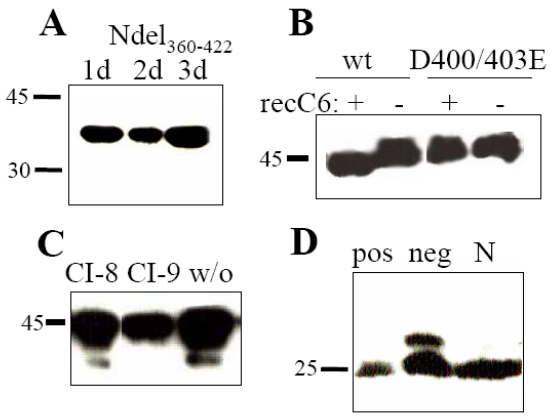

Fig. 13. Caspase-6 mediates cleavage of SARS-CoV N at C-terminal residues 400 and 403 by activation of the intrinsic apoptotic pathway. Vero E6 cells were transfected with a C-terminal deletion mutant of N (Ndel 360-422), lysed at day 1, 2 and 3 and analyzed in immunoblot (A). For *in vitro* caspase 6 cleavage assay a recombinant wild-type N (wt) and a double substitution mutant (D400/403E) were used. Each of them was incubated with recombinant caspase 6 (+) or with assay buffer (-). The cleavage of the protein was investigated by immunoblot (B). N-transfected Vero E6 cells were treated with 100 µM z-LEHD-FMK (CI-9) or 100 µM z-IETD-FMK (CI-8), or left untreated. Lysates were analysed in immunoblot (C). N or empty vector (neg) were transfected in Cos-1 cells. As a positive control Cos-1 cells were treated with staurosporine. Cells were lysed on day 3 and analyzed in Western blot using anti-bad antibody (D).

3.2.4 SUBCELLULAR LOCALIZATION OF SARS-COV N IN DIFFERENT CELL LINES

The caspase-mediated cleavage of Aleutian Mink disease virus NS1 protein alters the subcellular localization of this protein (Best *et al.*, 2003). To investigate whether the caspase-6 mediated cleavage of SARS-CoV N also influences its subcellular localization a nuclear and cytosolic fractionation assays were performed. At day 1, 2, and 3 post transfection of Vero E6, A549, Caco-2 and N2a nuclear fractions (n) were separated from cytosolic fractions (c) and examined by immunoblot. In Vero E6 **(Fig. 14A,** left panel) and in A549 **(Fig. 14B,** left panel) N is localised both in the cytoplasm and in the nucleus. Nuclear localization of N occurred at the second post transfection in Vero E6 cells and in A549 cells even at the first day after transfection. Moreover, both forms of N, full-length and cleaved N, were detected in the nucleus. In contrast, in Caco-2 cells **(Fig. 14C,** left panel) N was barely found in the nucleus. In N2a cells N was exclusively detected in cytosolic fractions **(Fig. 14D,** left panel).

To ensure the purity of nuclear and cytosolic fractions lysates were analysed with anti-

histone H3 in immunoblot. Histone H3 is known to stabilize the DNA in the nucleus and is excluded from the cytoplasm. Signals for H3 were only detected in the nuclear fractions, indicating that there is no substantial nuclear contamination of cytosolic fractions **(Fig. 14A, B, C, D;** middle panel). The immunoblot was re-probed with anti–Grb2 as a cytosol marker, to exclude contamination of the nuclear fraction by cytosolic proteins. Signals for Grb2 were only detected in the cytosolic fractions **(Fig. 14A, B, C, D;** right panel) confirming the purity of the nuclear fractions.

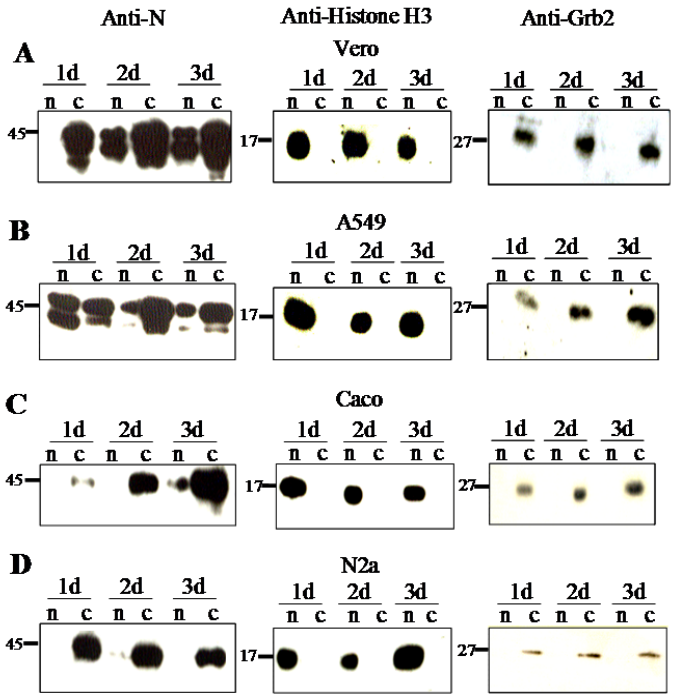

Fig. 14. Subcellular localization of SARS-CoV N analyzed by fractionation assay. Nuclear (n) and cytosolic (c) fractions of N transfected Vero E6 **(A),** A549 **(B),** CaCo-2 **(C)** and N2a **(D)** cells were separated at day one (1d), two (2d) and three (3d) post transfection. The fractions were analysed with the polyclonal serum against N (left panel) in immunoblot. Analysis with anti- histone H3 (middle panel) and anti-Grb2 antibodies (right panel) were performed to control the purity of nuclear and cytosolic fractions.

To confirm the data of the nuclear fractionation assay the subcellular localization of N was studied in A549, Vero E6, N2a and Caco-2 cells by an indirect immunofluorescence assay and confocal microscopy **(Fig. 15)**. At the second (data not shown) and third day post transfection N was stained with anti-N pAb followed by Cy3 labeled goat anti-rabbit antibody. For visulization of nuclei, Hoechst staining was used. N was predominantly localized in the

cytoplasm in all of the examined cell lines. However, at the second and the third day post transfection, N was found in the nucleus in ~ 5-10% of transfected Vero E6 and A549 cells **(Fig. 15A, B)**. In contrast to the nuclear localization of N in A549 and Vero E6, in Caco-2 and in N2a cells N was exclusively localized in the cytoplasm **(Fig. 15C, D)**.

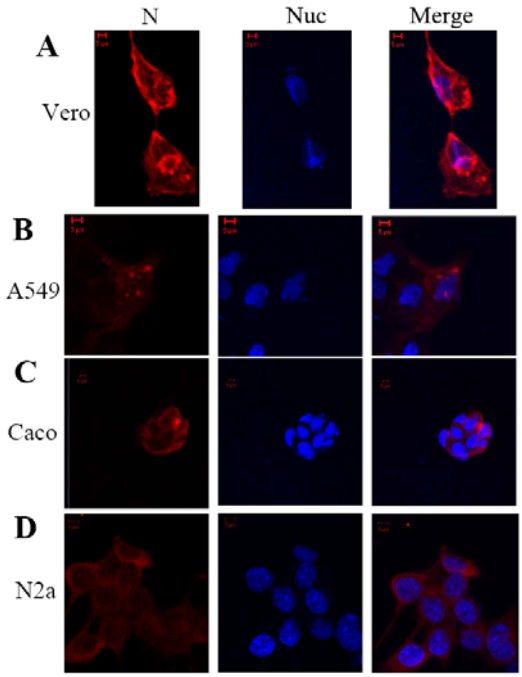

Fig. 15. Subcellular localization of SARS-CoV N analyzed by immunofluorescence assay. N transfected Vero E6 (A), A549 (B), Caco-2 (C) and N2a (D) were permeabilized at the second day post transfection. N (red) was stained with a polyclonal serum against N and with Cy3-conjugated goat-anti-rabbit secondary antibody (left panel) in the different cell lines. In the middle panel, the nuclei (blue) of cells were visualized by Hoechst staining. The merge of both stainings is shown in the right panel.

Taken together, a cell type-specific nuclear localisation of N was shown by subcellular fractionation and immunofluorescense assays. In the nucleus both full-length and cleaved N were found. Interestingly, nuclear localisation of N was detected in cell lines which exhibit a high virus propagation rate and also show caspase-mediated cleavage of N, indicating that cleavage of N and subcellular localisation are correlated.

3.2.5 MUTATION OF THE NUCLEAR LOCALISATION SIGNAL AT RESIDUES 257-265 PREVENTS CLEAVAGE OF N

Three potential nuclear localisation sequences (NLS) are embedded in the SARS-CoV N primary sequence (Rowland *et al.*, 2005). The N-terminal region of N contains a pat 7 motif (aa 38-44), the middle harbors a pat 4 and pat 7 sequence (aa 257-265), and finally the C-

terminal domain exhibits two bipartite, two pat 7 and one pat 4 motif (aa 369-390) **(Fig. 16A)**. Initially, the C-terminal nuclear localisation signal (360-422) of N was deleted to examine which NLS enables the most efficient nuclear localisation. Subcellular fractionation assay revealed that this deletion did not prevent the nuclear localisation of N (data not shown). Next the NLS in the middle part of N (Fig. 15A) was investigated in order to analyze whether the lysine residues present in this sequence mediate the transport of N into the nucleus. The three lysines which were found at positions 257, 258 and 262 were exchanged to glycins by site-directed mutagenesis (NLS II; **Fig. 16B**). Then Vero E6 cells were transfected with this substitution mutant (NLSII) of N and with wt N as a control. **(Fig. 16C)**. A nuclear fractionation assay was performed at day 2 and 3 post transfection, the fractions were examined by immunoblot. As expected wt N localised to the nucleus, however, the substitution mutant (NLS II) was not found in the nuclear fraction. Moreover, only the uncleaved full-length signal for NLS II was detectable indicating a correlation between nuclear localization and caspase mediated cleavage of N. Although it has already been demonstrated by immunfluorescence analysis in a previous study that the NLSII sequence of SARS-CoV is a general nuclear localization signal (You *et al.*, 2005), a further nuclear fractionation assay was performed to confirm this observation. Therefore, the NLSII sequence was fused to the N-terminus of the cytosolic protein Grb2 (NLSII-Grb2) and was as well as Grb2 alone expressed in Vero E6 cells. Two days after transfection nuclear and cytosolic fractions were separated and examined with anti-Grb2 antibody by immunoblot. In contrast to the nuclear fraction of Grb2, we detected a signal in the nuclear fraction of NLSII-Grb2 **(Fig. 16D)**, indicating that NLSII is a functional nuclear localization signal.

Several data in this study suggest a correlation between nuclear localisation of N and activation of an apoptotic pathway. To confirm this observation the phosphorylation state of Bad in N and NLSII transfected Cos-1 cells were investigated in a similar procedure as described in **Fig. 13 D**. Three days post transfection cells were lysed and analysed with an anti-Bad antibody by immunoblot **(Fig. 16E)**. In NLSII transfected cells both phosphorylated and dephosphorylated Bad was detected, in contrast to N-transfected cells exhibiting only the dephosphorylated form of Bad. To exclude that this effect is due to different expression levels of N and NLSII, an aliquot of the lysates was subjected to immunoblot analysis using anti-N antiserum. This immunoblot analysis revealed that the expression of N and NLSII was nearly the same **(Fig. 16F)**.

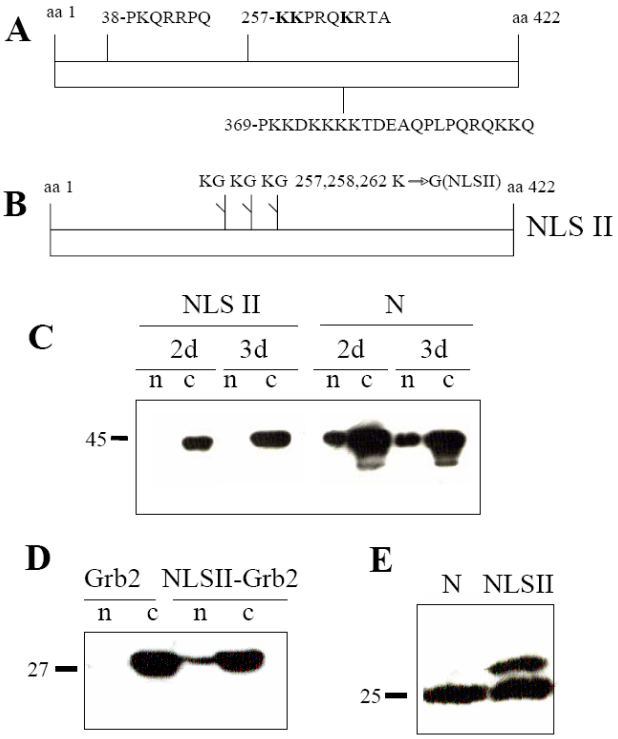

Fig. 16. Characterization of the functional nuclear localization signal of SARS-CoV N. Schematic description of the three potential NLSs (A) and of the substitution mutant in the middle of SARS-CoV N NLSII (B). NLSII and wt N were expressed in Vero E6 cells. After day 2 and 3 post transfection nuclei (n) and cytosol (c) were fractionated and subjected to immunoblot analysis (C). Vero E6 cells were transfected with Grb2 and NLSII-Grb2. At the second day post transfection the nuclear (n) and cytosolic (c) were separated and analyzed by immunoblot (D). N and NLSII were expressed in Cos-1 cells, lysed at the second day post transfection and analyzed with anti-Bad in immunoblot (D).

3.3 APOPTOTIC PROPERTIES OF SARS-COV 7A

3.3.1 IDENTIFICATION OF INTERACTORS OF THE SARS-COV 7A PROTEIN BY YEAST-TWO-HYBRID SCREEN

A Yeast-Two-Hybrid (Y2H) screen was performed to identify physically interacting proteins with the 7a protein. Based on the study on N the Caco-2 cell line which represents a model for persistent infection was chosen to generate a cDNA—library as prey. By using homologous recombination the cDNA from Caco-2 was fused in frame to the Gal4-transactivation domain vector (pGADT-7) and Orf7a was fused to the Gal4 binding domain (pGBKT-7). The constructs were transformed into haploid yeast cell strains AH109 and Y187, respectively, and mated. The screening exhibited a few positive yeast clones under

selective growth conditions and in α-galactosidase assay. Sequencing of the isolated plasmids and searching for homologous sequences by Blast Alghorithm revealed that most of the isolates were typically false positives. One of the isolate, however, was identified as the ER resident proapoptotic BH3-only protein Bik, and exhibited the complete sequence of this protein except two substitution mutations, one of which is silent **(Fig. 17)**. This candidate seemed to be a promising interactor of 7a due to the fact that both proteins, 7a as well as Bik, are predominately localized in the same cellular compartment which constitutes the subcellular precondition for an interaction *in vivo*. Furthermore, several studies have documented that 7a is involved in apoptotic processes and an interaction of 7a with a proapoptotic protein appears not absurdly. Therefore, a putative interaction of Bik and 7a was further analyzed in yeast by co-transformation of the isolated pGADT-Bik plasmid and pGBKT-7a and cultivation under selective nutrient conditions (QDO + gal). Again blue yeast cells were grown indicating an interaction of 7a and Bik in yeast.

Taken together, the BH3-only protein Bik was identified as an interactor of 7a by YH2 screen using a Caco-2 cDNA library as prey. Furthermore the interaction of both proteins could be confirmed in yeast by co-transformation.

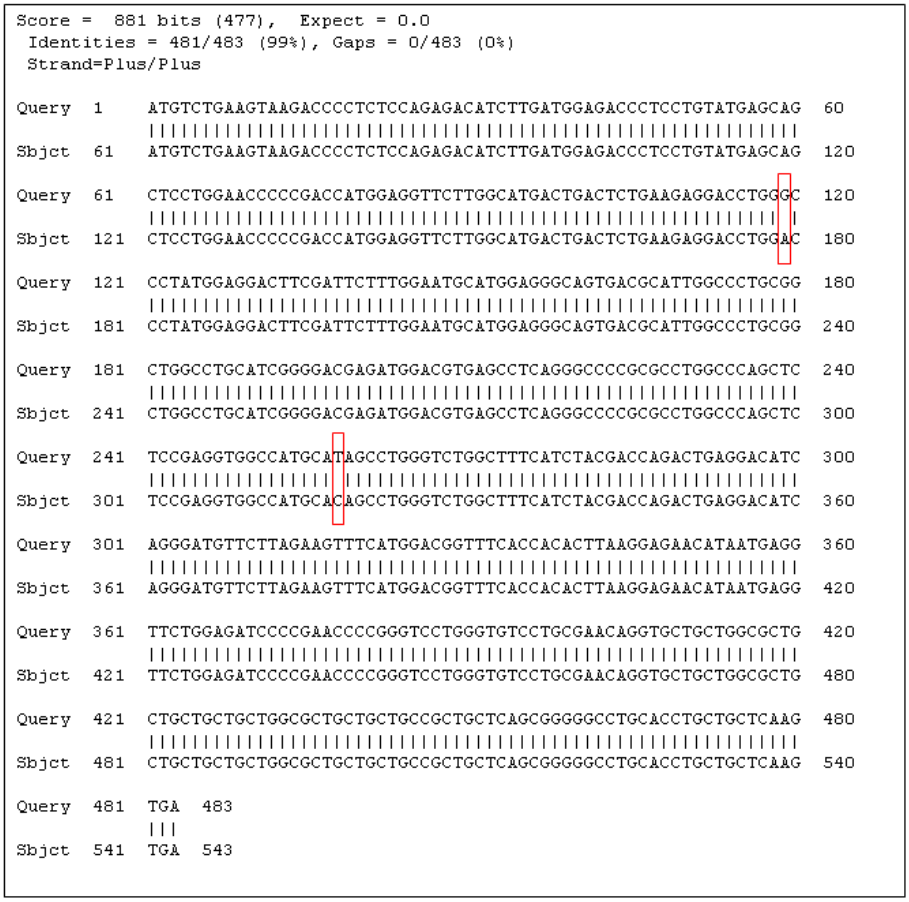

```
Score =  881 bits (477),  Expect = 0.0
 Identities = 481/483 (99%), Gaps = 0/483 (0%)
 Strand=Plus/Plus

Query  1    ATGTCTGAAGTAAGACCCCTCTCCAGAGACATCTTGATGGAGACCCTCCTGTATGAGCAG  60
            ||||||||||||||||||||||||||||||||||||||||||||||||||||||||||||
Sbjct  61   ATGTCTGAAGTAAGACCCCTCTCCAGAGACATCTTGATGGAGACCCTCCTGTATGAGCAG  120

Query  61   CTCCTGGAACCCCCGACCATGGAGGTTCTTGGCATGACTGACTCTGAAGAGGACCTGGGC  120
            ||||||||||||||||||||||||||||||||||||||||||||||||||||||||||| |
Sbjct  121  CTCCTGGAACCCCCGACCATGGAGGTTCTTGGCATGACTGACTCTGAAGAGGACCTGGAC  180

Query  121  CCTATGGAGGACTTCGATTCTTTGGAATGCATGGAGGGCAGTGACGCATTGGCCCTGCGG  180
            ||||||||||||||||||||||||||||||||||||||||||||||||||||||||||||
Sbjct  181  CCTATGGAGGACTTCGATTCTTTGGAATGCATGGAGGGCAGTGACGCATTGGCCCTGCGG  240

Query  181  CTGGCCTGCATCGGGGACGAGATGGACGTGAGCCTCAGGGCCCCGCGCCTGGCCCAGCTC  240
            ||||||||||||||||||||||||||||||||||||||||||||||||||||||||||||
Sbjct  241  CTGGCCTGCATCGGGGACGAGATGGACGTGAGCCTCAGGGCCCCGCGCCTGGCCCAGCTC  300

Query  241  TCCGAGGTGGCCATGCATAGCCTGGGTCTGGCTTTCATCTACGACCAGACTGAGGACATC  300
            |||||||||||||||| ||||||||||||||||||||||||||||||||||||||||||
Sbjct  301  TCCGAGGTGGCCATGCACAGCCTGGGTCTGGCTTTCATCTACGACCAGACTGAGGACATC  360

Query  301  AGGGATGTTCTTAGAAGTTTCATGGACGGTTTCACCACACTTAAGGAGAACATAATGAGG  360
            ||||||||||||||||||||||||||||||||||||||||||||||||||||||||||||
Sbjct  361  AGGGATGTTCTTAGAAGTTTCATGGACGGTTTCACCACACTTAAGGAGAACATAATGAGG  420

Query  361  TTCTGGAGATCCCCGAACCCCGGGTCCTGGGTGTCCTGCGAACAGGTGCTGCTGGCGCTG  420
            ||||||||||||||||||||||||||||||||||||||||||||||||||||||||||||
Sbjct  421  TTCTGGAGATCCCCGAACCCCGGGTCCTGGGTGTCCTGCGAACAGGTGCTGCTGGCGCTG  480

Query  421  CTGCTGCTGCTGGCGCTGCTGCTGCCGCTGCTCAGCGGGGGCCTGCACCTGCTGCTCAAG  480
            ||||||||||||||||||||||||||||||||||||||||||||||||||||||||||||
Sbjct  481  CTGCTGCTGCTGGCGCTGCTGCTGCCGCTGCTCAGCGGGGGCCTGCACCTGCTGCTCAAG  540

Query  481  TGA  483
            |||
Sbjct  541  TGA  543
```

Fig. 17. NCBI-Blast of 7a interactor Bik. The search of homologous sequence of a 7a interacting protein found in Y2H screen revealed 99% identity with the sequence of the BH3-only protein Bik. The complete sequence of Bik was isolated in the Y2H screen except two substitution mutations (indicated by red squares).

3.3.2 BIK IS EXPRESSED CELL-TYPE SPECIFICALLY AND 7A TENDS TO INDUCE APOPTOSIS IN A CELL-TYPE SPECIFIC MANNER

The expression of Bik is tissue-specific and the expression levels vary in different cell lines (Daniel *et al.*, 1999). To investigate the endogenous expression of Bik in the formerly used cell lines, Caco-2, A549, Vero E6 and Cos-7 were cultivated and lysed after one, two and three days. After protein content determination via Bradford assay, the lysates were analyzed with anti-Bik and anti-β-actin by immunoblot. β-actin was used as an internal loading control on the same blot. This analysis confirmed the study by Daniel et al., 1999 demonstrating that expression of Bik varied in different cell lines. Only in Caco-2 cells which delivered the cDNA for the Y2H screen a signal for Bik was detectable. In A549, Vero E6 and Cos-7, however, no protein expression of Bik was found **(Fig. 18A)**. Further experiments were done, similar to the

cell type specific induction of apoptosis by N, in which Caco-2 cells represent a model for persistent infection, in order to investigate the apoptotic features of 7a in Caco-2 and Vero E6 cells. Therefore, Caco-2 and Vero E6 cells were transfected with 7a or empty vector (mock). One day post transfection cells were lysed by RIPA-lysis buffer and protein content was determined by Bradford assay. The lysates were analyzed with caspase-3 antibody by immunoblot. In Caco-2 cells 7a expression does not increase levels of activated caspase-3 in comparison to mock-transfected cells **(Fig. 18B)**. In Vero E6, however, 7a was able to induce caspase-3 activation **(Fig. 18C)**, which is a hallmark of apoptosis. Three-hundred µg total protein content was required for active caspase-3 detection by Western blot analysis and the antibody was very instable. Due to this instability and unsensitivity/unspecifity of the caspase-3 antibody the experiments could not be reproduced during the time frame for this thesis. Therefore this experiment is very preliminary. In summary Bik is cell-type specific expressed and endogenous expression of it was only found in Caco-2 cells of the investigated cell lines. Furthermore 7a tends to induce apoptosis similar to N in a cell type specific manner.

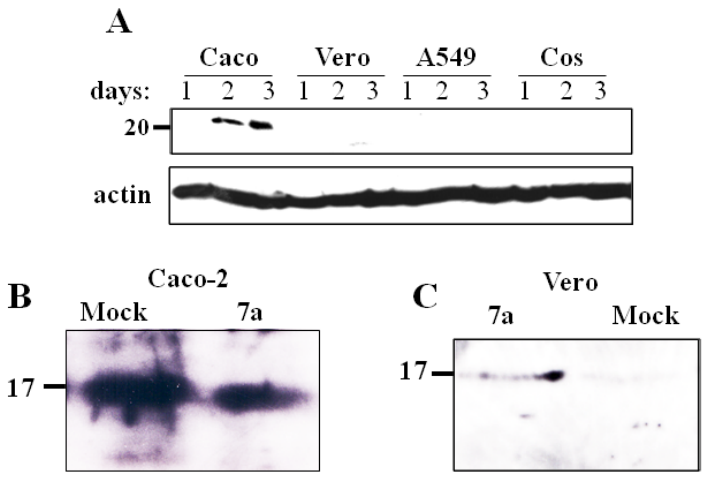

Fig. 18. Endogenous expression of Bik in different cell lines and cell type specific activation of caspase-3 by 7a expression. Caco-2, Vero E6, A549 and Cos-1 cells were seeded and lysed on day 1, 2 and 3 after cultivation. Cell lysates were analyzed with anti-Bik antibody and with anti-β actin antibody as a loading control by immunoblot (A). Caco-2 (B) and Vero E (C) were transfected with 7a or empty vector (mock), lysed at the first day post transfection and analyzed with anti-active caspase-3 antibody in Western blot.

3.3.3 VERIFICATION OF BIK-7A INTERACTION IN MAMMALIAN CELLS

The 7a-Bik interaction identified in the Y2H screen was further characterized in mammalian

cells to get insights into its biological relevance. Therefore, colocalization of both ER-resident proteins 7a and Bik were studied by indirect immunofluorescence staining and confocal microscopy. For this purpose, Vero E6 cells were co-transfected with Bik and HA-tagged 7a and fixed at the second day post transfection. The proteins were stained with rabbit-anti-Bik antibody and mouse-anti-HA antibody followed by Cy2 labeled anti-mouse and Cy3 labeled anti-rabbit antibodies. In several cells colocalization of Bik (red) and 7a (green) was visible, indicated as a yellow area in the overlay **(Fig. 19A)**.

The colocalization study only demonstrates a close proximity of 7a and Bik which is a pre-condition for protein interactions. To further confirm the interaction of 7a and Bik co-immunoprecipitation was performed. Vero E6 cells were again cotransfected with Bik and HA tagged 7a. After 48 h, the cells were harvested and lysed in Co-IP-buffer. Extracted proteins were immuno-precipitated with mouse anti-HA, conjugated to protein A-sepharose beads and analyzed with anti-Bik antibody by Western blot. As a positive control for the anti-Bik antibody a lysate of Vero E6 cells transfected with Bik was additionally analyzed **(Fig. 19B)**. Indeed, 7a-HA could be immuno-absorbed on Protein A Sepharose and the Western blot analysis revealed that 7a-HA was bound to Bik. In the mock transfected cells no specific signal for Bik was detected. Therefore, the 7a–Bik interaction found in Y2H could be confirmed by co-immunoprecipitation in mammalian cells. To investigate the relevance of this interaction during viral life cycle a similar co-immunoprecipitation experiment was done as described for transfected Vero E6 cells. Thus, Caco-2 cells were infected with SARS-CoV and lysed at the second day post infection. Complexes were immunoprecipitated by anti-7a antiserum and analyzed with anti-Bik antibody by immunoblot **(Fig. 19C)**. Using this approach, again an interaction between 7a and Bik was detected even during viral infection. As expected no Bik signal was found in cell lysate not treated with anti-7a antiserum.

Taken together, 7a and Bik colocalize in mammalian cells, as demonstrated by indirect immunofluorescence staining and confocal assay. Furthermore, the interaction of 7a and Bik which was found in yeast could be confirmed in mammalian cell lines by co-immunoprecipitation assays. Of note, the interaction of the viral accessory protein 7a with the BH3-only protein Bik has also been demonstrated during SARS-CoV infection of Caco-2 cells by co-immunoprecipitation assay, indicating a major importance of this interaction during SARS-CoV life cycle.

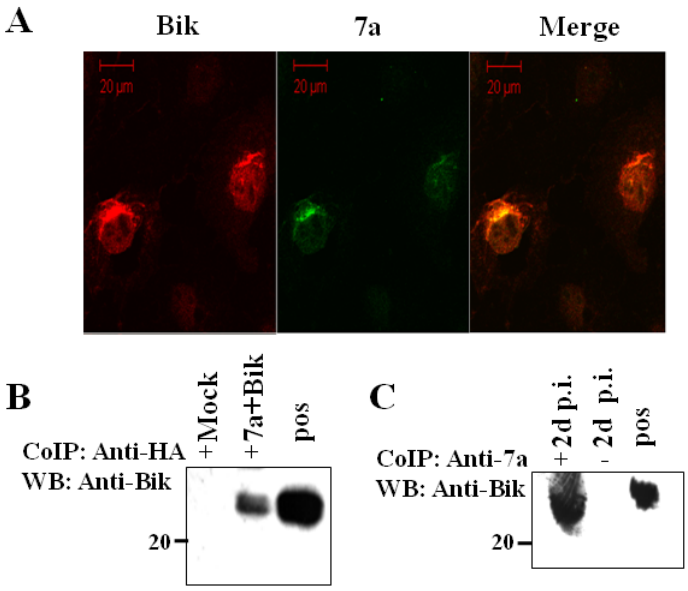

Fig. 19. Characterization of 7a–Bik interaction in mammalian cells. For colocalization study by immunofluorescence confocal assay 7a-HA and Bik were cotransfected into Vero E6 cells and cells were fixed and permeabilized at the second day post transfection. 7a-HA was stained with mouse-anti- HA followed by Cy2 labeled anti-mouse antibody (green) and Bik was stained with rabbit-anti-Bik followed by Cy3-conjugated anti-rabbit IgG (red). The merge of both staining shows a yellow area (A). Vero E6 cells were cotransfected with 7a-HA and Bik as well as left untransfected (mock). After 48 h cells were lysed, proteins were immunoprecipitated with anti-HA and analyzed with anti-Bik antibody in Western blot. As a size and antibody control, a Vero E6 cell lysate of cells transfected with Bik was additionally analyzed (pos) (B). Caco-2 cells were inoculated with SARS-CoV and lysed 2 days post infection. Proteins of the cell lysates were immunoprecipitated with anti-7a antiserum or left without antiserum (-) and were analyzed with anti-Bik antibody by immunoblot. A Bik transfected Vero E6 cell lysate served as a positive control (pos) (C).

3.3.4 MAPPING OF THE BINDING SITES OF 7A AND BIK BY Y2H AND VERIFICATION IN MAMMALIAN CELLS

In the next set of experiments the binding site of 7a to Bik was mapped by Y2H. Therefore the nucleotides coding for amino acids (aa) 16-46, 46-76, 76-106 and 93-123 of 7a were cloned in frame to the Gal4-transactivation domain **(Fig. 20A)**, full length Bik was fused to the Gal4 binding domain. For this screen only nucleotides of the mature form of 7a were used, without the nucleotides of the signal peptide. In a similar procedure as done for the Y2H screen before, the constructs were transformed into haploid yeast cells and were mated. Under selective nutrition conditions and in α-galactosidase assay positive clones were

selected. Positive yeast clones were only detected for the mated constructs 93-123 of 7a and Bik suggesting that aa 93-123 of 7a harbors the binding site. Using the same approach the binding site of Bik to 7a was mapped. The constructs coding for aa 1-33, 23-55, 40-70, 73-103, 104-133 and 134-160 of Bik **(Fig. 20B)** were transformed into AH109 yeast cells. Full length 7a in pGBK-T7 was transformed in Y187 yeast cells and mated with the six Bik constructs. A positive interaction under highly stringent conditions was only detected for the construct encoding aa 134-160 of Bik indicating that this region of Bik includes the binding site. Interestingly, both mapped binding sites of 7a and Bik contain the transmembrane domains of these proteins suggesting 7a and Bik interact via their transmembrane domains.

To investigate whether 7a and Bik interact through their transmembrane domains in physiological environment substitution mutants of both proteins were generated and a further co-immunoprecipitation experiment was performed. The transmembrane domain of Bik and 7a was exchanged by the transmembrane domain of human cytochrome b_5 which is also an ER-resident protein to facilitate the trafficking along the secretory pathway and mimicking a more natural situation for verification of the binding sites. Vero E6 cells were cotransfected once with the Bik substitution mutant (BikCb5) and full length 7a, twice with the 7a substitution mutant (7aCb5) and full-length Bik, once with full length 7a and Bik serving as a positive control and were mock transfected. Complexes were immunoprecipitated with anti-Bik and examined with 7a-antiserum in immunoblot **(Fig. 20C)**. As expected in 7a and Bik co-transfected cells 7a was coimmunoprecipitate. Even both forms of 7a were visible the mature (indicated by an arrow, ~15 kDa) and the immature (~17,5 kDa) product. In the antibody-specifity control (untransfected cells) as well as sepharose-specifity control (7aCb5 and Bik cotransfected cells without addition of anti-Bik antibody) no signal for 7a was detected, indicating the integrity of the procedure. Surprisingly, 7aCb5 as well as BikCb5 could be coimmunoprecipitated with Bik and 7a, respectively. This raises two possibilities: either the transmembrane domain is not the binding site during expression in mammalian cells or the interaction of 7a and Bik occurs with highly conserved sequences or sequence motifs in the transmembrane domain which are also present in cytochrome b_5. To verify these two hypotheses the transmembrane domain of 7a was deleted (termed 7aΔTM) and again a coimmunoprecipitation experiment was performed. Thus Vero E6 cells were cotransfected twice with 7a and Bik, once with 7aΔTM and Bik or were mock-transfected or with 7aΔTM alone **(Fig. 20D)**. In a similar procedure as previously described the coimmunoprecipitation experiment was performed. The immunoblot analysis revealed only the positive control exhibited signals consisting of two bands for the mature (indicated by an arrow) and immature 7a (~17,5 kDa), 7a and Bik co-transfected and treated with anti-Bik antibody. The negative controls 7a and Bik transfected cells without antibody treatment, as well as

expression of 7aΔTM alone and mock-transfected cells exhibited no signals for 7a in immunoblot, indicating again the integrity of the procedure. Of note, upon co-expression of 7aΔTM and Bik the two proteins did not interact. This suggests that the transmembran domain of 7a is the binding site to Bik and confirms the results of the Y2H mapping experiment.

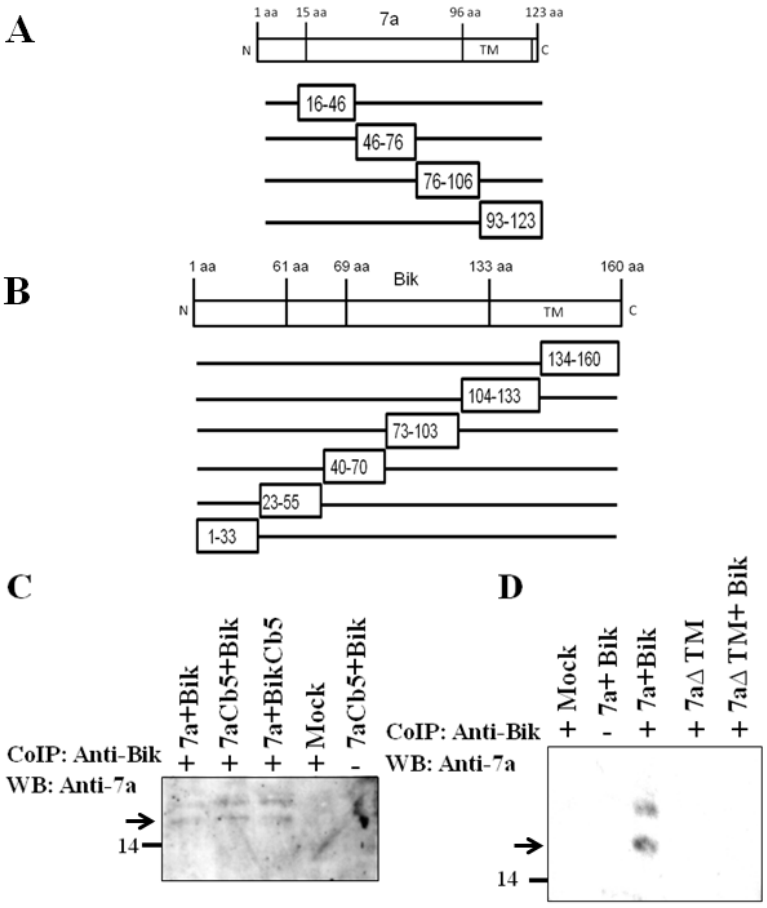

Fig. 20. Identification of the 7a-Bik binding site. Schematic illustration of full length 7a (A) and Bik (B) as well as the constructs coding for aa 16-46, 46-76, 76-106, 93-123 of 7a (A) and 1-33, 23-55, 40-70, 73-103, 104-133, 134-160 of Bik (B) which was used for the Y2H mapping. Vero E6 cells were cotransfected with 7a and Bik, transmembrane substitution mutant 7aCb5 and Bik, transmembrane substitution mutant BikCb5 and 7a or were mock-transfected. At the second day post transfection cells were lysed, immunoprecipitated with anti-bik or left without antibody and were analyzed with anti-7a antiserum by immunoblot (C). Vero E6 cells were cotransfected with 7a and Bik, transmembrane deletion mutant 7a Δ TM and Bik, or transfected with deletion mutant 7a Δ TM, or mock transfected. Protein complexes were immunoprecipitated with anti-Bik and analyzed with anti-7a antiserum by Western blot (D). The mature form of 7a was indicated by an arrow (C,D).

In summary, the BH3-only protein Bik was identified as an interactor of 7a by YH2 and the interaction was confirmed by Co-IP in mammalian cells. The transmembrane domain was

identfied as the binding site of 7a by Y2H and Co-IP.

3.3.5 INTERACTION OF 7A AND BIK HAS NO SIGNIFICANT EFFECT ON CASPASE-3 ACTIVITY

Both proteins, 7a as well as Bik, are well characterized as inducers of apoptosis. Therefore, the interaction of these two proteins stands to reason to influence their apoptotic potential. To investigate the effect of 7a and Bik interaction on their apoptotic property the active caspase-3 immunoblot assay was chosen. Vero E6 cells were transfected by Lipofectamine 2000 with empty vector (mock), 7a and Bik as well as cotransfected with 7a and Bik. At the first day post transfection cells were lysed in RIPA-lysis buffer. After protein content determination via Bradford assay 300 µg of protein of each lysate were analyzed with anti-active-caspase-3 by immunoblot **(Fig. 21A)**. As expected, the expression of both proapoptotic proteins 7a and Bik resulted in a considerable activation of caspase-3 in comparison to mock transfected Vero E6 cells. The co-expression of 7a and Bik seemed to have no substantial effect on the apoptotic potential of these proteins, because the expression of these proteins alone in comparison with co-expressed 7a and Bik do not alter the level of activated caspase-3. To ensure this finding the level of caspase-3 activation was analyzed in Caco-2 cells expressing 7a with and without silencing of endogenous Bik expression by siRNA. In pretests various siRNAs for silencing Bik expression in Caco-2 cells were evaluated and one of them, the HS4 siRNA was chosen for further experiments. In parallel, two series of Caco-2 transfection experiments were performed. One set was for the investigation of the level of activated caspase-3 during Bik knock down and 7a expression, the other one was to proof the transient knock down of Bik under the same conditions as the active caspase-3 assay. Therefore, Caco-2 cells were transiently transfected with the specific siRNA HS4 for silencing of Bik expression as well as a non specific siRNA (NS) as a control. At the second day post siRNA transfection the cells were again transfected twice with 7a or empty vector (mock). At the next day cells were lysed with RIPA-lysis buffer and the lysates were analyzed with anti-Bik **(Fig. 21B)** or anti-active-caspase-3 **(Fig. 21C)** by immunoblot. In addition, a lysate of cells overexpressing Bik was loaded and examined by Western blot analysis as an antibody control. Due to the instability and unsensitivity of the caspase-3 antibody (described above) the experiments could not be reproduced during the period of time for this thesis. However, this set of experiments was repreated later and confirmed the observation that the interaction of 7a and Bik do not significantly alter the level of active caspase-3 (C. Diemer and S. Gilch, personal communication).

Taken together, the interaction of 7a and Bik does not result in a significant alteration of caspase-3 activity.

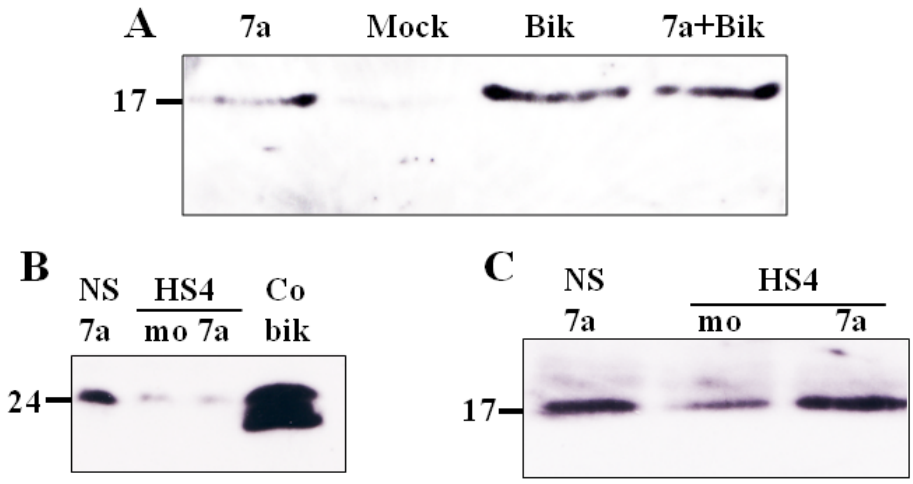

Fig. 21. Interaction of 7a and Bik do not influences their potential to activate caspase-3. Vero E6 cells were transfected with 7a, Bik mock or were cotransfected with 7a and Bik. After one day posttransfection cells were lysed and analyzed with anti-active-caspase-3 antibody by immunoblot (A). In double onsets Caco-2 cells were pretransfected with nonsilencing or HS4 siRNA. At the next day the cells were transfected with 7a or empty vector (mock). The cells were lysed at the second day post pretransfection and one set of the cell lysates was investigated with anti-Bik (B) the other set were analyzed with anti-active caspase-3 (C) by Western blot.

4 DISCUSSION

Among all coronaviruses, SARS-CoV causes the most serious infection in humans. SARS-CoV primarily leads to deleterious pulmonary pathological features in infected patients which could be elicited amongst others by apoptosis. Indeed in autopsy studies hallmarks of apoptosis were found in lung epithelial cells. Furthermore apoptosis was also observed in *in vitro* experiments when several cell lines were infected by SARS-CoV as well as expression studies of various SARS-CoV proteins. These observations indicate an important role of apoptosis during SARS-CoV replication and pathogenesis. To better understand modulation of host cell death by SARS-CoV and its possible contribution to the extraordinary aggressive SARS-CoV pathogenesis the apoptotic properties primarily of N were investigated in this study. In addition, one viral factor which could be responsible for the aggressive course of SARS-CoV is the unique protein 7a. This protein shows no sequence homology with any other known protein, therefore, it is of great interest to further characterize 7a by identifying interacting proteins via Y2H screen.

4.1 CELL-TYPE DIFFERENCES ARE CRUCIAL FOR THE APOPTOTIC POTENTIAL OF N

The study on the processing of SARS-CoV N by treatment of transiently transfected cells with caspase inhibitors revealed that N is cleaved by caspase-6. Cleavage of N by caspase-3 could not be excluded since caspase-3 is an activator of caspase-6. Inhibition of N-cleavage by CI-3 might be due to a blocked downstream activation of caspase-6. In addition, by recombinant caspase-6 assay, two features of N could be confirmed: first, that the processed N is in fact a cleavage product of caspase-6 and second that the caspase-6 cleavage site is located at residues 400 and 403 of N. For the N protein of TGEV, it was also shown that it is a substrate of caspases, with cleavage occurring upon induction of apoptosis during viral infection, pointing to a general feature and an important function of this processing (Eleouet *et al.*, 2000). Interestingly, the examination of different N transfected cell lines demonstrated that the caspase-6 mediated cleavage of N depends on the cell line. Caspase-6 is an effector caspase which is, once activated by initiator and effector caspases, mediating the morphological changes characteristic for apoptotic cell death, such as membrane blebbing and formation of apoptotic vesicles, cytoplasmic shrinkage as well as nuclear condensation and DNA fragmentation (Stennicke and Salvesen, 1998;Bratton *et al.*, 2000). The transactivation of caspase-6 is regulated by p53 and the induction of caspase-6 expression induces apoptotic signals that activate caspase-6 (MacLachlan and El Deiry, 2002). Since caspases are only active in cells undergoing apoptosis, these data support previous reports

demonstrating that N is a pro-apoptotic protein (Surjit *et al.*, 2004;Zhao *et al.*, 2006;Zhang *et al.*, 2007). Accordingly, in this study it was shown that N induces apoptosis by activation of the initiator caspase-9 as well as de-phosphorylation of proapoptotic Bad, which is indicative for intrinsic apoptosis activation. Taken together we demonstrate for the first time that the induction of apoptosis by SARS-CoV N is dependent on the cell type. We show that N processing is only observed in cells which are lytically infected by SARS-CoV, such as Vero E6 and A549 cells. In contrast, in CaCo-2 and the murine neuroblastoma cell line N2a, which we used as models for cells persistently infected (Chan *et al.*, 2004;Yamashita *et al.*, 2005) by SARS-CoV, no processing of N could be observed. Of note, the characterization of SARS-CoV pathogenesis *in vivo* by autopsied tissues from patients with SARS revealed viral signals in the lung with severe harm whereas in the intestine no apparent damage was observed despite detectable amounts of SARS-CoV in this organ (Ding *et al.*, 2004;To *et al.*, 2004a). Moreover, the majority of bat-SARS-CoVs and other CoV´s isolated from bats were found in the intestine, whereas none of the animals exhibit obvious signs of disease (Lau *et al.*, 2005;Watanabe *et al.*, 2010). First, this gives evidence that intestine is persistently infected by SARS-CoV. Second, this raises the question whether N is a decisive factor in the establishment of lytic or persistent infection. In infected Vero E6 cells it has been shown that the transcription factor STAT 3 is dephosphorylated and disappears from the nucleus (Mizutani *et al.*, 2004a), resulting in a decreased cell viability. In contrast, in Vero E6 subclones persistently infected with SARS-CoV the anti-apoptotic proteins Bcl-2 and Bcl-$_{XL}$ were up-regulated. Here, transient expression of N triggered phosphorylation of Akt and JNK, possibly leading to the establishment of persistence (Mizutani *et al.*, 2006). For N-transfected Cos-1 cells it was reported that p38 MAPK and JNK as well as caspase-3 and -7 are upregulated (Surjit *et al.*, 2004). Possibly, in colon cells N activates the Akt or STAT3 pathways or inhibits the MAPK pathway and, consequently, prevents the induction of apoptosis to facilitate viral persistence. Remarkably, in human intestinal epithelial cells the PI3/Akt, MAPK and ERK pathways are involved in cell survival, depending on the differentiation state of the cells (Franke *et al.*, 1997;Gauthier *et al.*, 2001). Therefore, the different regulation of survival pathways in various cell lines may also inhibit potential interactions of N with pro-apoptotic signals. Furthermore, the caspase-6 mediated cleavage of SARS-CoV N may be essential to enable the interaction of SARS-CoV N with proteins of pro- or antiapoptotic pathways which would be crucial for viral pathogenesis.

4.2 N IS BOTH INDUCER AND SUBSTRATE OF APOPTOTIC EXECUTION

Induction of apoptosis by viruses is very common during infection. This has also been

observed in SARS-CoV infected Vero E6 cells (Mizutani *et al.*, 2004b), raising the general question whether the induction of apoptosis is host defence or is even favourable for the viral life cycle. In case of host defence, the infected cell initiates apoptosis to hold spread of progeny virus in bay. However, a growing number of viruses were shown to adapt to the host cell death machinery to promote viral propagation. In some cases viruses capitalize caspases to cleave their own proteins for enhancing viral replication or establishing persistence (Best and Bloom, 2004). Coronavirus-induced apoptosis occurs upon infection of cells with TGEV. Upon induction of apoptosis, it has been demonstrated that the nucleocapsid protein of TGEV serves as a substrate for caspase-6 and -7 in infected cells (Eleouet *et al.*, 2000). The induction of apoptosis in TGEV infected cells, however, could also be initiated by other viral proteins during infection. In the case of the SARS-CoV N, we definitely showed in this study that N itself is inducer and subsequently the substrate of caspase-6, because the N expression alone without additional apoptotic stimuli activated caspase-6, resulting in processing of N. This is in contrast to many other viral proteins, which either activate or are target of caspases. Therefore, the two features of SARS-CoV N, namely to be both inducer of apoptosis and substrate of caspase-6, suggest that caspase-6 activity and subsequent processing of N have other roles during viral life cycle than simply induction of apoptosis to defence the virus. In general, the nucleocapsid protein would be an appropriate target for fending of viral propagation, since this protein is essential for viral assembly. Moreover, only full length N is packaged in the virion during TGEV infection (Eleouet *et al.*, 2000), indicating that caspase-6 processing might inhibit viral assembly. On the other hand, although N cleavage occurs in Vero E6 cells, high viral titers are achieved in this cell line. Furthermore, the caspase cleavage sites of N are highly conserved sequences, suggesting an important role for the viral life cycle.

4.3 CASPASE-6 ACTIVITY CORRELATES WITH NUCLEAR LOCALIZATION OF N

When we analysed the subcellular localisation of N in different cell lines, we found that, depending on the cell line which is used, N was located in the nucleus. This feature was observed in Vero E6 and in A549 cells, both cell lines known to be lytically infected by SARS-CoV. In contrast, in cell lines serving as models for persistent infection, N was predominantly or exclusively distributed in the cytoplasm. Interestingly, when nuclear localisation of N was compared with caspase-6 activity and processing of N, the two features significantly correlated. This means that only in cells exhibiting nuclear localization of N the protein was processed by caspase-6. This raises two possibilities: Either N is translocated to the nucleus leading to the induction of caspase-6 activity, or N can only be imported into the nucleus if

caspase-6 is active during apoptotic processes. An example for such a mechanism is provided by the NS1 protein of Aleutian mink disease parvovirus (Best *et al.*, 2003). In contrast, SARS-CoV N appears to be imported into the nucleus and to activate subsequently the apoptotic cascade leading to its own processing. This was shown by using a triple substitution mutant of N. Here, the three lysine residues of the predicted NLS between aa 257 and 265 were exchanged by glycins. Remarkably, this mutant was not imported into the nucleus anymore, clearly demonstrating for the first time that this stretch contains a functional NLS. Even more interesting, this mutant was not cleaved in Vero E6 cells and Bad was not de-phosphorylated, indicating that apoptosis and subsequently caspase-6 were not activated. This leads to the conclusion that nuclear localization of N is essential for induction of caspase-6 activity. Of note, we found both the processed and the full-length N within the nucleus. This seems to be consequent, since caspase-6 mediated cleavage of N does not impair the nuclear localization sequence and subsequent nuclear import of the processed form of N. Furthermore, a structural protein of the nuclear lamina, lamin A, is one of the major substrate of caspase-6. Processing of lamin A during apoptosis leads to intensified permeability of the nuclear pores (Best and Bloom, 2004). This might allow N to enter the nuclei of apoptotic cells non-specifically by passive diffusion. Arguing against this hypothesis is the finding that in the fractionation assays the marker protein grb-2 was detectable exclusively within the cytoplasmic fraction.

In this report, we show that N is specifically imported into the nucleus of transfected cells via its NLS, a feature which has also been observed for the N proteins of several other coronaviruses, e.g. IBV, MHV (Wurm *et al.*, 2001), or the related porcine reproductive and respiratory syndrome virus (PRRSV) (Rowland *et al.*, 1999). It has been described for PRRSV that deletion of the nuclear localisation signal of N led to a shorter viremia. Persistence of these NLS-deletion mutants was observed, but detailed analysis revealed that nuclear localisation of the N protein of these viruses was restored by point mutations within the nuclear localisation signal, resulting in a functional NLS (Lee *et al.*, 2006). These data indicate that nuclear localisation of N could have the potential to modulate pathogenicity of viruses. In addition, some MHV strains cause fulminant hepatitis in mice, dependent on N and the infected cell type. Here, N acts as a transcription factor, yet not directly but in connection with a host factor (Ning *et al.*, 2003).

Taken together, N-induced apoptosis leads to caspase-6 dependent processing of N in a cell type specific manner. The cell type specifity of this scenario might be evoked by the activation of survival pathways by cells which are infected persistently by SARS-CoV. If N enters the nucleus, apoptosis is induced via the intrinsic pathway and, thereby, caspase-6 activation results in the processing of N. Within the nucleus, N could in addition act as

transcription factor, either directly **(Fig. 22)** or dependent on host factors. This model underlines the possibility that the nuclear localization of N might be involved in the pathogenicity of SARS-CoV.

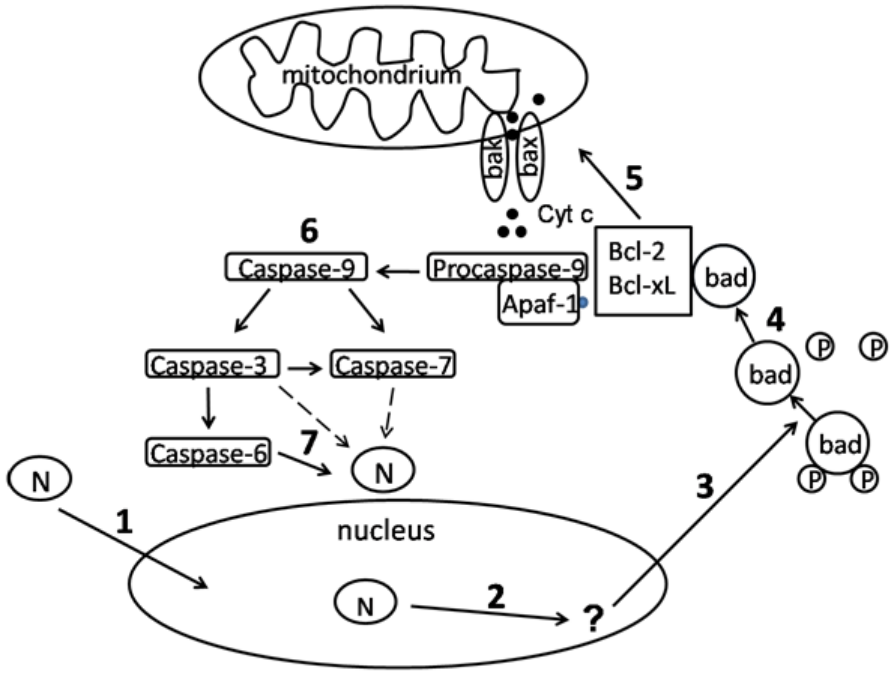

Fig. 22. Hypothetical model for correlation of SARS-CoV N nuclear localization and activation of caspases (Diemer *et al.*, 2008). During lytic infection SARS-CoV N translocates in the nucleus (1) and may activate gene expression or interact with nuclear compounds (2) resulting in dephosphorylation of Bad (3). Dephosphorylated Bad is able to interact with Bcl-2 and Bcl-xl(4). This interaction liberates Bax and Bak from prosurvival Bcl proteins and facilitates insertion of Bax and Bak into the mitochondrial membrane (5). The resulting membrane permeabilization enables cytochrome C efflux which triggers the activation of procaspase-9 by binding of Apaf-1. Once caspase-9 is activated the caspase cascade occurs and effector caspases are activated (6). After all N is cleaved by caspase-6, additional cleavage may occur by caspase-7 and/or caspase-6.

4.4 CELL-TYPE SPECIFICALLY EXPRESSED BH3-ONLY PROTEIN BIK INTERACTS WITH 7A

The BH3-only protein Bik was identified as an interacting protein of 7a by Y2H screen and the interaction was confirmed in yeast and mammalian cells, even during SARS-CoV infection. Although several Y2H screens with 7a were already performed, none of these studies used a cDNA library generated from cells or tissues of the gastrointestinal tract (Fielding *et al.*, 2006;Hanel and Willbold, 2007;Vasilenko *et al.*, 2010). As discussed above

the gastrointestinal tract seems to be a target for persistent infection of SARS-CoV *in vivo* and the Caco-2 cell line represents a model for persistent SARS-CoV infection *in vitro*. Therefore, we decided to prepare a Caco-2- cDNA library as prey for the Y2H screen, to possibly find a cell-type specific interacting protein of 7a. Indeed, we found that the 7a interactor Bik is, among the investigated cell lines, cell-type specifically expressed only in Caco-2 cells. However, this observation does not reflect the situation *in vivo*. *In vivo,* the mRNA expression of Bik is very restricted to kidney and pancreas, lung, liver, placenta, prostate as well as testis tissues, and no expression of Bik was found in the small intestine and colon tissues (Daniel *et al.*, 1999). Apparently, Bik expression in tumor-derived or immortalised cell lines is induced or down-regulated, respectively, during immortalization. Our data demonstrated, in line with the study of Daniel and colleagues, that in immortalized cell lines derived from kidney and lung no Bik protein expression was detectable, whereas in Caco-2 cell line originating from the small intestine considerable expression of Bik was found. Obviously, the cell line model concerning Bik expression is inversed to the situation of Bik expression *in vivo* and indicates an important role of Bik during tumorgenesis. Since the endogenous Bik of Caco-2 cells harbours two substitution mutations at position 119 bp and 258 bp, we asked whether these mutations may influence the apoptotic properties of Bik, thereby benefitting the tumorgenesis of Caco-2 cells. The codon analysis revealed that the mutation at position 258 bp is a silent mutation (His →His), but that the mutation at 119 bp (40 aa) caused an amino acid (aa) substitution from Glycin (G) to aspatate acid (D). Mutations in the Bik gene to promote tumorgenesis in different cell lines are controversally discussed (Castells *et al.*, 1999;Abdel-Rahman *et al.*, 1999;Arena *et al.*, 2003). However, none of the found mutations in these studies includes a mutation at residue 40. Moreover, substitutions at the phosphorylation site at aa T33 and / or S35 to D, mimic phosphorylation and even enhance the apoptotic potential of Bik (Lan *et al.*, 2007). Furthermore, the BH3 domain (aa 61-69) and aa 120-134 are the responsible motifs for the Bik-induced apoptotic activity (Elangovan and Chinnadurai, 1997). In addition, the transmembrane domain of Bik harbours a cleavage site GG (aa 153-154) of a Rhomboid protease (RHBDD1) which regulates the stability and apoptotic activity of Bik by processing and subsequent degradation (Wang *et al.*, 2008b). Since the substitution (aa 40) of Bik found in Caco-2 cells is not embedded in one of the apoptotic motifs, it will most likely not influence the apoptotic potential of Bik.

4.5 THE TRANSMEMBRANE DOMAINS OF 7A AND BIK ARE SITES OF INTERACTION

7a is targeted to the ER-lumen with its C-terminal domain and Bik is anchored with its C-

terminus to the ER membrane directing the N-terminal domain to the cytosol (Nelson *et al.*, 2005;Wang *et al.*, 2008b;Boumela *et al.*, 2011). Due to the different orientation during ER-membrane integration of these two proteins the most probable interaction site of both proteins seems to be the transmembrane domain **(Fig. 23)**. This assumption could be confirmed in this study by Y2H mapping and CoIP. The identification of the interaction site of both proteins, 7a as well as Bik, was performed to further characterize the interaction and primarily to generate a tool to analyze the biological function of this interaction. The first hint that the transmembrane domain or motifs of this sequence are the interaction site of proteins, 7a as well as Bik, has been delivered by the Y2H mapping experiment. Next, we decided to generate a transmembrane substitution mutant of 7a and Bik to facilitate the trafficking along the secretory pathway for CoIP experiments. Therefore, we generated transmembrane substitution mutants of both 7a and Bik. Here, the original transmembrane domain was exchanged with the transmembrane domain of human cytochrome b_5. Cytochrome b_5 is an ER resident protein and its transmembrane domain has been commonly fused to proteins in various studies to restrict their localization to the ER (Pedrazzini E, 1996). Surprisingly, we found again an interaction by CoIP experiments despite the substitution. This raises two possibilities: either the transmembrane domains which were identified in the Y2H mapping are not the binding sites of 7a and Bik, or the binding sites consist of a highly conserved sequence motif within the transmembrane regions. Later, it was confirmed by CoIP that 7a in which the transmembrane domain was deleted failed to interact with Bik. This finding is in line with a previous study in which the transmembrane domain of 7a was also identified as the interaction site for antiapoptotic Bcl-2 proteins. In addition, it was demonstrated that 7a lacking the transmembrane domain has a reduced apoptotic activity (Tan *et al.*, 2007).

The transmembrane substitution mutant of Bik also still interacts with full length 7a and in the Y2H mapping the transmembrane domain of Bik was identified as the interaction site with 7a. These findings indicate that the interaction site of Bik is also embedded in the transmembrane domain. The transmembrane domain of Bik harbours a sequence GG (aa 153-154) which influences the apoptotic potential of Bik, as mentioned above (Wang *et al.*, 2008b). Therefore, the interaction of 7a and Bik through their transmembrane domain indicates an important effect on their apoptotic properties. The transmembrane domain is basically important for the insertion in the target membrane. Although both proteins, 7a as well as Bik, are predominantly localized to the ER, they also were found in other organelles such as mitochondria. In a previous study it was demonstrated that the restriction of Bcl-2 proteins to mitochondria or ER triggers distinct apoptotic pathways (W Zhu, 1996). These observations indicate that through the interaction of 7a and Bik via an obviously conserved motif of the transmemberane domains, a confinement of these two proteins to the ER, which

is a central place in regulation of apoptosis, may occur.

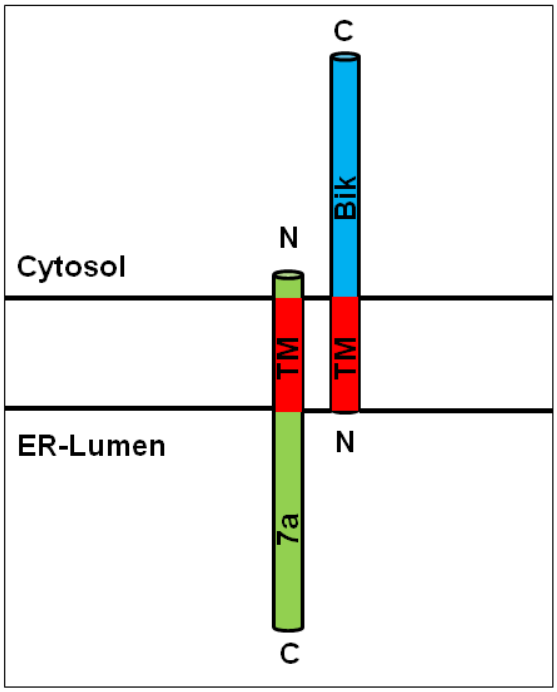

Fig. 23. Schematic illustration of the integration of 7a and Bik in the ER-membrane. The positions of the C- and N-terminus of 7a (green) and Bik (blue) during ER-membrane integration indicates that the interaction site of these two proteins is most likely the transmembrane domain (TM, red).

4.6 7A AND BIK INTERACTION DOES NOT ALTER THE ACTIVATION LEVEL OF CASPASE-3

Due to the previous findings and the fact that both proteins, 7a as well as Bik, are strong inducers of apoptosis we assumed that the interaction of these two proteins would influence their apoptotic properties. Therefore, we investigated the biological relevance of the interaction by active caspase-3 immunoblot analysis. Co-expression of Bik and 7a, in comparison to the expression of each protein alone, does not alter the activation of caspase-3. Further experiment with silenced endogenous Bik in Caco-2 cells by a specific siRNA combined with overexpression of 7a has also no effect on caspase-3 activation in comparison to 7a expression without silencing of Bik. In both experiments neither an increase nor a reduction of activated caspase-3 was found. This raises two possibilities: either the interaction indeed has no effect on apoptotic cell death or the insensitivity (as described in results) of the active caspase-3 assay obscures a significant alteration. The fact that Bik has also the competence to induce caspase-independent autophagic cell death (Rashmi *et al.*, 2008) would offer an explanation for a possible inability of the 7a/Bik

interaction to effect the level of active caspase-3. In contrast to this possibility is that the induction of apoptosis and subsequent activation of caspase-3 by 7a was documented in several studies (Tan *et al.*, 2004;Kopecky-Bromberg *et al.*, 2006;Tan *et al.*, 2007).

One possible mechanism in which the 7a and Bik interaction can interfere with the apoptotic machinery could be masking of the cleavage site of Rhomboid protease (RHBDD1) in the Bik transmembrane domain (Wang *et al.*, 2008b) which would enhance the stability of Bik and its ability to induce apoptosis. This scenario would indicate a proapoptotic function of the interaction of 7a and Bik. Another option for the involvement of the 7a/Bik interaction in apoptotic mechanisms at the ER is a potential binding competition of Bip (GRP78). Bip is an ER-associated protein with antiapoptotic properties, it also has the competence to interact with Bik (Fu *et al.*, 2007,Gorbatyuk *et al.*, 2010) as well as with 7a, as identified by Martha Schneider (diploma thesis) in our laboratory. The interaction of Bip with Bik reduces apoptosis in breast cancer cells and also seems to have antiapoptotic effects during expression of a misfolded protein P23H Rhodopsin (Gorbatyuk *et al.*, 2010). Moreover, interferon γ, which was highly elevated in serum of SARS-CoV patients during acute phase of infection, induces high levels of Bik expression and mediates cell death through the translocation of phosphor-extracellular kinase (ERK 1/2) in mouse airway epithelial cells (MAEC). Bik knock-out MAECs were resistant to interferon γ induced ER stress. It was suggested that the lack of Bik expression enables Bip to display its antiapoptotic properties; in this scenario, the interaction of Bik and Bip would have a proapoptotic role (Mebratu YA, 2008). Apparently depending on the induced apoptotic pathway and the balance between Bik and Bip proteins, it is decided whether the interaction of these two proteins is pro- or anti-apoptotic. 7a could compete the interaction with and between Bik and Bip and could direct the apoptotic property of the interaction, depending on the induced apoptotic pathway and the presence of Bik. Of note, Bik is not expressed in the small intestine as well as colon. Maybe the failure of Bik and subsequently the lack of interaction with 7a during SARS-CoV infection contribute to attenuation of apoptosis.

Taken together, the BH3-only protein Bik was identified as an interacting protein of 7a even during SARS-CoV infection. The interaction site of 7a and most likely of Bik is embedded in the transmembrane domain, and by this interaction the two proteins could be restricted to the ER. Although a significant alteration of activated caspase-3 by the interaction of 7a and Bik was not observed, possibly because of the insensitivity of the test system, a putative apoptotic regulation point at the ER by competitive binding of 7a with Bik or Bip is suggested.

REFERENCES

Abdel-Rahman,W.M., Arends,M.J., Wyllie,A.H. (1999). Death pathway genes Fas (Apo-1/CD95) and Bik (Nbk) show no mutations in colorectal carcinomas. Cell Death and Differentiation *6*, 387-388.

Abreu,M.T., Arnold,E.T., Chow,J.Y., Barrett,K.E. (2001). Phosphatidylinositol 3-kinase-dependent pathways oppose Fas-induced apoptosis and limit chloride secretion in human intestinal epithelial cells. Implications for inflammatory diarrheal states. J.Biol.Chem. *276*, 47563-47574.

Arena,V., Martini,M., Luongo,M., Capelli,A., Larocca,L.M. (2003). Mutations of the BIK gene in human peripheral B-cell lymphomas. Genes Chromosomes Cancer. *38*, 91-96.

Ashkenazi A. (2002). Targeting death and decoy receptors of the tumour-necrosis factor superfamily. Nat Rev Cancer *2*, 420-430.

Best,S.M., Bloom,M.E. (2004). Caspase activation during virus infection: more than just the kiss of death? Virology *320*, 191-194.

Best,S.M., Shelton,J.F., Pompey,J.M., Wolfinbarger,J.B., Bloom,M.E. (2003). Caspase cleavage of the nonstructural protein NS1 mediates replication of Aleutian mink disease parvovirus. J Virol. *77*, 5305-5312.

Booth,C.M., Matukas,L.M., Tomlinson,G.A., Rachlis,A.R., Rose,D.B., Dwosh,H.A., Walmsley,S.L., Mazzulli,T., Avendano,M., Derkach,P., Ephtimios,I.E., Kitai,I., Mederski,B.D., Shadowitz,S.B., Gold,W.L., Hawryluck,L.A., Rea,E., Chenkin,J.S., Cescon,D.W., Poutanen,S.M., Detsky,A.S. (2003). Clinical features and short-term outcomes of 144 patients with SARS in the greater Toronto area. JAMA *289*, 2801-2809.

Bordi,L., Castilletti,C., Falasca,L., Ciccosanti,F., Calcaterra,S., Rozera,G., Di Caro,A., Zaniratti,S., Rinaldi,A., Ippolito,G., Piacentini,M., Capobianchi,M.R. (2006). Bcl-2 inhibits the caspase-dependent apoptosis induced by SARS-CoV without affecting virus replication kinetics. Arch.Virol. *151*, 369-377.

Bosch,B.J., de Haan,C.A., Smits,S.L., Rottier,P.J. (2005). Spike protein assembly into the coronavirion: exploring the limits of its sequence requirements. Virology *334*, 306-318.

Boumela,I., Assou,S., Aouacheria,A., Haouzi,D., Dechaud,H., Handyside,A., Hamamah,S. (2011). Involvement of BCL2 family members in the regulation of human oocyte and early embryo survival and death: gene expression and beyond. Reproduction. *141*, 549-561.

Boyd,J.M., Gallo,G.J., Elangovan,B., Houghton,A.B., Malstrom,S., Avery,B.J., Ebb,R.G., Subramanian,T., Lutz,R.J., et.al. (1995). Bik, a novel death-inducing protein shares a distinct sequence motif with Bcl-2 family proteins and interacts with viral and cellular survival-promoting proteins. Oncogene. *11*, 1921-1928.

Bratton,S.B., MacFarlane,M., Cain,K., Cohen,G.M. (2000). Protein complexes activate distinct caspase cascades in death receptor and stress-induced apoptosis. Exp.Cell Res *256*, 27-33.

Breiman,R.F., Evans,M.R., Preiser,W., Maguire,J., Schnur,A., Li,A., Bekedam,H., Mackenzie,J.S. (2003). Role of China in the quest to define and control severe acute respiratory syndrome. Emerg.Infect.Dis. *9*, 1037-1041.

Cantrell,D.A. (2001). Phosphoinositide 3-kinase signalling pathways. J.Cell Sci. *114*, 1439-1445.

Castells,A., Ino,Y., Louis,D.N., Ramesh,V., Gusella,J.F., Rustgi,A.K. (1999). Mapping of a target region of allelic loss to a 0.5-cM interval on chromosome 22q13 in human colorectal cancer. Gastroenterology. *117*, 831-837.

Chan,P.K., To,K.F., Lo,A.W., Cheung,J.L., Chu,I., Au,F.W., Tong,J.H., Tam,J.S., Sung,J.J., Ng,H.K. (2004). Persistent infection of SARS coronavirus in colonic cells in vitro. J Med.Virol. *74*, 1-7.

Chau,T.N., Lee,K.C., Yao,H., Tsang,T.Y., Chow,T.C., Yeung,Y.C., Choi,K.W., Tso,Y.K., Lau,T., Lai,S.T., Lai,C.L. (2004). SARS-associated viral hepatitis caused by a novel coronavirus: report of three cases. Hepatology *39*, 302-310.

Chen,Y.Y., Shuang,B., Tan,Y.X., Meng,M.J., Han,P., Mo,X.N., Song,Q.S., Qiu,X.Y., Luo,X., Gan,Q.N., Zhang,X., Zheng,Y., Liu,S.A., Wang,X.N., Zhong,N.S., Ma,D.L. (2005). The protein X4 of severe acute respiratory syndrome-associated coronavirus is expressed on both virus-infected cells and lung tissue of severe acute respiratory syndrome patients and inhibits growth of Balb/c 3T3 cell line. Chin Med.J (Engl.) *118*, 267-274.

Cheng,P.K., Wong,D.A., Tong,L.K., Ip,S.M., Lo,A.C., Lau,C.S., Yeung,E.Y., Lim,W.W. (2004). Viral shedding patterns of coronavirus in patients with probable severe acute respiratory syndrome. Lancet *363*, 1699-1700.

Cheng,V.C.C., Lau,S.K.P., Woo,P.C.Y., Yuen,K.Y. (2007). Severe acute respiratory syndrome coronavirus as an agent of emerging and reemerging infection. Clinical Microbiology Reviews *20*, 660-+.

Chow,K.C., Hsiao,C.H., Lin,T.Y., Chen,C.L., Chiou,S.H. (2004). Detection of severe acute respiratory syndrome-associated coronavirus in pneumocytes of the lung. Am.J Clin.Pathol. *121*, 574-580.

Christian Eggert und Utz Fischer (2003). RNA-Interferenz: Ein neues Werkzeug zur Analyse der Genfunktion. BIOspektrum *9*, 372-374.

Cinatl,J., Hoever,G., Morgenstern,B., Preiser,W., Vogel,J.U., Hofmann,W.K., Bauer,G., Michaelis,M., Rabenau,H.F., Doerr,H.W. (2004). Infection of cultured intestinal epithelial cells with severe acute respiratory syndrome coronavirus. Cellular and Molecular Life Sciences *61*, 2100-2112.

Daniel,P.T., Pun,K.T., Ritschel,S., Sturm,I., Holler,J., Dörken,B., Brown,R. (1999). Expression of the death gene Bik/Nbk promotes sensitivity to drug-induced apoptosis in corticosteroid-resistant T-cell lymphoma and prevents tumor growth in severe combined immunodeficient mice. Blood. *94*, 1100-1107.

Diemer C, Schneider M, Schätzl HM, Gilch S (2010). Modulation of Host Cell Death by SARS Coronavirus Proteins. In: Molecular Biology of the SARS-Coronavirus, ed. Sunil K Lal Springer, 231-245.

Diemer,C., Schneider,M., Seebach,J., Quaas,J., Frosner,G., Schatzl,H.M., Gilch,S. (2008). Cell type-specific cleavage of nucleocapsid protein by effector caspases during SARS coronavirus infection. Journal of Molecular Biology *376*, 23-34.

Ding,Y., He,L., Zhang,Q., Huang,Z., Che,X., Hou,J., Wang,H., Shen,H., Qiu,L., Li,Z., Geng,J., Cai,J., Han,H., Li,X., Kang,W., Weng,D., Liang,P., Jiang,S. (2004). Organ distribution of severe acute respiratory syndrome (SARS) associated coronavirus (SARS-CoV) in SARS patients: implications for pathogenesis and virus transmission pathways. J Pathol. *203*, 622-630.

Drosten,C., Chiu,L.L., Panning,M., Leong,H.N., Preiser,W., Tam,J.S., Gunther,S., Kramme,S., Emmerich,P., Ng,W.L., Schmitz,H., Koay,E.S. (2004). Evaluation of advanced reverse transcription-PCR assays and an alternative PCR target region for detection of severe acute respiratory syndrome-associated coronavirus. J Clin.Microbiol *42*, 2043-2047.

Drosten,C., Gunther,S., Preiser,W., van der Werf,S., Brodt,H.R., Becker,S., Rabenau,H., Panning,M., Kolesnikova,L., Fouchier,R.A.M., Berger,A., Burguiere,A.M., Cinatl,J., Eickmann,M., Escriou,N., Grywna,K., Kramme,S., Manuguerra,J.C., Muller,S., Rickerts,V., Sturmer,M., Vieth,S., Klenk,H.D., Osterhaus,A.D.M.E., Schmitz,H., Doerr,H.W. (2003b). Identification of a novel coronavirus in patients with severe acute respiratory syndrome. New England Journal of Medicine *348*, 1967-1976.

Drosten,C., Gunther,S., Preiser,W., van der Werf,S., Brodt,H.R., Becker,S., Rabenau,H., Panning,M., Kolesnikova,L., Fouchier,R.A.M., Berger,A., Burguiere,A.M., Cinatl,J., Eickmann,M., Escriou,N., Grywna,K., Kramme,S., Manuguerra,J.C., Muller,S., Rickerts,V., Sturmer,M., Vieth,S., Klenk,H.D., Osterhaus,A.D.M.E., Schmitz,H., Doerr,H.W. (2003a). Identification of a novel coronavirus in patients with severe acute respiratory syndrome. New England Journal of Medicine *348*, 1967-1976.

Eickmann,M., Becker,S., Klenk,H.D., Doerr,H.W., Stadler,K., Censini,S., Guidotti,S., Masignani,V., Scarselli,M., Mora,M., Donati,C., Han,J.H., Song,H.C., Abrignani,S., Covacci,A., Rappuoli,R. (2003). Phylogeny of the SARS coronavirus. Science *302*, 1504-1505.

Elangovan,B., Chinnadurai,G. (1997). Functional dissection of the pro-apoptotic protein Bik. Heterodimerization with anti-apoptosis proteins is insufficient for induction of cell death. J Biol Chem. *272*, 24494-24498.

Eleouet,J.F., Slee,E.A., Saurini,F., Castagne,N., Poncet,D., Garrido,C., Solary,E., Martin,S.J. (2000). The viral nucleocapsid protein of transmissible gastroenteritis coronavirus (TGEV) is cleaved by caspase-6 and -7 during TGEV-induced apoptosis. J Virol. *74*, 3975-3983.

Fang,X., Ye,L., Timani,K.A., Li,S., Zen,Y., Zhao,M., Zheng,H., Wu,Z. (2005). Peptide domain involved in the interaction between membrane protein and nucleocapsid protein of SARS-associated coronavirus. J Biochem Mol Biol. *38*, 381-385.

Fielding,B.C., Gunalan,V., Tan,T.H., Chou,C.F., Shen,S., Khan,S., Lim,S.G., Hong,W., Tan,Y.J. (2006). Severe acute respiratory syndrome coronavirus protein 7a interacts with hSGT. Biochem Biophys Res Commun. *343*, 1201-1208.

Fielding,B.C., Tan,Y.J., Shuo,S., Tan,T.H., Ooi,E.E., Lim,S.G., Hong,W., Goh,P.Y. (2004). Characterization of a unique group-specific protein (U122) of the severe acute respiratory syndrome coronavirus. J Virol. *78*, 7311-7318.

Franke,T.F., Kaplan,D.R., Cantley,L.C. (1997). PI3K: downstream AKTion blocks apoptosis. Cell *88*, 435-437.

Fu,Y., Li,J., Lee,A.S. (2007). GRP78/BiP inhibits endoplasmic reticulum BIK and protects human breast cancer cells against estrogen starvation-induced apoptosis. Cancer Res. *67*, 3734-3740.

Fulda S (2006). Extrinsic versus intrinsic apoptosis pathways in anticancer chemotherapy. Oncogene *25*, 4798-4811.

Gauthier,R., Harnois,C., Drolet,J.F., Reed,J.C., Vezina,A., Vachon,P.H. (2001). Human intestinal epithelial cell survival: differentiation state-specific control mechanisms. Am.J Physiol Cell Physiol *280*, C1540-C1554.

Germain,M., Mathai,J.P., McBride,H.M., Shore,G.C. (2005). Endoplasmic reticulum BIK initiates

DRP1-regulated remodelling of mitochondrial cristae during apoptosis. EMBO J. *24*, 1546-1556.

Germain,M., Mathai,J.P., Shore,G.C. (2002). BH-3-only BIK functions at the endoplasmic reticulum to stimulate cytochrome c release from mitochondria. J Biol Chem. *277*, 18053-18060.

Gonzalez,J.M., Gomez-Puertas,P., Cavanagh,D., Gorbalenya,A.E., Enjuanes,L. (2003). A comparative sequence analysis to revise the current taxonomy of the family Coronaviridae. Arch.Virol. *148*, 2207-2235.

Gorbatyuk,M.S., Knox,T., LaVail,M.M., Gorbatyuk,O.S., Noorwez,S.M., Hauswirth,W.W., Lin,J.H., Muzyczka,N., Lewin,A.S. (2010). Restoration of visual function in P23H rhodopsin transgenic rats by gene delivery of BiP/Grp78. Proc Natl Acad Sci U S A. *107*, 5961-5966.

Green,D.R. (2000). Apoptotic pathways: paper wraps stone blunts scissors. Cell *102*, 1-4.

Gu,J., Gong,E., Zhang,B., Zheng,J., Gao,Z., Zhong,Y., Zou,W., Zhan,J., Wang,S., Xie,Z., Zhuang,H., Wu,B., Zhong,H., Shao,H., Fang,W., Gao,D., Pei,F., Li,X., He,Z., Xu,D., Shi,X., Anderson,V.M., Leong,A.S. (2005). Multiple organ infection and the pathogenesis of SARS. J Exp.Med. *202*, 415-424.

Guan,Y., Zheng,B.J., He,Y.Q., Liu,X.L., Zhuang,Z.X., Cheung,C.L., Luo,S.W., Li,P.H., Zhang,L.J., Guan,Y.J., Butt,K.M., Wong,K.L., Chan,K.W., Lim,W., Shortridge,K.F., Yuen,K.Y., Peiris,J.S.M., Poon,L.L.M. (2003). Isolation and characterization of viruses related to the SARS coronavirus from animals in Southern China. Science *302*, 276-278.

Haijema,B.J., Volders,H., Rottier,P.J. (2004). Live, attenuated coronavirus vaccines through the directed deletion of group-specific genes provide protection against feline infectious peritonitis. J Virol. *78*, 3863-3871.

Han,J., Sabbatini,P., White,E. (1996). Induction of apoptosis by human Nbk/Bik, a BH3-containing protein that interacts with E1B 19K. Mol Cell Biol. *16*, 5857-5864.

Hanel,K., Willbold,D. (2007). SARS-CoV accessory protein 7a directly interacts with human LFA-1. Biological Chemistry *388*, 1325-1332.

He,R., Leeson,A., Andonov,A., Li,Y., Bastien,N., Cao,J., Osiowy,C., Dobie,F., Cutts,T., Ballantine,M., Li,X. (2003). Activation of AP-1 signal transduction pathway by SARS coronavirus nucleocapsid protein. Biochem Biophys Res Commun. *311*, 870-876.

Hegde,R., Srinivasula,S.M., Ahmad,M., Fernandes-Alnemri,T., Alnemri,E.S. (1998). Blk, a BH3-containing mouse protein that interacts with Bcl-2 and Bcl-xL, is a potent death agonist. J Biol Chem. *273*, 7783-7786.

Hofmann,H., Pohlmann,S. (2004). Cellular entry of the SARS coronavirus. Trends Microbiol *12*, 466-472.

Huang,C., Ito,N., Tseng,C.T., Makino,S. (2006a). Severe acute respiratory syndrome coronavirus 7a accessory protein is a viral structural protein. J Virol. *80*, 7287-7294.

Huang,C., Narayanan,K., Ito,N., Peters,C.J., Makino,S. (2006b). Severe acute respiratory syndrome coronavirus 3a protein is released in membranous structures from 3a protein-expressing cells and infected cells. J Virol. *80*, 210-217.

Jeffers,S.A., Tusell,S.M., Gillim-Ross,L., Hemmila,E.M., Achenbach,J.E., Babcock,G.J., Thomas,W.D., Jr., Thackray,L.B., Young,M.D., Mason,R.J., Ambrosino,D.M., Wentworth,D.E., Demartini,J.C., Holmes,K.V. (2004). CD209L (L-SIGN) is a receptor for severe acute respiratory

syndrome coronavirus. Proc.Natl.Acad.Sci.U.S A *101*, 15748-15753.

Kan,B., Wang,M., Jing,H.Q., Xu,H.F., Jiang,X.G., Yan,M.Y., Liang,W.L., Zheng,H., Wan,K.L., Liu,Q.Y., Cui,B.Y., Xu,Y.M., Zhang,E.M., Wang,H.X., Ye,J.R., Li,G.H., Li,M.H., Cui,Z.G., Qi,X.B., Chen,K., Du,L., Gao,K., Zhao,Y.T., Zou,X.Z., Feng,Y.J., Gao,Y.F., Hai,R., Yu,D.Z., Guan,Y., Xu,J.G. (2005). Molecular evolution analysis and geographic investigation of severe acute respiratory syndrome coronavirus-like virus in palm civets at an animal market and on farms. Journal of Virology *79*, 11892-11900.

Kanzawa,N., Nishigaki,K., Hayashi,T., Ishii,Y., Furukawa,S., Niiro,A., Yasui,F., Kohara,M., Morita,K., Matsushima,K., Lee,M.Q., Masuda,T., Kannagi,M. (2006). Augmentation of chemokine production by severe acute respiratory syndrome coronavirus 3a/X1 and 7a/X4 proteins through NF-kappa B activation. Febs Letters *580*, 6807-6812.

Knoops,K., Kikkert,M., van den Worm,S.H.E., Zevenhoven-Dobbe,J.C., van der Meer,Y., Koster,A.J., Mommaas,A.M., Snijder,E.J. (2008). SARS-coronavirus replication is supported by a reticulovesicular network of modified endoplasmic reticulum. Plos Biology *6*, 1957-1974.

Kopecky-Bromberg,S.A., Martinez-Sobrido,L., Frieman,M., Baric,R.A., Palese,P. (2007). Severe acute respiratory syndrome coronavirus open reading frame (ORF) 3b, ORF 6, and nucleocapsid proteins function as interferon antagonists. J.Virol. *81*, 548-557.

Kopecky-Bromberg,S.A., Martinez-Sobrido,L., Palese,P. (2006). 7a protein of severe acute respiratory syndrome coronavirus inhibits cellular protein synthesis and activates p38 mitogen-activated protein kinase. J Virol. *80*, 785-793.

Krähling,V., Stein,D.A., Spiegel,M., Weber,F., Mühlberger,E. (2009). Severe acute respiratory syndrome coronavirus triggers apoptosis via protein kinase R but is resistant to its antiviral activity. J Virol. *83*, 2298-2309.

Ksiazek,T.G., Erdman,D., Goldsmith,C.S., Zaki,S.R., Peret,T., Emery,S., Tong,S., Urbani,C., Comer,J.A., Lim,W., Rollin,P.E., Dowell,S.F., Ling,A.E., Humphrey,C.D., Shieh,W.J., Guarner,J., Paddock,C.D., Rota,P., Fields,B., DeRisi,J., Yang,J.Y., Cox,N., Hughes,J.M., LeDuc,J.W., Bellini,W.J., Anderson,L.J. (2003). A novel coronavirus associated with severe acute respiratory syndrome. N.Engl.J Med. *348*, 1953-1966.

Kulik,G., Klippel,A., Weber,M.J. (1997). Antiapoptotic signalling by the insulin-like growth factor I receptor, phosphatidylinositol 3-kinase, and Akt. Mol.Cell Biol. *17*, 1595-1606.

Lai,M.M. (2003). SARS virus: the beginning of the unraveling of a new coronavirus. J Biomed.Sci. *10*, 664-675.

Lan,K.L., Yen,S.H., Liu,R.S., Shih,H.L., Tseng,F.W., Lan,K.H. (2007). Mutant Bik gene transferred by cationic liposome inhibits peritoneal disseminated murine colon cancer. Clin Exp Metastasis. *24*, 461-470.

Lang,Z.W., Zhang,L.J., Zhang,S.J., Meng,X., Li,J.Q., Song,C.Z., Sun,L., Zhou,Y.S., Dwyer,D.E. (2003). A clinicopathological study of three cases of severe acute respiratory syndrome (SARS). Pathology *35*, 526-531.

Lau,S.K., Woo,P.C., Li,K.S., Huang,Y., Tsoi,H.W., Wong,B.H., Wong,S.S., Leung,S.Y., Chan,K.H., Yuen,K.Y. (2005). Severe acute respiratory syndrome coronavirus-like virus in Chinese horseshoe bats. Proc.Natl.Acad.Sci.U.S A *102*, 14040-14045.

Lee,C., Hodgins,D., Calvert,J.G., Welch,S.K., Jolie,R., Yoo,D. (2006). Mutations within the nuclear

localization signal of the porcine reproductive and respiratory syndrome virus nucleocapsid protein attenuate virus replication. Virology *346*, 238-250.

Lee,N., Hui,D., Wu,A., Chan,P., Cameron,P., Joynt,G.M., Ahuja,A., Yung,M.Y., Leung,C.B., To,K.F., Lui,S.F., Szeto,C.C., Chung,S., Sung,J.J.Y. (2003). A major outbreak of severe acute respiratory syndrome in Hong Kong. New England Journal of Medicine *348*, 1986-1994.

Leong,W.F., Tan,H.C., Ooi,E.E., Koh,D.R., Chow,V.T. (2005). Microarray and real-time RT-PCR analyses of differential human gene expression patterns induced by severe acute respiratory syndrome (SARS) coronavirus infection of Vero cells. Microbes.Infect. *7*, 248-259.

Leung,W.K., To,K.F., Chan,P.K., Chan,H.L., Wu,A.K., Lee,N., Yuen,K.Y., Sung,J.J. (2003). Enteric involvement of severe acute respiratory syndrome-associated coronavirus infection. Gastroenterology *125*, 1011-1017.

Li MH (2004). [Difference and significance of T-lymphocyte subsets in differential diagnosis between severe acute respiratory syndrome and common atypical pneumonia]. Chinese *18*, 137-141.

Li,W.D., Shi,Z.L., Yu,M., Ren,W.Z., Smith,C., Epstein,J.H., Wang,H.Z., Crameri,G., Hu,Z.H., Zhang,H.J., Zhang,J.H., McEachern,J., Field,H., Daszak,P., Eaton,B.T., Zhang,S.Y., Wang,L.F. (2005). Bats are natural reservoirs of SARS-like coronaviruses. Science *310*, 676-679.

Lim,P.L., Kurup,A., Gopalakrishna,G., Chan,K.P., Wong,C.W., Ng,L.C., Se-Thoe,S.Y., Oon,L., Bai,X., Stanton,L.W., Ruan,Y., Miller,L.D., Vega,V.B., James,L., Ooi,P.L., Kai,C.S., Olsen,S.J., Ang,B., Leo,Y.S. (2004). Laboratory-acquired severe acute respiratory syndrome. N.Engl.J Med. *350*, 1740-1745.

Lu HY (2005). Clinical features of probable severe acute respiratory syndrome in Beijing. World J Gastroenterol *11*, 2971-2974.

MacLachlan,T.K., El Deiry,W.S. (2002). Apoptotic threshold is lowered by p53 transactivation of caspase-6. Proc.Natl.Acad.Sci.U.S A *99*, 9492-9497.

Marra,M.A., Jones,S.J., Astell,C.R., Holt,R.A., Brooks-Wilson,A., Butterfield,Y.S., Khattra,J., Asano,J.K., Barber,S.A., Chan,S.Y., Cloutier,A., Coughlin,S.M., Freeman,D., Girn,N., Griffith,O.L., Leach,S.R., Mayo,M., McDonald,H., Montgomery,S.B., Pandoh,P.K., Petrescu,A.S., Robertson,A.G., Schein,J.E., Siddiqui,A., Smailus,D.E., Stott,J.M., Yang,G.S., Plummer,F., Andonov,A., Artsob,H., Bastien,N., Bernard,K., Booth,T.F., Bowness,D., Czub,M., Drebot,M., Fernando,L., Flick,R., Garbutt,M., Gray,M., Grolla,A., Jones,S., Feldmann,H., Meyers,A., Kabani,A., Li,Y., Normand,S., Stroher,U., Tipples,G.A., Tyler,S., Vogrig,R., Ward,D., Watson,B., Brunham,R.C., Krajden,M., Petric,M., Skowronski,D.M., Upton,C., Roper,R.L. (2003). The Genome sequence of the SARS-associated coronavirus. Science *300*, 1399-1404.

Marshansky,V., Wang,X., Bertrand,R., Luo,H., Duguid,W., Kanaan,N., Wu,J. (2001). Proteasomes modulate balance among proapoptotic and antiapoptotic Bcl-2 family members and compromise functioning of the electron transport chain in leukemic cells. J Immunol. *166*, 3130-3142.

Marzi,A., Gramberg,T., Simmons,G., Moller,P., Rennekamp,A.J., Krumbiegel,M., Geier,M., Eisemann,J., Turza,N., Saunier,B., Steinkasserer,A., Becker,S., Bates,P., Hofmann,H., Pohlmann,S. (2004). DC-SIGN and DC-SIGNR interact with the glycoprotein of Marburg virus and the S protein of severe acute respiratory syndrome coronavirus. J Virol. *78*, 12090-12095.

Masters,P.S. (2006). The molecular biology of coronaviruses. Adv.Virus Res *66*, 193-292.

Mathai JP,G.M.S.GC. (2005). BH3-only BIK regulates BAX,BAK-dependent release of Ca2+ from

endoplasmic reticulum stores and mitochondrial apoptosis during stress-induced cell death. J Biol Chem. *280*, 23829-23836.

Mazzulli,T., Farcas,G.A., Poutanen,S.M., Willey,B.M., Low,D.E., Butany,J., Asa,S.L., Kain,K.C. (2004). Severe acute respiratory syndrome-associated coronavirus in lung tissue. Emerg.Infect.Dis. *10*, 20-24.

Mebratu YA,D.B.E.C.T.Y. (2008). The BH3-only protein Bik/Blk/Nbk inhibits nuclear translocation of activated ERK1/2 to mediate IFNgamma-induced cell death. J Cell Biol. *183*, 429-439.

Mizutani,T., Fukushi,S., Ishii,K., Sasaki,Y., Kenri,T., Saijo,M., Kanaji,Y., Shirota,K., Kurane,I., Morikawa,S. (2006). Mechanisms of establishment of persistent SARS-CoV-infected cells. Biochem Biophys Res Commun. *347*, 261-265.

Mizutani,T., Fukushi,S., Murakami,M., Hirano,T., Saijo,M., Kurane,I., Morikawa,S. (2004a). Tyrosine dephosphorylation of STAT3 in SARS coronavirus-infected Vero E6 cells. FEBS Lett. *577*, 187-192.

Mizutani,T., Fukushi,S., Saijo,M., Kurane,I., Morikawa,S. (2004b). Importance of Akt signaling pathway for apoptosis in SARS-CoV-infected Vero E6 cells. Virology *327*, 169-174.

Mizutani,T., Fukushi,S., Saijo,M., Kurane,I., Morikawa,S. (2004c). Phosphorylation of p38 MAPK and its downstream targets in SARS coronavirus-infected cells. Biochem Biophys Res Commun. *319*, 1228-1234.

Mizutani,T., Fukushi,S., Saijo,M., Kurane,I., Morikawa,S. (2005). JNK and PI3k/Akt signaling pathways are required for establishing persistent SARS-CoV infection in Vero E6 cells. Biochim.Biophys Acta *1741*, 4-10.

Nelson,C.A., Pekosz,A., Lee,C.A., Diamond,M.S., Fremont,D.H. (2005). Structure and intracellular targeting of the SARS-coronavirus Orf7a accessory protein. Structure *13*, 75-85.

Nicholls,J.M., Butany,J., Poon,L.L., Chan,K.H., Beh,S.L., Poutanen,S., Peiris,J.S., Wong,M. (2006). Time course and cellular localization of SARS-CoV nucleoprotein and RNA in lungs from fatal cases of SARS. PLoS Med. *3*, e27.

Nikrad M,J.T.P.H.C.L.A.J.K.AS. (2005). The proteasome inhibitor bortezomib sensitizes cells to killing by death receptor ligand TRAIL via BH3-only proteins Bik and Bim. Mol Cancer Ther. *4*, 443-449.

Ning,Q., Lakatoo,S., Liu,M., Yang,W., Wang,Z., Phillips,M.J., Levy,G.A. (2003). Induction of prothrombinase fgl2 by the nucleocapsid protein of virulent mouse hepatitis virus is dependent on host hepatic nuclear factor-4 alpha. J Biol.Chem. *278*, 15541-15549.

Normile,D. (2004). Infectious diseases. Second lab accident fuels fears about SARS. Science *303*, 26.

Parashar,U.D., Anderson,L.J. (2004). Severe acute respiratory syndrome: review and lessons of the 2003 outbreak. Int.J Epidemiol. *33*, 628-634.

Pedrazzini E,V.A.B.N. (1996). A mutant cytochrome b5 with a lengthened membrane anchor escapes from the endoplasmic reticulum and reaches the plasma membrane. Proc Natl Acad Sci U S A. *93*, 4207-4212.

Peiris,J.S., Chu,C.M., Cheng,V.C., Chan,K.S., Hung,I.F., Poon,L.L., Law,K.I., Tang,B.S., Hon,T.Y., Chan,C.S., Chan,K.H., Ng,J.S., Zheng,B.J., Ng,W.L., Lai,R.W., Guan,Y., Yuen,K.Y. (2003a). Clinical

progression and viral load in a community outbreak of coronavirus-associated SARS pneumonia: a prospective study. Lancet *361*, 1767-1772.

Peiris,J.S., Guan,Y., Yuen,K.Y. (2004). Severe acute respiratory syndrome. Nat.Med. *10*, S88-S97.

Peiris,J.S.M., Lai,S.T., Poon,L.L.M., Guan,Y., Yam,L.Y.C., Lim,W., Nicholls,J., Yee,W.K.S., Yan,W.W., Cheung,M.T., Cheng,V.C.C., Chan,K.H., Tsang,D.N.C., Yung,R.W.H., Ng,T.K., Yuen,K.Y. (2003b). Coronavirus as a possible cause of severe acute respiratory syndrome. Lancet *361*, 1319-1325.

Pfefferle,S., Krähling,V., Ditt,V., Grywna,K., Mühlberger,E., Drosten,C. (2009). Reverse genetic characterization of the natural genomic deletion in SARS-Coronavirus strain Frankfurt-1 open reading frame 7b reveals an attenuating function of the 7b protein in-vitro and in-vivo. Virol J *6*, 1-17.

Poutanen,S.M., Low,D.E., Henry,B., Finkelstein,S., Rose,D., Green,K., Tellier,R., Draker,R., Adachi,D., Ayers,M., Chan,A.K., Skowronski,D.M., Salit,I., Simor,A.E., Slutsky,A.S., Doyle,P.W., Krajden,M., Petric,M., Brunham,R.C., McGeer,A.J. (2003). Identification of severe acute respiratory syndrome in Canada. N.Engl.J Med. *348*, 1995-2005.

Prentice,E., Jerome,W.G., Yoshimori,T., Mizushima,N., Denison,M.R. (2004). Coronavirus replication complex formation utilizes components of cellular autophagy. J Biol.Chem. *279*, 10136-10141.

Qiu,M., Shi,Y., Guo,Z., Chen,Z., He,R., Chen,R., Zhou,D., Dai,E., Wang,X., Si,B., Song,Y., Li,J., Yang,L., Wang,J., Wang,H., Pang,X., Zhai,J., Du,Z., Liu,Y., Zhang,Y., Li,L., Wang,J., Sun,B., Yang,R. (2005). Antibody responses to individual proteins of SARS coronavirus and their neutralization activities. Microbes.Infect. *7*, 882-889.

Rashmi,R., Pillai,S.G., Vijayalingam,S., Ryerse,J., Chinnadurai,G. (2008). BH3-only protein BIK induces caspase-independent cell death with autophagic features in Bcl-2 null cells. Oncogene. *27*, 1366-1375.

Reggiori,F., Monastyrska,I., Verheije,M.H., Cali,T., Ulasli,M., Bianchi,S., Bernasconi,R., de Haan,C.A.M., Molinari,M. (2010). Coronaviruses Hijack the LC3-I-Positive EDEMosomes, ER-Derived Vesicles Exporting Short-Lived ERAD Regulators, for Replication. Cell Host & Microbe *6*, 500-508.

Reilley,B., Van Herp,M., Sermand,D., Dentico,N. (2003). SARS and Carlos Urbani. N Engl J Med *348*, 1951-1952.

Ren,L., Yang,R., Guo,L., Qu,J., Wang,J., Hung,T. (2005). Apoptosis induced by the SARS-associated coronavirus in Vero cells is replication-dependent and involves caspase. DNA Cell Biol. *24*, 496-502.

Rota,P.A., Oberste,M.S., Monroe,S.S., Nix,W.A., Campagnoli,R., Icenogle,J.P., Penaranda,S., Bankamp,B., Maher,K., Chen,M.H., Tong,S., Tamin,A., Lowe,L., Frace,M., DeRisi,J.L., Chen,Q., Wang,D., Erdman,D.D., Peret,T.C., Burns,C., Ksiazek,T.G., Rollin,P.E., Sanchez,A., Liffick,S., Holloway,B., Limor,J., McCaustland,K., Olsen-Rasmussen,M., Fouchier,R., Gunther,S., Osterhaus,A.D., Drosten,C., Pallansch,M.A., Anderson,L.J., Bellini,W.J. (2003). Characterization of a novel coronavirus associated with severe acute respiratory syndrome. Science *300*, 1394-1399.

Rowland,R.R., Chauhan,V., Fang,Y., Pekosz,A., Kerrigan,M., Burton,M.D. (2005). Intracellular localization of the severe acute respiratory syndrome coronavirus nucleocapsid protein: absence of nucleolar accumulation during infection and after expression as a recombinant protein in vero cells. J Virol. *79*, 11507-11512.

Rowland,R.R., Kervin,R., Kuckleburg,C., Sperlich,A., Benfield,D.A. (1999). The localization of porcine reproductive and respiratory syndrome virus nucleocapsid protein to the nucleolus of infected cells and identification of a potential nucleolar localization signal sequence. Virus Res *64*, 1-12.

Ruchaud,S., Korfali,N., Villa,P., Kottke,T.J., Dingwall,C., Kaufmann,S.H., Earnshaw,W.C. (2002). Caspase-6 gene disruption reveals a requirement for lamin A cleavage in apoptotic chromatin condensation. EMBO J. *21*, 1967-1977.

Sawicki,S.G., Sawicki,D.L., Siddell,S.G. (2006). A Contemporary View of Coronavirus Transcription. J Virol. *81*, 20-29.

Schaecher,S.R., Mackenzie,J.M., Pekosz,A. (2007). The ORF7b protein of severe acute respiratory syndrome coronavirus (SARS-CoV) is expressed in virus-infected cells and incorporated into SARS-CoV particles. Journal of Virology *81*, 718-731.

Schneider, M. Molekulare Mechanismen des SARS-Coronavirus: Charakterisierung des akzessorischen 7a-Proteins und Effekt des proteasomalen Inhibitors MG-132 auf die virale Replikation. 1-145. 2011. Lehrstuhl für Biofunktionalität der Lebensmittel.

Ref Type: Thesis/Dissertation

Shen,S., Lin,P.S., Chao,Y.C., Zhang,A., Yang,X., Lim,S.G., Hong,W., Tan,Y.J. (2005). The severe acute respiratory syndrome coronavirus 3a is a novel structural protein. Biochem Biophys Res Commun. *330*, 286-292.

Shi,X., Gong,E., Gao,D., Zhang,B., Zheng,J., Gao,Z., Zhong,Y., Zou,W., Wu,B., Fang,W., Liao,S., Wang,S., Xie,Z., Lu,M., Hou,L., Zhong,H., Shao,H., Li,N., Liu,C., Pei,F., Yang,J., Wang,Y., Han,Z., Shi,X., Zhang,Q., You,J., Zhu,X., Gu,J. (2005). Severe acute respiratory syndrome associated coronavirus is detected in intestinal tissues of fatal cases. Am.J Gastroenterol. *100*, 169-176.

Shi,Z.L., Hu,Z.H. (2008). A review of studies on animal reservoirs of the SARS coronavirus. Virus Research *133*, 74-87.

Shieh,W.J., Hsiao,C.H., Paddock,C.D., Guarner,J., Goldsmith,C.S., Tatti,K., Packard,M., Mueller,L., Wu,M.Z., Rollin,P., Su,I.J., Zaki,S.R. (2005). Immunohistochemical, in situ hybridization, and ultrastructural localization of SARS-associated coronavirus in lung of a fatal case of severe acute respiratory syndrome in Taiwan. Hum.Pathol. *36*, 303-309.

Snijder,E.J., Bredenbeek,P.J., Dobbe,J.C., Thiel,V., Ziebuhr,J., Poon,L.L., Guan,Y., Rozanov,M., Spaan,W.J., Gorbalenya,A.E. (2003). Unique and conserved features of genome and proteome of SARS-coronavirus, an early split-off from the coronavirus group 2 lineage. J Mol Biol. *331*, 991-1004.

Song,H.D., Tu,C.C., Zhang,G.W., Wang,S.Y., Zheng,K., Lei,L.C., Chen,Q.X., Gao,Y.W., Zhou,H.Q., Xiang,H., Zheng,H.J., Chern,S.W., Cheng,F., Pan,C.M., Xuan,H., Chen,S.J., Luo,H.M., Zhou,D.H., Liu,Y.F., He,J.F., Qin,P.Z., Li,L.H., Ren,Y.Q., Liang,W.J., Yu,Y.D., Anderson,L., Wang,M., Xu,R.H., Wu,X.W., Zheng,H.Y., Chen,J.D., Liang,G., Gao,Y., Liao,M., Fang,L., Jiang,L.Y., Li,H., Chen,F., Di,B., He,L.J., Lin,J.Y., Tong,S., Kong,X., Du,L., Hao,P., Tang,H., Bernini,A., Yu,X.J., Spiga,O., Guo,Z.M., Pan,H.Y., He,W.Z., Manuguerra,J.C., Fontanet,A., Danchin,A., Niccolai,N., Li,Y.X., Wu,C.I., Zhao,G.P. (2005). Cross-host evolution of severe acute respiratory syndrome coronavirus in palm civet and human. Proc.Natl.Acad.Sci.U.S A *102*, 2430-2435.

Stadler,K., Masignani,V., Eickmann,M., Becker,S., Abrignani,S., Klenk,H.D., Rappuoli,R. (2003). SARS--beginning to understand a new virus. Nat.Rev.Microbiol *1*, 209-218.

Stennicke,H.R., Salvesen,G.S. (1998). Properties of the caspases. Biochim.Biophys Acta *1387*, 17-31.

Suggs,S.V., Wallace,R.B., Hirose,T., Kawashima,E.H., Itakura,K. (1981). Use of Synthetic Oligonucleotides As Hybridization Probes .3. Isolation of Cloned Cdna Sequences for Human Beta-2-Microglobulin. Proceedings of the National Academy of Sciences of the United States of America-Biological Sciences *78*, 6613-6617.

Surjit,M., Kumar,R., Mishra,R.N., Reddy,M.K., Chow,V.T., Lal,S.K. (2005). The severe acute respiratory syndrome coronavirus nucleocapsid protein is phosphorylated and localizes in the cytoplasm by 14-3-3-mediated translocation. J Virol. *79*, 11476-11486.

Surjit,M., Lal,S.K. (2008). The SARS-CoV nucleocapsid protein: A protein with multifarious activities. Infection Genetics and Evolution *8*, 397-405.

Surjit,M., Liu,B., Jameel,S., Chow,V.T., Lal,S.K. (2004). The SARS coronavirus nucleocapsid protein induces actin reorganization and apoptosis in COS-1 cells in the absence of growth factors. Biochem J *383*, 13-18.

Tan,Y.J., Fielding,B.C., Goh,P.Y., Shen,S., Tan,T.H., Lim,S.G., Hong,W. (2004). Overexpression of 7a, a protein specifically encoded by the severe acute respiratory syndrome coronavirus, induces apoptosis via a caspase-dependent pathway. J Virol. *78*, 14043-14047.

Tan,Y.X., Tan,T.H., Lee,M.J., Tham,P.Y., Gunalan,V., Druce,J., Birch,C., Catton,M., Fu,N.Y., Yu,V.C., Tan,Y.J. (2007). Induction of apoptosis by the severe acute respiratory syndrome coronavirus 7a protein is dependent on its interaction with the Bcl-XL protein. J.Virol. *81*, 6346-6355.

Tang,X.C., Zhang,J.X., Zhang,S.Y., Wang,P., Fan,X.H., Li,L.F., Li,G., Dong,B.Q., Liu,W., Cheung,C.L., Xu,K.M., Song,W.J., Vijaykrishna,D., Poon,L.L., Peiris,J.S., Smith,G.J., Chen,H., Guan,Y. (2006). Prevalence and genetic diversity of coronaviruses in bats from China. J Virol. *80*, 7481-7490.

Thiel,V., Ivanov,K.A., Putics,A., Hertzig,T., Schelle,B., Bayer,S., Weissbrich,B., Snijder,E.J., Rabenau,H., Doerr,H.W., Gorbalenya,A.E., Ziebuhr,J. (2003). Mechanisms and enzymes involved in SARS coronavirus genome expression. J Gen Virol. *84*, 2305-2315.

Timani,K.A., Liao,Q., Ye,L., Zeng,Y., Liu,J., Zheng,Y., Ye,L., Yang,X., Lingbao,K., Gao,J., Zhu,Y. (2005). Nuclear/nucleolar localization properties of C-terminal nucleocapsid protein of SARS coronavirus. Virus Res *114*, 23-34.

To,K., Tong,J.H.M., Chan,P.K.S., Au,F.W.L., Chim,S.S.C., Chan,K.C.A., Cheung,J.L.K., Liu,E.Y.M., Tse,G.M.K., Lo,A.W.I., Lo,Y.M.D., Ng,H.K. (2004). Tissue and cellular tropism of the coronavirus associated with severe acute respiratory syndrome: an in-situ hybridization study of fatal cases. Journal of Pathology *202*, 157-163.

To,K.F., Lo,A.W. (2004). Exploring the pathogenesis of severe acute respiratory syndrome (SARS): the tissue distribution of the coronavirus (SARS-CoV) and its putative receptor, angiotensin-converting enzyme 2 (ACE2). J Pathol. *203*, 740-743.

Tsang,K.W., Mok,T.Y., Wong,P.C., Ooi,G.C. (2003). Severe acute respiratory syndrome (SARS) in Hong Kong. Respirology. *8*, 259-265.

Tyrrell,D.A. (1965). Viruses and Acute Respiratory Infections. British Medical Journal *2*, 822-&.

Vasilenko,N., Moshynskyy,I., Zakhartchouk,A. (2010). SARS coronavirus protein 7a interacts with human Ap(4)A-hydrolase. Virology Journal *7*.

Verma,S., Zhao,L.J., Chinnadurai,G. (2001). Phosphorylation of the pro-apoptotic protein BIK:

mapping of phosphorylation sites and effect on apoptosis. J Biol Chem. *276*, 4671-4676.

W Zhu,A.C.G.W.W.L.Z.P.B.L.a.D.W.A. (1996). Bcl-2 mutants with restricted subcellular location reveal spatially distinct pathways for apoptosis in different cell types. EMBO J *15*, 4130-4141.

Wang,H., Mao,Y., Ju,L., Zhang,J., Liu,Z., Zhou,X., Li,Q., Wang,Y., Kim,S., Zhang,L. (2004). Detection and monitoring of SARS coronavirus in the plasma and peripheral blood lymphocytes of patients with severe acute respiratory syndrome. Clin.Chem. *50*, 1237-1240.

Wang,H.L., Yang,P., Liu,K.T., Guo,F., Zhang,Y.L., Zhang,G.Y., Jiang,C.Y. (2008). SARS coronavirus entry into host cells through a novel clathrin- and caveolae-independent endocytic pathway. Cell Research *18*, 290-301.

Wang,L.F., Shi,Z.L., Zhang,S.Y., Field,H., Daszak,P., Eaton,B.T. (2006). Review of bats and SARS. Emerging Infectious Diseases *12*, 1834-1840.

Wang,Y., Guan,X., Fok,K.L., Li,S., Zhang,X., Miao,S., Zong,S., Koide,S.S., Chan,H.C., Wang,L. (2008). A novel member of the Rhomboid family, RHBDD1, regulates BIK-mediated apoptosis. Cell Mol Life Sci. *65*, 3822-3829.

Watanabe,S., Masangkay,J.S., Nagata,N., Morikawa,S., Mizutani,T., Alviola,P., Omatsu,T., Ueda,N., Iha,K., Taniguchi,S., Fujii,H., Tsuda,S. (2010). Bat coronaviruses and experimental infection of bats, the Philippines. Emerg Infect Dis *16*, 1217-1223.

WHO. Summary of probable SARS cases with onset of illness from 1. November 2003 to 31. July 2003. 2011.

Ref Type: Internet Communication

Woo P.C. (2009). Coronavirus diversity, phylogeny and interspecies jumping. Exp Biol Med *234*, 1117-1127.

Woo,P.C., Lau,S.K., Li,K.S., Poon,R.W., Wong,B.H., Tsoi,H.W., Yip,B.C., Huang,Y., Chan,K.H., Yuen,K.Y. (2006). Molecular diversity of coronaviruses in bats. Virology *351*, 180-187.

Wu,D.L., Tu,C.C., Xin,C., Xuan,H., Meng,Q.W., Liu,Y.G., Yu,Y.D., Guan,Y.T., Jiang,Y., Yin,X.N., Crameri,G., Wang,M.P., Li,C.W., Liu,S.W., Liao,M., Feng,L., Xiang,H., Sun,J.F., Chen,J.D., Sun,Y.W., Gu,S.L., Liu,N.H., Fu,D.X., Eaton,B.T., Wang,L.F., Kong,X.G. (2005). Civets are equally susceptible to experimental infection by two different severe acute respiratory syndrome coronavirus isolates. Journal of Virology *79*, 2620-2625.

Wurm,T., Chen,H., Hodgson,T., Britton,P., Brooks,G., Hiscox,J.A. (2001). Localization to the nucleolus is a common feature of coronavirus nucleoproteins, and the protein may disrupt host cell division. J Virol. *75*, 9345-9356.

Xu,X., Gao,X. (2004). Immunological responses against SARS-CoV infections in humans. Cellular & Molecular Imunology *1*, 119-122.

Yamashita,M., Yamate,M., Li,G.M., Ikuta,K. (2005). Susceptibility of human and rat neural cell lines to infection by SARS-coronavirus. Biochem Biophys Res Commun. *334*, 79-85.

Yan,H., Xiao,G., Zhang,J., Hu,Y., Yuan,F., Cole,D.K., Zheng,C., Gao,G.F. (2004). SARS coronavirus induces apoptosis in Vero E6 cells. J Med.Virol. *73*, 323-331.

Yan,X., Hao,Q., Mu,Y., Timani,K.A., Ye,L., Zhu,Y., Wu,J. (2006). Nucleocapsid protein of SARS-CoV activates the expression of cyclooxygenase-2 by binding directly to regulatory elements for

nuclear factor-kappa B and CCAAT/enhancer binding protein. Int.J Biochem Cell Biol. *38*, 1417-1428.

Yang,Z.Y., Huang,Y., Ganesh,L., Leung,K., Kong,W.P., Schwartz,O., Subbarao,K., Nabel,G.J. (2004). pH-dependent entry of Severe acute respiratory syndrome coronavirus is mediated by the spike glycoprotein and enhanced by dendritic cell transfer through DC-SIGN. Journal of Virology *78*, 5642-5650.

Ye,J., Zhang,B., Xu,J., Chang,Q., McNutt,M.A., Korteweg,C., Gong,E., Gu,J. (2007). Molecular pathology in the lungs of severe acute respiratory syndrome patients. Am J Pathol *170*, 538-545.

You,J., Dove,B.K., Enjuanes,L., Dediego,M.L., Alvarez,E., Howell,G., Heinen,P., Zambon,M., Hiscox,J.A. (2005). Subcellular localization of the severe acute respiratory syndrome coronavirus nucleocapsid protein. J Gen Virol. *86*, 3303-3310.

Yount,B., Roberts,R.S., Sims,A.C., Deming,D., Frieman,M.B., Sparks,J., Denison,M.R., Davis,N., Baric,R.S. (2005). Severe acute respiratory syndrome coronavirus group-specific open reading frames encode nonessential functions for replication in cell cultures and mice. J Virol. *79*, 14909-14922.

Yuan,X., Wu,J., Shan,Y., Yao,Z., Dong,B., Chen,B., Zhao,Z., Wang,S., Chen,J., Cong,Y. (2006). SARS coronavirus 7a protein blocks cell cycle progression at G0/G1 phase via the cyclin D3/pRb pathway. Virology *346*, 74-85.

Zhang,L., Wei,L., Jiang,D., Wang,J., Cong,X., Fei,R. (2007). SARS-CoV nucleocapsid protein induced apoptosis of COS-1 mediated by the mitochondrial pathway. Artif.Cells Blood Substit.Immobil.Biotechnol. *35*, 237-253.

Zhang,Q.L., Ding,Y.Q., He,L., Wang,W., Zhang,J.H., Wang,H.J., Cai,J.J., Geng,J., Lu,Y.D., Luo,Y.L. (2003). [Detection of cell apoptosis in the pathological tissues of patients with SARS and its significance]. Chinese *23*, 770-773.

Zhang,X., Wu,K., Wang,D., Yue,X., Song,D., Zhu,Y., Wu,J. (2007). Nucleocapsid protein of SARS-CoV activates interleukin-6 expression through cellular transcription factor NF-kappaB. Virology.

Zhao,G., Shi,S.Q., Yang,Y., Peng,J.P. (2006). M and N proteins of SARS coronavirus induce apoptosis in HPF cells. Cell Biol.Toxicol. *22*, 313-322.

Zhao,X., Nicholls,J.M., Chen,Y.G. (2008). Severe acute respiratory syndrome-associated coronavirus nucleocapsid protein interacts with Smad3 and modulates transforming growth factor-beta signaling. J Biol Chem. *283*, 3272-3280.

Zhao,Z., Thackray,L.B., Miller,B.C., Lynn,T.M., Becker,M.M., Ward,E., Mizushima,N.N., Deninson,M.R., Virgin IV,H.W. (2007). Coronavirus Repliction Does Not Require the Autophagy Gene ATG5. Autophagy *3*, 581-585.

Zheng,B.J., Wong,K.H., Zhou,J., Wong,K.L., Young,B.W., Lu,L.W., Lee,S.S. (2004). SARS-related virus predating SARS outbreak, Hong Kong. Emerg.Infect.Dis. *10*, 176-178.

Zhong,N.S., Zheng,B.J., Li,Y.M., Poon,L.L.M., Xie,Z.H., Chan,K.H., Li,P.H., Tan,S.Y., Chang,Q., Xie,J.P., Liu,X.Q., Xu,J., Li,D.X., Yuen,K.Y., Peiris,J.S.M., Guan,Y. (2003). Epidemiology and cause of severe acute respiratory syndrome (SARS) in Guangdong, People's Republic of China, in February, 2003. Lancet *362*, 1353-1358.

Zhu,H., Zhang,L., Dong,F., Guo,W., Wu,S., Teraishi,F., Davis,J.J., Chiao,P.J., Fang,B. (2005). Bik/NBK accumulation correlates with apoptosis-induction by bortezomib (PS-341, Velcade) and

other proteasome inhibitors. Oncogene. *24*, 4993-4999.

ABBREVIATIONS

% (v/v)	Volume percentage
% (w/v)	Weight percentage
°C	Degree Celsius
µ	Mikro
A	Adenine, Ampere
Aa	Aminoacid
Ab	Antibody
Amp	Ampicillin
ACE2	Angiotensin-Converting Enzyme 2
APS	Ammoniumpersulfate
ATF6	activating transcription factor 6
ATP	Adenosintriphosphat
bp	Basepair
Bcl-2	B-cell lymphoma-2
Bik	BCL-2 interacting killer
BiP	immunoglobulin heavy chain binding protein
BSA	Bovines Serumalbumin
c	concentration
C	Cytosin
CDC	Center for Disease Control
CoV	Coronavirus
CRM-1	Chromosomal region maintenance 1
C-Terminus	Carboxy-Terminus
da	Dalton
dest.	destilled
DMEM	Dulbeccos Modified Eagle Medium
DMSO	Dimethylsulfoxid
DMV	Doublemembranevesicle
DNA	Deoxyribonucleicacid
DNAse	Deoxyribonuclease
dNTPs	Desoxyribonucleosidtriphosphate
d	day
ds	double stranded
DOC	Deoxycholate
DTT	Dithriothreitol

E	Envelope
EDTA	Ethylenediamine-N,N,N´,N´-Tetraacetate 2
EGFP	Enhanced green fluorescent protein
ER	Endoplasmic reticulum
EtBr	Ethidiumbromide
EtOH	Ethanol
FCS	Fetal calf serum
Fig	Figure
FECV	feline Coronavirus
FIPV	feline Peritonitisvirus
g	gramm
G	Guanin
GAPDH	Glycerinaldehyde-3-phosphate-Dehydrogenase
GFP	green fluorescent protein
h	hour
HA	Hemagglutinin
hu	Human
IF	Immunofluorescence
Ig	Immune globuline
IFN	Interferon
IRE1	Inositol requiring enzyme 1
JNK	C-Jun terminal kinase
k	Kilo
kb	Kilo base pair
kDa	Kilo Dalton
l	Liter
Lac	Lactacystin
LB	Luria-Bertrani
M	Molar, Matrix
m	Milli, Meter
MAPK	Mitogen-activated protein kinase
Mcs	Multiple cloning site
MEM	Modified Eagle Medium
MetOH	Methanol
MHC	major histocompatibility complex
MHV	murines Hepatitisvirus

min	Minute
MOI	multiplicity of infection
mRNA	messenger RNA
N	Nuleocapsid
NF	nuclear factor
n	nano
nsp	Non-structuralprotein
nt	Nucleotide
N-Terminus	Amino-Terminus
OD	Optical density
ORF	Open reading frame
PBS	Phosphate buffered saline
PKR	Protein kinase R
PVDF	Polyvinyl difluoride
RIPA	Radioimmunoprecipitation assay buffer
rpm	Rotation per minute
RT	Room temperature
S	Spike, Svedberg, second
ss	single stranded
SARS	severe acute respiratory syndrome
SDS	Sodium dodecyle sulfate
sgRNA	subgenome RNA
T	Thymidine
TEMED	N,N,N´,N´-Tetramethylethylendiamin
Tris	Tris-(hydroxymethyl-)aminomethan
U	Unit
UPR	Unfolded protein response
UV	Ultraviolett
V	Volume
W	Watt
WB	Western Blot
WHO	World Health Organization
wt	wild type

PUBLICATIONS

Diemer C, Schneider M, Schätzl HM, Gilch S; S.K. Lal (ed.) *Molecular Biology of SARS-CoV:*"Modulation of host cell death by SARS-CoV proteins." Springer Verlag Berlin 2010

Diemer C, Schneider M, Seebach J, Quaas J, Fösner G, Schätzl HM, Gilch S. „ Cell-type specific cleavage of nucleocapsid protein by effector caspases during SARS coronavirus infection." JMB, 2008.

Krammer C. Suhre MH, Kremmer E, Diemer C, Hess S, Schätzl HM, Scheibel T, Vorberg I. „Prion protein / protein interactions: fusion with yeast Sup35p-NM modulates cytosolic PrP aggregation in mammalian cells." FASEB J., 2007

Cosma A, Nagaraj R, Staib C, Diemer C, Wopfner F, Schätzl H, Busch DH, Sutter G, Goebel FD, Erfle V. „Evaluation of modified vaccinia virus Ankara as an alternative vaccine against smallpox in chronically HIV type 1-infected individuals undergoing HAART." AIDS Res Hum Retroviruses, 2007.

ACKNOWLEDGEMENT

Mein herzlichster Dank gilt Herrn Professor Hermann M. Schätzl, dass er mir die Möglichkeit gegeben hat meine Doktorarbeit in seiner Arbeitsgruppe durchzuführen. Für die fortwährende Diskussionsbereitschaft, hervoragende Betreuung, Geduld und dass er mir trotz eigener beruflicher Veränderung, die Möglichkeit einer Babypause einräumte und mir so das Beenden dieser Arbeit ermöglichte.

Mein besonderer Dank gilt Herrn Professor Bauer für das Interesse und die bereitwillige Übernahme der Betreuung meiner Doktorarbeit.

Dr. Sabine Gilch möchte ich ganz herzlich danken für die hervorragende Betreuung, unzähligen Ratschläge und Diskussionen, im Besonderen auch, dass sie mich in die Praxis der Virologie und des S3-Labor Betriebs einführte, mir mit ihrem umfassenden Wissen stets zur Seite stand.

Bei Dr. Alexa Ertmer, Dr. Carmen Krammer und Dr. Ina Vorberg möchte ich mich ganz herzlich für die unzähligen praktischen sowie wissenschaftlichen Ratschläge und Diskussionen, insbesondere was das Klonieren betrifft, bedanken.

Mein besonderer Dank gilt Dr. Alexa Ertmer für die vielen Aufmunterungen, Unterstützung und Diskussionen schon morgens früh um 6 Uhr. Für die großartige Freundschaft, die sich daraus entwickelte und die trotz der großen Entfernung und über die Jahre hinweg immer noch Bestand hat.

Bei Dr. Carmen Krammer, die mich schon seit dem ersten Semester begleitet, möchte ich mich für die treue, langjährige Freundschaft, den Zuspruch und den lustigen, geselligen Treffen (u. a. „Weihnachtstradition“) bedanken.

Christian Bach möchte ich ganz herzlich für die Unterstützung in jeglichen IT-Belangen danken.

Bei der gesamten Schätzl AG und Vorberg AG insbesondere, Dr. Max Nunziante, Martha Schneider Christopher Bruns, Christian Bach, Doris Pelz und Kata Masic möchte ich mich ganz herzlich für die Hilfe, Ratschläge, die freundschaftliche, lustige und angenehme Zusammenarbeit bedanken.

Mein innigster Dank gilt Christoph Wex für die jahrelange Unterstützung schon während des Studiums, den vielen Aufmunterungen und einfach, dass Du immer für mich da warst und bist!